UNLV Theses, Dissertations, Professional Papers, and Capstones

December 2016

Canovas Canyon Rhyolites, Jemez Volcanic Field, New Mexico: Discrete Source Magmas, or a Potential Caldera Forming Magma System?

Penelope Marie Padmore
University of Nevada, Las Vegas

CANOVAS CANYON RHYOLITES, JEMEZ VOLCANIC FIELD, NEW MEXICO:
DISCRETE SOURCE MAGMAS, OR A POTENTIAL CALDERA FORMING
MAGMA SYSTEM?

By

Penelope Marie Padmore

Bachelor of Arts – Theater Arts
Salem State College
1989

Bachelor of Science – Geology
Salem State College
1999

Master of Education – Special Education
Grand Canyon University
2011

A thesis submitted in partial fulfillment
of the requirements for the

Master of Science – Geoscience

Department of Geoscience
College of Sciences
The Graduate College

University of Nevada, Las Vegas
December 2016

Thesis Approval

The Graduate College
The University of Nevada, Las Vegas

November 18, 2016

This thesis prepared by

Penelope Marie Padmore

entitled

Canovas Canyon Rhyolites, Jemez Volcanic Field, New Mexico: Discrete Source Magmas, or a Potential Caldera Forming Magma System?

is approved in partial fulfillment of the requirements for the degree of

Master of Science – Geoscience
Department of Geoscience

Terry Spell, Ph.D.   Kathryn Hausbeck Korgan, Ph.D.
Examination Committee Chair   *Graduate College Interim Dean*

Shichun Huang, Ph.D.
Examination Committee Member

Rodney V. Metcalf, Ph.D.
Examination Committee Member

Dennis Bazlinski, Ph.D.
Graduate College Faculty Representative

ABSTRACT

Canovas Canyon Rhyolites, Jemez Volcanic Field, New Mexico: Discrete source magmas, or a potential caldera forming magma system?

by

Penelope M. Padmore
Dr. Terry Spell, Examination Committee Chair
Associate Professor of Geology
University of Nevada, Las Vegas

The Jemez volcanic field (JVF), New Mexico, is a caldera-forming volcanic field located at the junction of the Rio Grande Rift and the Jemez Lineament. The JVF is one of three large North American caldera-forming systems, including Long Valley, California and Yellowstone Plateau volcanic field, Wyoming, which have been active during the Quaternary. Because portions of the JVF are unusually well preserved, it offers a rare opportunity to study how such systems develop. Insight into the history of caldera-forming systems will contribute to the understanding of their potential future behavior. In the case of Yellowstone and Long Valley, that insight could contribute to more accurate prediction of the future activity of these two potentially active systems. This research focuses on the nature of the Canovas Canyon Rhyolite (CCR). These domes and flows were the product of the first significant rhyolitic volcanism in the JVF, beginning about 13 Ma (Gardner, et al., 1986). Timing of the eruptions; over a ~4 Ma time period, as well as the areal extent (more than 50 km^2), make it unlikely that the CCR was produced by one long lived magma system.

Models which describe the formation of silicic caldera-forming systems can be broadly grouped into two categories: **A**. Those which postulate large, thermally stable, long lived magma bodies which develop chemical and thermal gradients, such as the model developed by Hildreth,

(1981) and Halliday, et al., (1989); **B**. Models in which silicic volcanism is produced by smaller, individual batches of melt (Huppert and Sparks, 1988b). In the second type of model, caldera-forming magma chambers are ephemeral and only occur in the last stage of development of the system, prior to the culminating eruption.

Major and trace element geochemistry trends rule out any of the sampled units having been produced by the same magma system. Nd, Sr, and Pb isotope ratios indicate that the CCR are products of fractional crystallization of associated basalts, with up to 50% crustal assimilation. The CCR best fits model B; a rhyolite produced in small, ephemeral, independent magma systems

ACKNOWLEDGMENTS

inspiration, and finally, I would also like to thank Educate, Empower and Succeed, Arizona, for allowing me the time off to complete my thesis.

DEDICATION

I would like to dedicate this thesis to my mom, Joan Padmore, in gratitude for her help and support, and for our mutual appreciation of rocks.

TABLE OF CONTENTS

LIST OF TABLES

LIST OF FIGURES

CHAPTER 1

INTRODUCTION

The Jemez Mountains Volcanic Field (JMVF), New Mexico is the location of the Valles Caldera. The Valles Caldera is the type locality for large, resurgent ash-flow calderas (Smith and Bailey, 1968). There have been numerous eruptions in the volcanic field, some as old as 16 Ma, and others as young as 70 ka. It has twice produced a silicic magma system large enough to culminate in two significant caldera forming eruptions. The first occurred at 1.608 ± 0.010 Ma (Spell et al., 1996), and produced the Toledo Caldera, along with the 400 km^3 Dense Rock Equivalent (DRE) Otowi member of the Bandelier Tuff. The second eruption produced the Valles Caldera at 1.225 ± 0.008 Ma (Spell et al., 1996), and the 250 km^3 DRE Tshirege Member of the Bandelier Tuff (Spell, et al, 1993).

The JMVF (Fig. 1.01) is located at the intersection of the Jemez Lineament and the Rio Grande Rift. The Jemez Lineament is a northwest trending line of volcanic centers which extends from the San Carlos Volcanic Field in Arizona, to the Raton/Clayton Volcanic Field in New Mexico. The lineament coincides with the suture zone of the Yavapai and Mazatzal Terranes, which converged at about 1.65 to 1.60 Ga. during the Mazatzal Orogeny (Magnani, et al., 2004). The Rio Grande Rift is a north-south trending series of *en echelon* basins, which formed to accommodate spreading from Colorado to Mexico, beginning about 29 Ma (Morgan, et al., 1986). While both the Jemez Lineament and the Rio Grande Rift have produced volcanism, the JMVF is the most significant volcanic field of either feature.

While syn- and post caldera rhyolites have received a great deal of research attention, pre- caldera rhyolites, and in particular, the oldest rhyolites, have not been as extensively studied since the amount of exposure is limited. Whereas andesite and basalt dominate the JMVF, episodes of silicic volcanism have punctuated its eruptive history. The Canovas Canyon Rhyolite (CCR), is the oldest significant rhyolite produced in the JMVF. The CCR consists of a series of small volume eruptions which occurred in the southern JMVF. Erupted between 12 - 7 Ma (Justet, 2003; Gardner, 1985), the CCR has the potential to reveal a great deal about the nature of the Jemez volcanic system during its earliest stages of development. This study focuses on the petrogenesis of the CCR, and the development of JMVF's magmatic system at the time of the CCR eruptions.
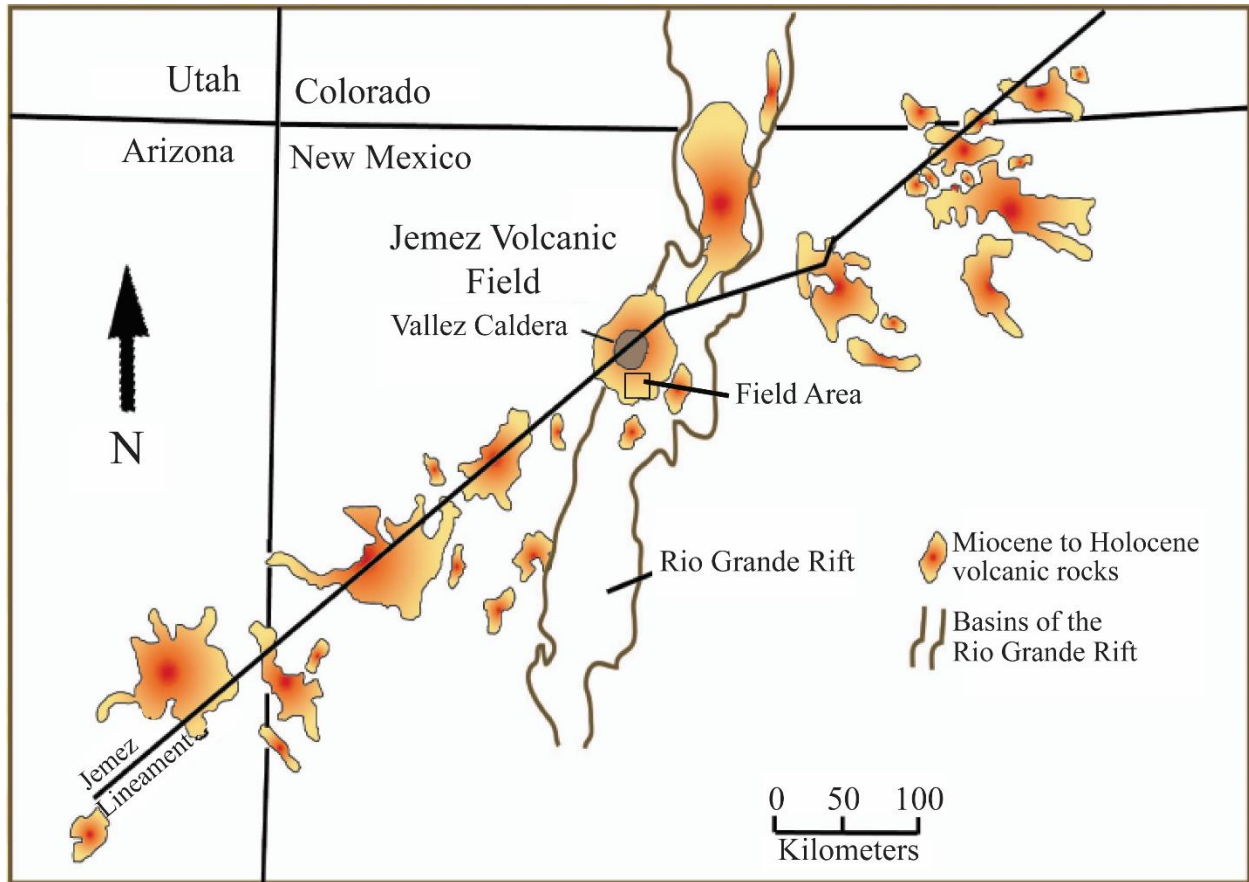
Figure 1.01. Location of the Jemez Volcanic Field at the juncture of the Rio Grande Rift and the Jemez Lineament. After Perry et al. (1987). The black box shows the field area mapped in Figure 5. Figure from Gibler, (2007).

1.1 Purpose and Scope

Large, caldera forming eruptions such as those which produced the Valles Caldera can have catastrophic effects not only on their immediate vicinities, but on global climate as well. Among historical eruptions which have affected populations by lowering temperatures and causing crop failure, the greatest was the eruption of Tambora, Indonesia, in 1815. The volume of ash it injected into the atmosphere has been estimated to be about 50 km^3. In the years immediately following, average global temperature was reduced by up to 2° C, causing famine, epidemics, and social upheaval in areas as far away as western Europe (Oppenheimer, 2003).

Aside from Tambora, there are a number of other volcanic systems throughout the world which could potentially affect global populations through reducing the amount of solar energy that reaches the Earth's surface, these include Taupo, New Zealand, as well as Yellowstone and Long Valley, both found in the United States. Another threat posed by such systems is to populations in their vicinity, which could be affected by ashfalls and pyroclastic flows. The JMVF itself could present a potential hazard to Santa Fe, Albuquerque, and the Los Alamos National Laboratory. The most recent volcanism in the Jemez Volcanic Field is the East Fork member of the Valles Rhyolite which has been recently dated to about 68.3 ± 1.5 ka (Zimmerer, et al., 2015). The most recent volcanism may signify the beginning of a new cycle of volcanic activity (Wolff and Gardner, 1995).

The United States hosts three of the largest continental caldera-forming systems in the world; Yellowstone, Long Valley, and the Jemez Volcanic Field, (JMVF) New Mexico. All three systems have all been active during the Quaternary. While their tectonic settings differ, all three are comparable in volume and composition. Both Long Valley and Yellowstone continue to undergo episodes of tumescence (Johnson, et al., 2002; Hill et al., 2003). The record of volcanic activity in a system such as the Jemez could provide valuable insight into the future behavior of other systems (Lipman, 1984). Figure 1.02 shows the relative volume of several eruptions including three historical eruptions.
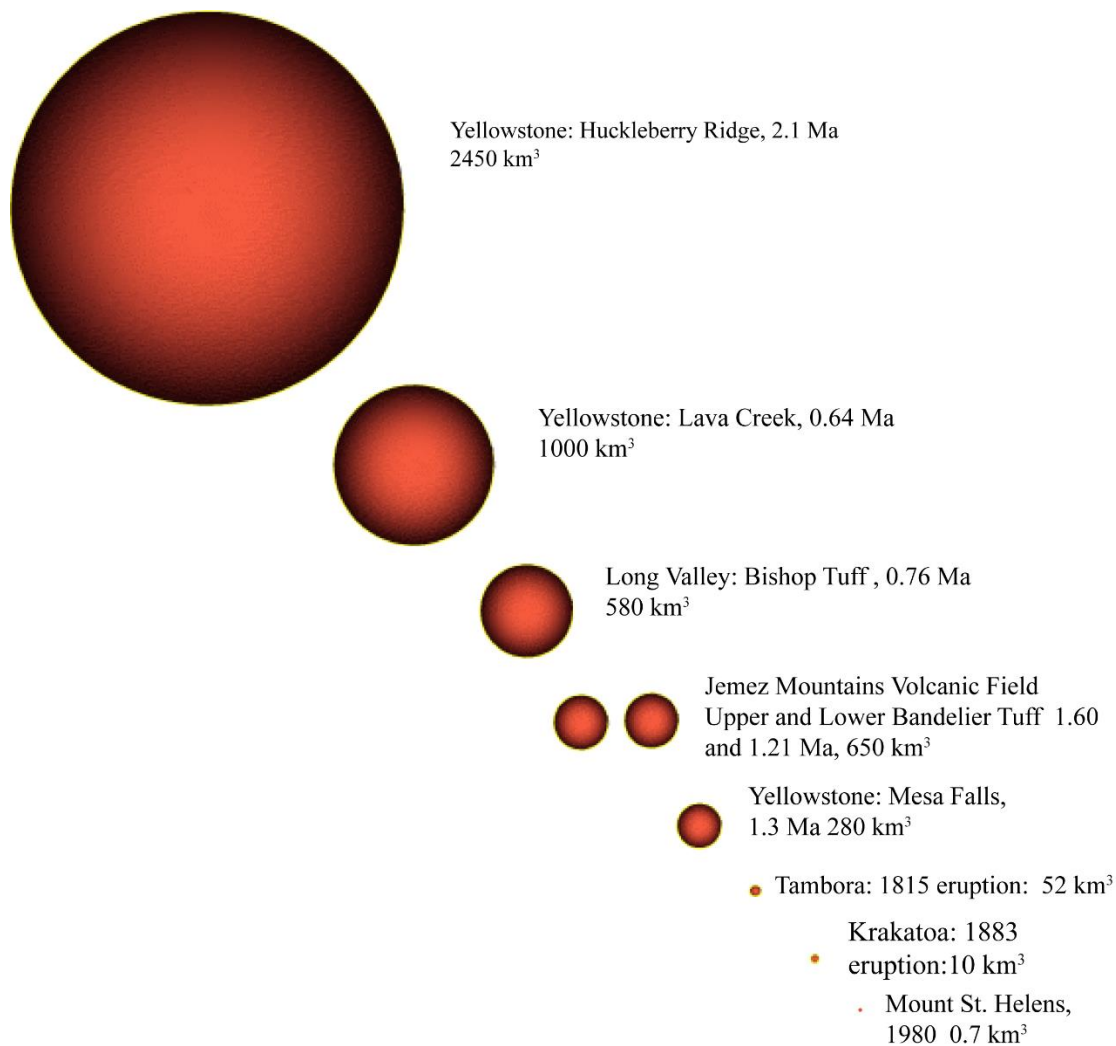
Figure 1.02. Comparison of volumes of Yellowstone, Jemez, Long Valley and other historical eruptions (USGS Volcano Hazards Program 2016; Hildreth and Wilson, 2007, Self, 1992).

1.2 Current Models

Many of the models which have been proposed for the development of silicic magma systems in continental caldera-forming volcanic fields such as the JMVF can be broadly grouped into two end-member categories; those in which large, persistent magma systems develop over million year timescales, and those in which eruptions tap multiple smaller independent batches of

magma and in which large magma systems only develop during caldera-forming stages. While

all such systems are driven by basalt injection, the interactions between the intruding basalt and

the host rocks are very different. In the Huppert and Sparks (1988a) model, open system

processes dominate and small aliquots of basalt are heavily contaminated from partial melting of

host crustal rocks. Rhyolite is primarily generated by episodic remelting of granitic crustal rocks,

and generated on short time scales (Sparks et al., 1990). Batches of discrete rhyolitic melts form

over much shorter time scales, generated by separate basalt injections into the mid to deep crust.

The models which fit this category include those by Huppert and Sparks (1988a; 1988b) and

Perry et al., (1990). In these models, large magma chambers are more ephemeral features which

form after smaller batches of melt coalesce into a single large chamber, capable of producing a

large-scale caldera-forming eruption. While this model does not exclude the possibility of the

existence of pluton sized magma systems remaining in the crust for up to 1 Ma, it does

 In contrast to the Perry et al., (1990)/Huppert and Sparks (1988a) model described

above, in this second type of model, pluton sized, thermally stable magma bodies remain viable

within the crust for up to 1-2 million years (Smith, 1979; Hildreth, 1981; Halliday et al., 1989).

These massive magma chambers become chemically and thermally stratified over time, and

convection cells develop within the distinct layers due to thermal, density and chemical

gradients. Small rhyolitic eruptions from such a system such as this would sample magma

located at the apex of the chamber (Hildreth, 1979). These minor, effusive eruptions tap magma

which is >70% silica, usually enriched in Sc, Mn, and depleted in Ba, Sr, P, and Mg (Bacon et

al., 1981).

If a single eruption of sufficiently large volume, such as an ash flow tuff, withdraws a

large enough volume of magma from the top layers of the magma chamber, a typical feature of

such eruptions is that the earliest products at the base of the ash flow tuff are more evolved than subsequent layers (Smith, 1979). The magma chamber empties from the top down. After such an eruption, these large chambers appear to recover their chemical gradients on a timescale of hundreds of thousands of years, as evidenced by a relationship between the length of time between eruptions and the extent to which the magma has evolved. In such systems, stratification is produced by the precipitation of crystals from basalt injections, separation of melt from crystals, followed by separate layers continuing to evolve (Schmitt et al., 2002). While such long lived systems can produce caldera forming massive eruptions, it is also possible for them to produce small, localized eruptions which only tap the apex of the magma chamber, where the most rhyolitic melt can accumulate. Small eruptions from such a single system may have as much as a 300 ka age range (Bachmann and Bergantz, 2004).

Results from research on the CCR are anticipated to indicate which model best fits the magma system at the time it produced these rhyolites. A Huppert and Sparks (1988a) type model might be indicated if the isotope signatures are more consistent with the crustal rocks in the area than with basalts which are interbedded with the CCR. Major and trace element chemistry would not be expected to show systematic variation with time, and would also be expected to have a wider range of values than would a single, long lived system. Table 1.01 summarizes the implications of results for the CCR. In general, evidence which indicates a lack of fractionation between the units, or fractionation from a common source would tend to favor model B. Indications that the rhyolites were descended from a common source, or that latter rhyolites were derived from older units would tend to favor model A.

Parameter	Persistent single magma chamber (Smith, 1979; Hildreth, 1981; Perry et al., 1990, Halliday et al., 1989	Ephemeral magma systems (Huppert & Sparks, 1988a and 1988b)
Major Elements	Systematic variability over time.	Greater variability among rhyolites.
		Evolution of rhyolites not related to timing between eruptions
Trace Elements	More evolved magmas produced after longer residence times.	No little correlation among trace elements from different units.
Petrographic results	Equilibrium assemblages	Evidence of disequilibrium more likely due to more open system processes
$^{40}Ar/^{39}Ar$ Dating	All eruptions similar in age.	Ages spanning millions of years are unlikely to be from the same system.
Pb isotopes	Pb isotopes similar to associated basalts.	More likely to be similar to crustal rocks due to assimilation.
$^{87}Sr/^{86}Sr$	More uniform $^{87}Sr/^{86}Sr$ ratios	Larger array of values showing varying levels of crustal contamination.
		Sr signature more likely to be dominated by crustal contamination.
ε_{Nd}	Limited range of values, clearly related to parental basalt	$^{143}Nd/^{144}Nd$ vs. $^{87}Sr/^{86}Sr$ ratios which indicate two or more possible sources

Table 1.01. Comparison of two end member models and possible results.

CHAPTER 2

GEOLOGIC SETTING AND HISTORY

2.1 Structure

The Jemez Volcanic Field (JVMF) is an approximately 1,600 km^3 volcanic complex located on the western rim of the Española Basin, at the juncture of the Jemez Lineament and the Rio Grande Rift. The Rio Grande Rift (RGR) consists of a series of north-trending *en echelon* basins which extends from Colorado through New Mexico, Texas and into Chihuahua, Mexico and it is the only feature east of the Colorado Plateau which is the result of regional Cenozoic extension (Aldrich et al., 1986). The Jemez Lineament (JL) is a line of volcanic fields and faulting which extends from southeastern Arizona to northeastern New Mexico, coincident with the remnant of a Proterozoic convergent plate boundary. Because of the concentration of tectonic activity at this juncture of the RGR and the JL, the JMVF is the most productive volcanic field of the Jemez Lineament (Chapin, et al, 2004). This focusing of tectonic activity has also resulted in a long-lived magmatic system (Gardner, 1985).

The Rio Grande Rift began forming during the early Oligocene, with evidence of rifting in the southern part of New Mexico as early as 37 Ma (Aldrich, et al.., 1986). There is a dearth of volcanism along the RGR relative to other rift zones due to the lithospheric conditions at the time of RGR inception. At that time, a low strain rate coupled with an elevated geotherm caused the lower lithosphere to deform ductilely. While the crust accommodated strain through normal faulting and the creation of rift basins (Figure 2.01), the lower lithosphere thinned uniformly over an area up to four times the width of the surface expression of extension, preventing

localized upwelling of mantle and small scale convection which would tend to favor volcanism

(Wilson, et al., 2005). The regional stress field and the extension in the area has varied from

ENE-SW, to a roughly NE-SW direction (Morgan, et al., 1986). The rate of extension has also

fluctuated significantly, and the volume of volcanism in the JMVF can be correlated with the

variation in rates of extension (Heiken et al., 1990). The current rate of extension along the RGR

is about 0.1 cm per year. Within the Jemez itself, extension along the Parajito fault system has

been between 0.5 mm and 0.7 mm per year, over the last 1.1 Ma (Golombek, 1981).
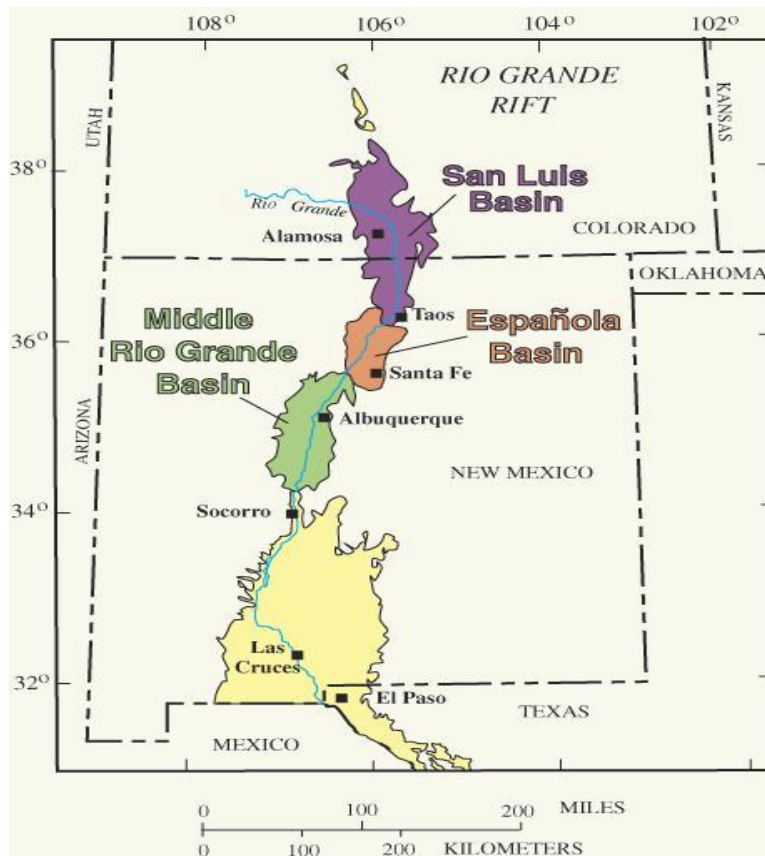
Figure 2.01. The basins which make up the northern Rio Grande Rift, image courtesy of the
USGS, from "Measuring Rio Grande Rift Crustal Deformation."

The Española Basin, which hosts the JMVF on its western edge, began forming at about

25 Ma (Izett and Obradovich, 2001). The Velarde Graben is the active sub-basin of the Española. Its western boundary is the Parajito Fault Zone which cuts the Tshirege member on the eastern side of the JMVF. Along the Parajito Fault Zone which there has been approximately 100 meters of vertical displacement. The volcanic field itself is located on the Jemez bench, an upraised area which defines the northwest boundary of the Española Basin (Golombek, 1981).
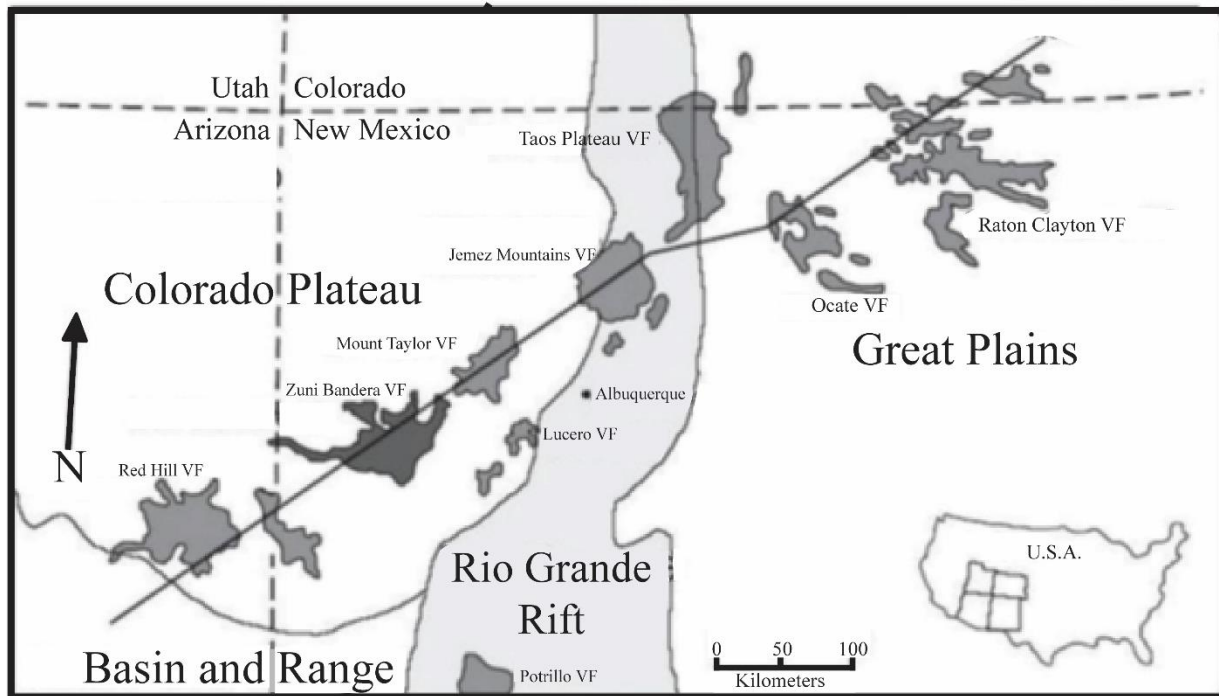
Figure 2.02. The volcanic fields of the Jemez Lineament. From Suneson (2012).

The Jemez Lineament is a crustal scale tectonic feature which occurs in the suture zone between the Yavapai and Mazatzal Proterozoic provinces. The Mazatzal Province docked against the Yavapai Province at about 1.68 -1.65 Ga, during the Mazatzal Orogeny (Magnani, et al, 2002). The lineament stretches from SE Arizona to NW New Mexico, and is approximately 100 km wide (Figure 2.02). Underlain by low seismic velocity mantle, it is marked by Tertiary to Quaternary volcanic centers, faulting, and uplift. The suture zone (Figure 2.03 and 2.04) consists

of complex folds and thrusts which are the result of the original collision during the Proterozoic. The suture is an area of weakness which has allowed mantle material to well up into the crust, as well as being a locus for tectonic deformation (Magnani, et al., 2004). From seismic studies of the Jemez Lineament, Magnani, et al. (2002; 2004) described the complex geometry of this ancient subduction zone (Figure 2.04), and showed that features in the mid to lower crust such as thrust faults and recumbent folds may provide areas of weakness where magma rose and created some of the volcanic fields such as the Ocate and Raton.
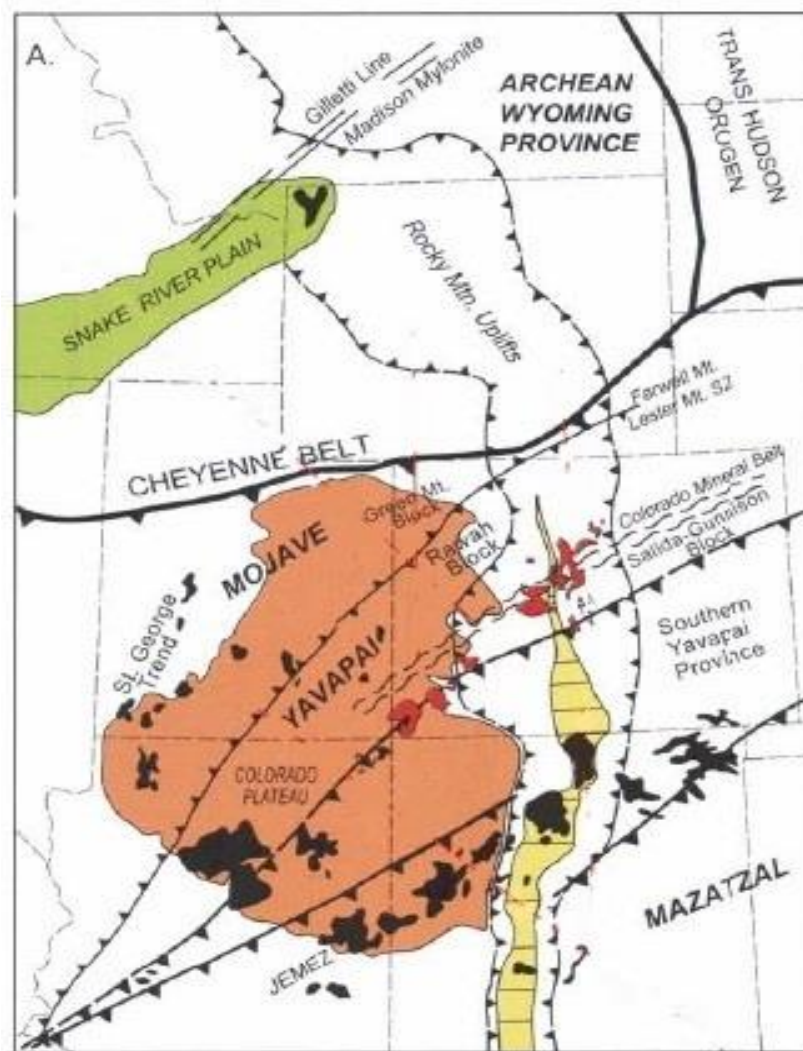
 Figure 2.03. The Rio Grande Rift (pale yellow), volcanic fields of the Jemez Lineament, Colorado Plateau (pale orange) Colorado Mineral Belt (orange), as well as the Mojave, Yavapai and Masatzal provinces. From Karlstrom et al., 2002.

A south-dipping reflector, interpreted to be the remains of a descending slab, plunges

from a depth of about 10 km to a depth of about 35 km directly underneath the lineament itself. A

seismic reflection study by Levander et al. (2004) found relatively thin lower crust, 41-44 km,

above an area of lower (7.7 to 7.8 km/sec) seismic velocity in the upper mantle. South dipping

negative P and S velocity anomalies which extend from a depth of about 150 km to the base of

the crust, along with bright seismic reflectors in the crust are interpreted to be a partially molten

(1% melt) mantle, with mantle basalt intruding into the lower crust (Wisniewski and Pazzaglia,

2002).
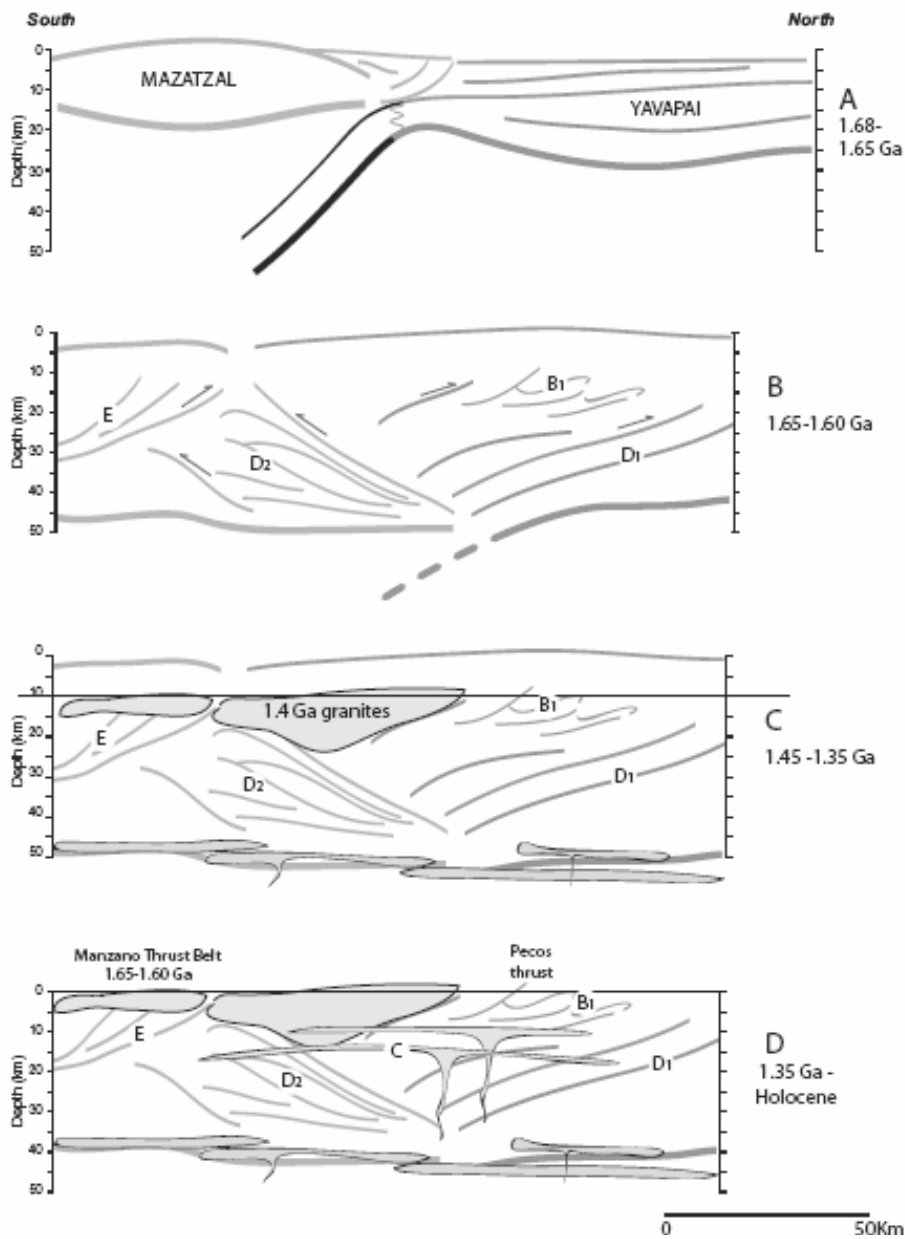
Figure 2.04. Development of the lithospheric structure of the Jemez Lineament northeast of the JMVF. In A, the Mazatzal overrides Yavapai to the north, and a prism of Mazatzal sediments are deposited on top of the Yavapai. B: Because of continuing compression, a complex zone of thrusts and folding form, followed by a magmatic event at about 1.4 Ga. In C, uplift causes exposure of intrusions, and in D, basalt underplating, such as that which feeds the JMVF occurs, controlled by preexisting structure. Figure from Magnani et al. (2004).

Faulting within the area of the JVMF is either on-strike with the Rio Grande Rift (approximately

15

north trending) or the Jemez Lineament (northeast trending). However, the Jemez Lineament

seems to control more recent volcanic activity within the JMVF (Self, et al., 1986). Several

features which are on strike with the Jemez Lineament found in and around the area of the Jemez

Volcanic Field, include faults within the Valles Caldera, the alignment of the Toldeo embayment,

and the Jemez Fault Zone (Gardner, 1986).

2.2 History of Volcanism in the JVMF

The earliest volcanism in the Espanola Basin dates to about 25 Ma, near the time of the

inception of basin. The earliest products of the JMVF itself is the mid to late Miocene Keres

Group. which are found south of the Valles Caldera. The Polvadera Group occurs in the central

and northern JVMF, and dates between 10.8 Ma to 2.0 Ma (Singer and Kudo, 1986). The latest

stages of volcanism in the Jemez produced the Tewa Group, which consists of the upper and

lower Bandelier Tuff, the Cerro Toledo Rhyolite, Cerro Rubio Quartz Latite, the Valles Rhyolite,

and the most recent El Cajete. Smith, et al., 1970 formalized the stratigraphy of the JVMF,

summarized in Figure 2.05.
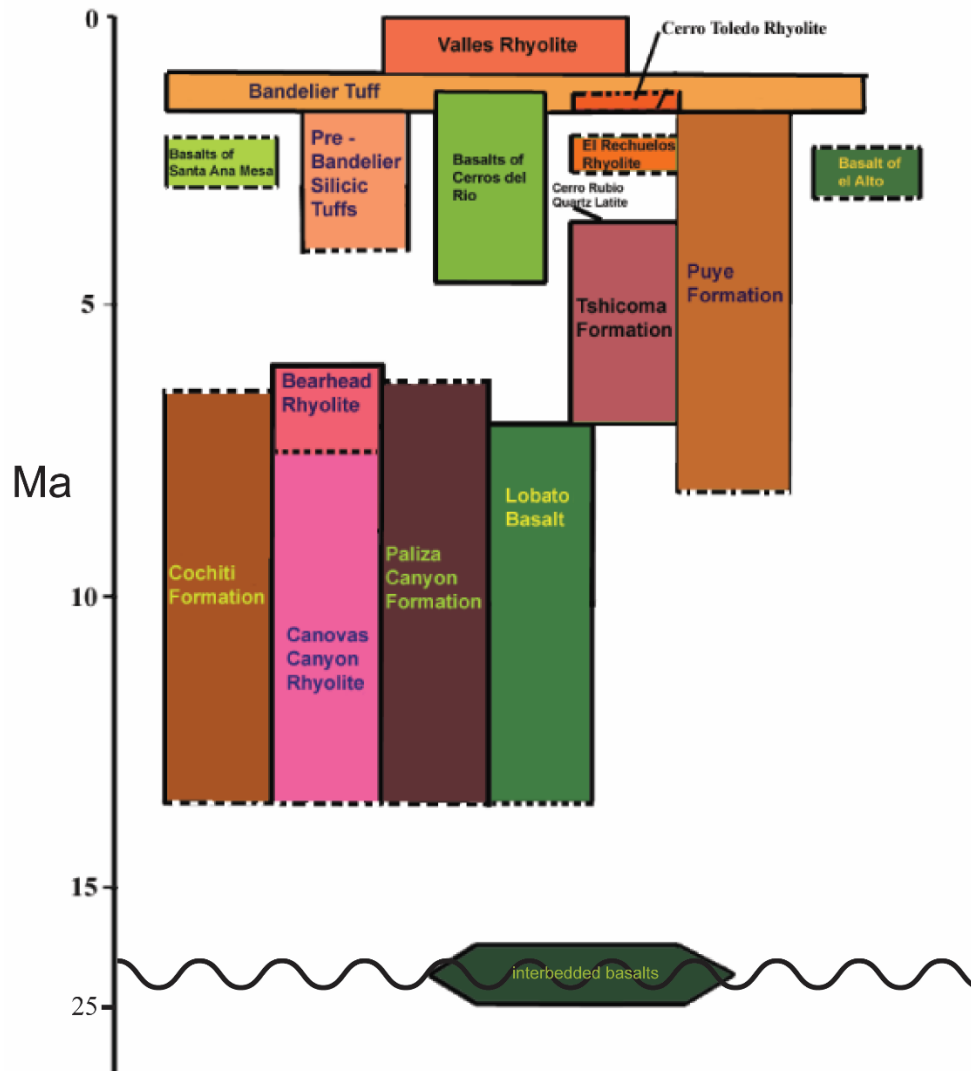
Figure 2.05. Jemez Volcanic Field formalized stratigraphy, after Bailey, et al., 1970, Gardner, 1985, Loeffler, et al., 1988 and Heiken *et al.*, 1990. Dotted lines indicate uncertainty. The diagram also represents a cross section of the volcanic field, from south, on the left, to north on the right. The oldest group, The Keres Group, were produced from about 13 Ma to 6 Ma. The oldest rhyolite of the Keres Group is the Canovas Canyon Rhyolite.

The earliest lavas within the JVMF were mafic flows interbedded with Santa Fe basin fill sediments. From 25 Ma to 16.5 Ma, thinly bedded nephelinites and basanites, including the most primitive lava found in the area of the JVMF; a 16% MgO nephelinite, erupted in the area which later became the JVMF (Gardner et al., 1986). At about ~13 Ma, the main volcanism associated

17

with the Jemez began with the extrusion of the Keres Group. The Keres Group is predominantly andesitic and basaltic, but also includes two formations of high silica rhyolite: the Canovas Canyon Rhyolite (CCR) and the younger Bearhead Rhyolite. Although the Bearhead and the Canovas Canyon Rhyolites are petrographically indistinguishable, recent ^{40}Ar/^{39}Ar dating indicates that there was a time span of about 1.2 Ma between cessation of CCR eruptions and inception of the Bearhead Rhyolite eruptions (Justet and Spell, 2001). Ellisor et al., (1996) dates the CCR between 12.4 to 8.8 Ma. Gardner and Goff (1984) dated the CCR from 12.4 to 9.2.

From 10 to 7 Ma, basalt, high silica rhyolites and andesite continued to erupt, coinciding with an increase in regional extension. A lull in extension from 7 to 4 Ma coincided with decreased volcanic activity. However, during this period, from about 7 Ma to 2 Ma, the dacitic/rhyolitic Tschicoma Formation erupted in the central and eastern Jemez, with the main volume being produced between 5 Ma to 3 Ma . At about 4 Ma, faulting and basaltic volcanism resumed in areas around the main volcanic field (Gardner, 1985).

At about 1.61 Ma, the Lower Bandelier Tuff, which is the The Ottowi Member, erupted, accompanied by formation of the Toledo Caldera (Spell, et al., 1996). Smaller intracaldera domes and tuffs then erupted over the next few hundred thousand years. The Toledo Caldera was later overprinted by the larger Valles Caldera, at about 1.23 Ma (Spell, et al., 1996) during the eruption of the Upper Bandelier Tuff ; the Tshirege Member. The two calderas are nearly coincident in their locations (Stix et al., 1988). The post collapse rhyolite domes within the caldera comprise the Valles Rhyolite, which includes domes and ignimbrites inside the caldera, such as the El Cajete Pumice. The El Cajete has been dated using thermo-luminescence and carbon-14 dating to between 50 to 60 ka (Reneau et al., 1996). According to some workers, the

Jemez may be entering a new phase of activity after more than 400,000 years of relative quiescence (Wolff and Gardner, 1995).

Justet (2003) concluded, based in part on extensive $^{40}Ar/^{39}Ar$ geochronology, that volcanism in the JVMF occurred in 2 major cycles, each approximately 3 Ma in duration. The first stage, which produced the Keres Group, occurred from about 9.8 Ma, to 6.0 Ma, and the second from about 3.8 Ma to 50 ka. Between these two phases there was a lull in volcanism which lasted about 2.2 Ma. The earliest stage of both cycles lasted between 1.8 to 1.9 Ma, and produced large volumes of mafic to intermediate lava. The next stage was a lull in volcanism lasting about 0.3 to 0.8 Ma. During the final stage in each of these phases, large silicic systems formed at shallow levels. The products of these final stages are the Bearhead Rhyolite in the first cycle, and the Bandelier Tuff in the second.

Basalt underplating continues to drive volcanism in the Jemez, as it has for approximately 25 Ma, even prior to the formation of the Espanola Basin. As regional extension stretches the lithosphere, basalt intrudes the lower to middle crust from the mantle. Figure 2.06 shows a recent tomographic study by Aprea et al. (2000) of seismic data from the area of the Valles Caldera. There are several horizontal layers of high velocity material, interpreted to be mafic sills (purple). The green area is a low velocity region interpreted to be a potential magma system currently beneath the Valles Caldera.
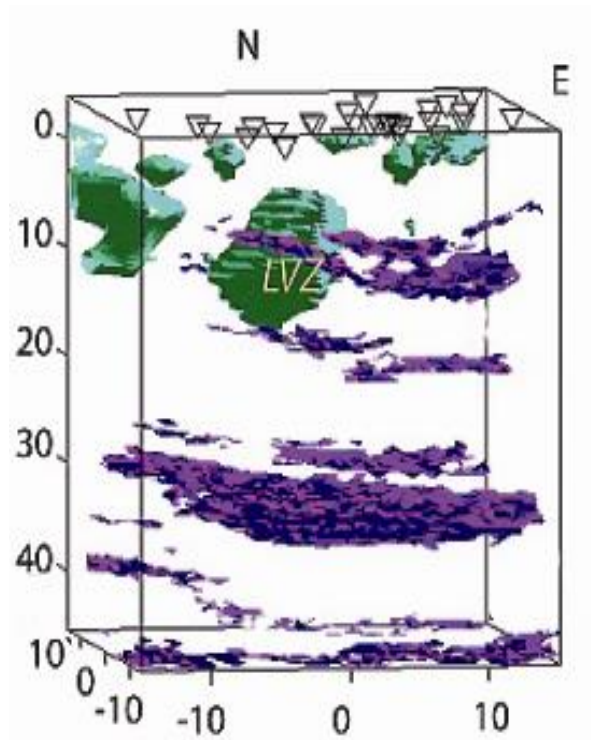
Figure 2.06. Tomographic image of the crust and upper mantle beneath the Valles Caldera, JVMF. Purple areas represent zones of higher velocities. In the transitional area between the lower crust and upper mantle, 30-40 km depth, these are interpreted as evidence of basaltic underplating. Green area marked LVZ (Low Velocity Zone) is interpreted as the remnants of a magma system beneath Valles Caldera. Triangles are seismic stations. Depth and distance are in km. From Aprea et al. (2000).

CHAPTER 3

STUDY AREA

The entire field area is located south of the Valles Caldera, where there are numerous exposures of the Canovas Canyon Rhyolite (Figure 3.01, inset). The CCR occurs as volcanic domes, plugs, shallow intrusions, lava flows and tuffs, and is interbedded with Paliza Canyon basalt and andesite. Sampling locations were chosen based on the original field work and mapping of Smith, et al., (1970). The field area, mostly covered with pine and deciduous forest, is remote, with many sample locations are only accessible on foot. The study area occurs within the Santa Fe National Forest and the tribal lands of the Pueblo of the Jemez. Steve Blodgett of the Pueblo of the Jemez granted permission for access to tribal lands for this research. The USGS 7.5 Quadrangle maps which cover the study area include The Redondo Peak, Bear Springs Peak, and Ponderosa. Figure 3.02 is a more recent geologic map of the area provided by S. A. Kelley. Sampling for this study was conducted in July, 2005 and again in May 2006 when it was completed.
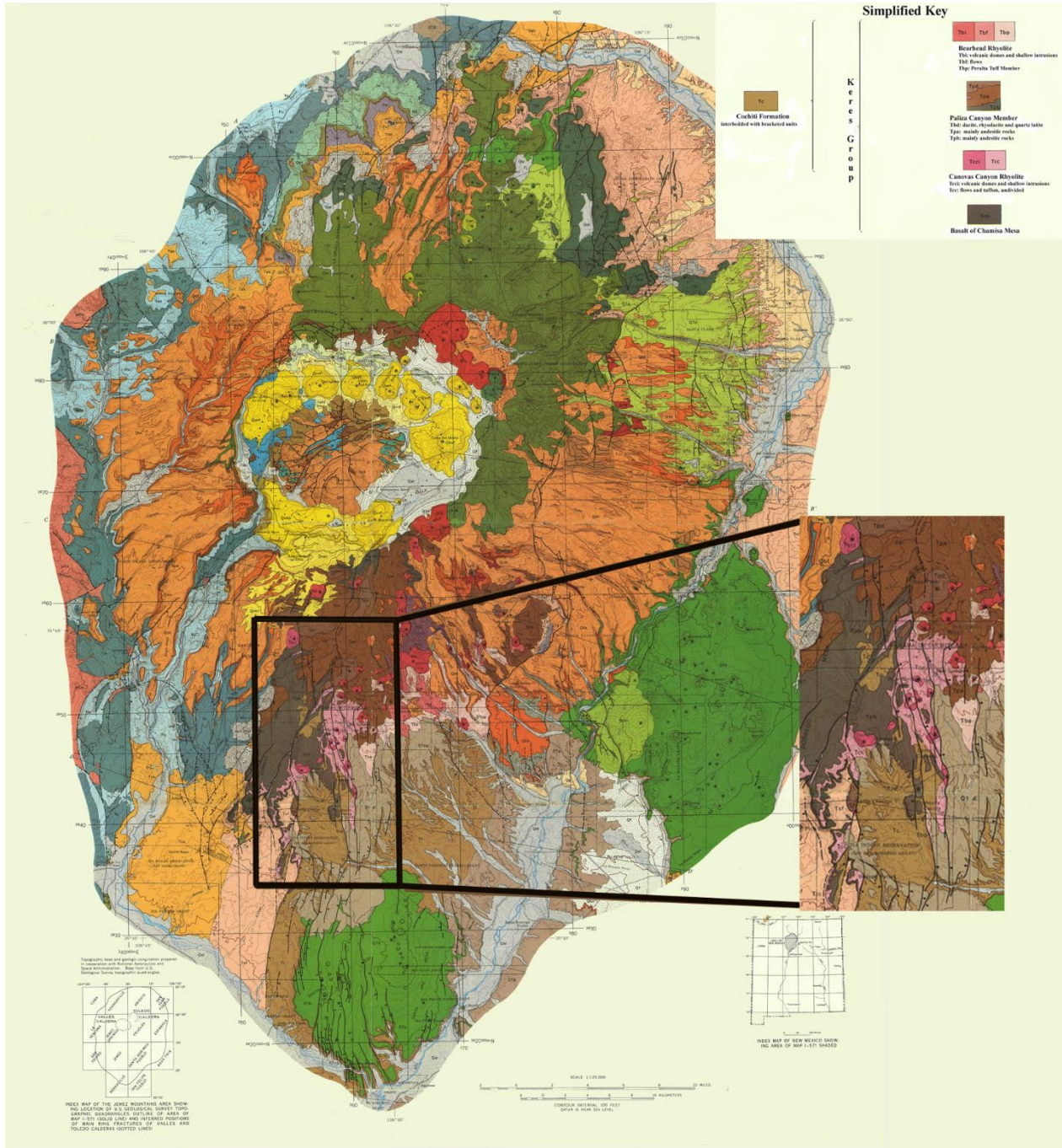
Figure 3.01. Geologic map of Smith, et al., 1970, with the field area inset.

Samples were named using the following convention: CC for Canovas Canyon, two or three letters denoting the area from which the samples were taken, and four digits denoting the

year of sampling and its chronological order in the individual field area (Table 3.01).
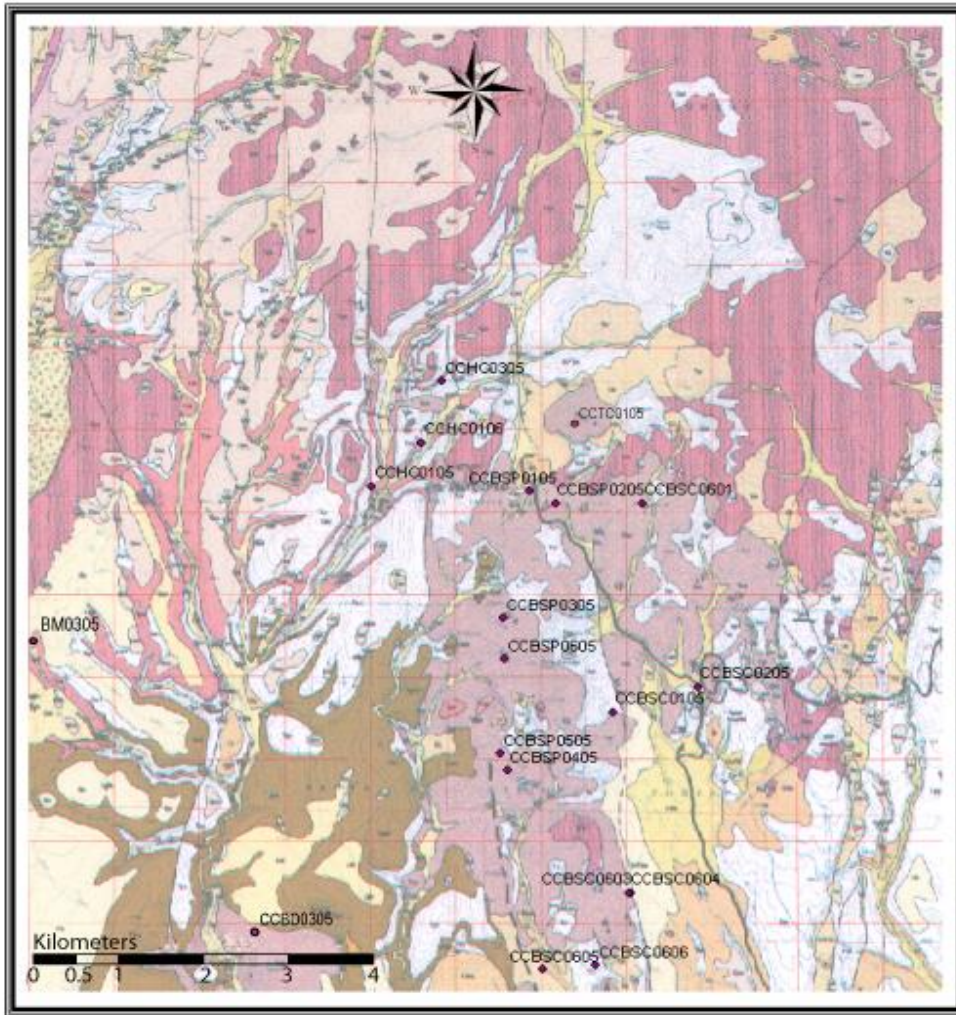
Canovas Canyon Rhyolite

Figure 3.02. Geologic map of the field area with sample names and locations (draft of map provided by Shari Kelley and Kirt Kemper of the New Mexico Bureau of Geology and Mines (NMBGM), modified from Smith, et al., 1970. The Valles Caldera lies to the north of the field area.

Sample abbreviation	Area sampled
BSP	Bear Springs Peak
BSC	Bear Springs Canyon
HC	Hondo Canyon
TC	Tres Cerros
BM	Borego Mesa
BD	Borego Dome

Table 3.01. Abbreviations for areas sampled. The abbreviations are incorporated into all

sample numbers.

CHAPTER 4

PREVIOUS WORK

Initial work was done on the Jemez during the early 1960's to early 1970's including identification of the Valles type resurgent caldera, creation of a detailed geologic map of the Jemez, along with a formalized stratigraphy, and paleomagnetism, geochemical and K/Ar analysis (Ross and Smith, 1961; Ross, et al., 1961; Smith, et al., 1961; Bailey, et al., 1969; Doell et al., 1968; Smith, et al., 1970). Whereas extensive research on syn- and post caldera rhyolites has been done, less is known about the earlier rhyolites such as the Canovas Canyon Rhyolite. The CCR has only been sampled as part of larger studies on the Keres Group itself, (Guilbeau, 1982; Gardner and Goff, 1984; Gardner, 1985). It has also been researched as part of studies on the development of volcanism in the Jemez, Justet (2003) or as part of studies of regional volcanism (Leudke and Smith, 1978).

4.1 Summary of Geochronological, Geochemical data and Modeling

K/Ar data from a Paliza Canyon Basalt which which was interbedded with the CCR indicated an age of 13.2 ± 3.3 to 6.74 ± 0.47 Ma (Gardner and Goff, 1984). Justet (2003), presented geochemistry and petrography on samples of the CCR. The range in $^{40}Ar/^{39}Ar$ dates include 9.3 ± 0.05 Ma to 6.86 ± 0.04 Ma. Gardner (1985) concluded that the CCR was likely the result of a partial melt of depleted source rock which had lower incompatible element

25

abundances than the local Precambrian granite. Both the Bearhead Rhyolite and the CCR appear to have evolved independently from other Keres Group rocks, possibly as melts of lower crustal granulite (Gardner and Goff, 1984). In contrast, the other Keres Group rock types: basalts, andesites, and dacites were most effectively modeled as the results of fractional crystallization with crustal contamination.

Guilbeau (1982) sampled the CCR and mapped volcanic domes of both the CCR and the Bearhead Rhyolite as part of a master's degree thesis. Based on the variation in $^{87}Sr/^{86}Sr$ isotope ratios as well as petrogenetic modeling, he concluded that the high silica rhyolites of the Keres Group (both the CCR and the Bearhead Rhyolite) were most likely unrelated to the intermediate and mafic rocks of the Paliza Canyon. Basalt fractionation could have produced the andesitic magmas, and fractional crystallization of the andesites could have produced the dacites, however, the CCR and Bearhead Rhyolite were not the products of that fractional crystallization trend. Rather, the rhyolites were more likely the result of melting of a depleted crustal source (Guilbeau, 1982).

Ellisor et al. (1996) concluded that all Keres Group volcanic rocks could be explained as having developed along one of three possible paths of Assimilation/Fractional Crystallization (AFC) of an OIB mantle-derived magma with between 12-20% crustal contamination with mafic lower crust, felsic lower crust and/or upper crust. Other workers have also concluded that in order to explain the array of isotope signatures and trace element chemistry found in the earliest rocks of the Keres Group, multiple crustal contaminants must have been involved (Rowe, et al., 2007).

CHAPTER 5

SAMPLING STRATEGIES AND ANALYTICAL METHODS

5.1 Sampling and sample preparation

Based on the geologic mapping of Bailey, et al. (1970) and more recent mapping by the

New Mexico Department of Mines and Minerals, samples from outcrops of Canovas Canyon

Rhyolite (CCR) domes and flows were collected during July 2005 and May, 2006. Single

samples were collected from flows and domes rather than tuffs with the exception of an isolated

outcrop in Hondo Canyon. This sampling strategy was chosen for two reasons. First, volcanic

tuffs are susceptible to weathering and alteration. Second, due to the distribution of tuffs over

much wider areas than either flows or plugs, it is difficult to accurately associate tuffs with their

vents. Volcanic breccias were not analyzed for this study. This research was focused on finding

the relationships between the various units of the CCR, rather than looking for heterogeneity in

the units themselves, therefore, the best sample from each unit was chosen for analysis, rather

than studying multiple samples from each unit.

Samples were cleaned of weathered surfaces and examined for suitability for analysis.

All samples showed some degree of alteration. Of the samples collected, the 16 which were least

altered were chosen for further study. Billets were cut from 15 of the samples and sent to

Spectrographics for thin section preparation. The thin section for one sample, BSP0105, was

prepared by hand by Alex Roy at UNLV. Based on an examination of the 16 thin sections, 15

samples were identified as being appropriate for major, trace and isotope geochemistry. Of these,

nine were deemed appropriate for geochronological analysis based on the presence of dateable

phenocrysts and degree of alteration.

To process samples for analyses, samples were broken by hand and pumiceous sample material and weathered surfaces were removed. These samples were then shattered into chips approximately 0.2 to 0.7 cm in size. Chips from each of these samples were selected for grinding. Each sample was powered in a tungsten carbide mill for three minutes. A tungsten carbide mortar and pestle were chosen instead of agate because of the hardness of some the samples. Approximately 10 grams of this material was then packed and shipped to the Peter Hooper GeoAnalytical Lab at Washington State University for trace element analysis using ICPMS, and 10 grams were sent to the Stable Isotope Geochemistry Lab at the University of Kentucky for isotope analysis. Powered sample was used for X-ray fluorescence analysis at UNLV for major and trace elements. The remainder of the crushed sample was used to hand pick mineral separates of plagioclase, biotite or sanidine for geochronology.

5.2 Petrography

Modal percentages of minerals were determined by point counting thin sections at 600 points per slide.

5.3 Loss on Ignition

Loss on Ignition (LOI) was determined by placing the samples in pre-weighed carbon crucibles, and heating them in a 110º C oven for 30 minutes. The crucibles were then cooled in a desiccating cabinet and reweighed to measure the amount of free moisture in the sample. The

reweighed crucibles were then heated for 2 hours at 900° C in and reweighed in order to measure the mass of moisture liberated from within minerals.

5.4 X-Ray Fluorescence for major and trace element geochemistry

X-Ray fluorescence (XRF) analyses were performed at the University of Nevada, Las Vegas, using a PANalytical Axios Advanced Sequential X-ray Fluorescence Spectrometer. After the samples had been analyzed for LOI, they were prepared in the following manner: For major element geochemistry, 30.00 grams of samples were mixed with tetraborate flux and fused at 1110° C for thirty minutes. The resulting fused bead was then polished on a disk grinder before being analyzed. For trace element geochemistry 12 grams of sample was added to 3 grams of powdered wax and agitated in a vial for three minutes. The sample-impregnated wax was then pressed into disks and analyzed.

5.5 ICP-MS Trace Elements

Approximately 10 grams of powdered sample was sent to the Peter Hooper GeoAnalytical Lab at Washington State University for ICP-MS (inductively coupled plasma mass spectrometry) to determine the trace element concentrations of REE (rare earth elements) and Ba, Rb, Y, Nb, Cs, Hf, Ta, Pb, Th Sr and Zr. The procedure used by the laboratory was done to ensure the removal of SiO_2 and B and to completely dissolve all minerals including resistant crystals such as garnet and zircon. Two grams of powdered sample were mixed with an equal amount of lithium tetraborate flux, and fused in a carbon crucible at 1000° C for 30 minutes. The

fusion bead was then powdered using an iron shatterbox, and 250 mg of the resulting powder

was dissolved on a hotplate in Teflon vial, at 110° C. The solution used to dissolve the powdered

bead consists of the following: 6 ml HF; 2 ml HNO_3; and 2 ml $HClO_4$. After heating, 3 mL

HNO_3, 8 drops H_2O_2, 5 drops of HF, and the In, Re and Ru in-house standards were added. The

mixture was diluted to a volume of 60 mL, resulting in a final dilution of 1:240. The instruments

used to analyze the samples included a Sciex Elan model 250 ICP-MS with a Babington

nebulizer, Brooks mass flow controllers and a water cooled spray chamber. In order to minimize

the formation of metal oxides, samples were introduced into the Ar plasma at a rate of 1.0 ml per

minute using a peristaltic pump and an automatic sampler, with plasma power at 1500 watts.

Multi element mode was used, where the time for analysis of each element totals 5 seconds (10

repeats of 0.5 seconds per element). Isotope selection for each of the elements was based on

relative abundances, and selected in order to minimize the potential for isobaric and oxide

interference (Knaak, et al., 1994). Precision and accuracy analysis were provided by the

Geoanalytical Lab at Washington State University and are included in Appendix B.

5.6 Thermal Ionization Mass Spectrometry

In order to determine the isotope ratios of Sr, Nd and Pb isotopes, approximately 10

grams of powdered sample was sent to the Isotope Geochemistry Lab at the University of Kansas

for thermal ionization spectrometry. Sm/Nd sample preparation uses a Teflon powder-HDEHP

column procedure (Patchett and Ruiz, 1987). High temperature dissolution in Krogh-type bombs

insures that refractory minerals are decomposed (Krogh, 1973). Nd data are referenced to La

Jolla standard $^{143}Nd/^{144}Nd = 0.511860$.

Samples for Rb/Sr geochemistry were dissolved using HF and HNO_3 acid in sealed Teflon dissolution vessels. Elemental separation is accomplished using HCl elution on cation exchange columns. Sr data are referenced to NBS-987 $^{87}Sr/^{86}Sr = 0.71025$. Sr data are normalized to $^{86}Sr/^{88}Sr = 0.1194$. U/Pb sample preparation was based on Krogh (1973, 1982). Pb data are normalized to NBS-981, $^{207}Pb/^{208}Pb = 0.91464$. TIMS analysis was done on a fully automated VG Sector variable 6-collector system, Daly multiplier and an ion counting system. Precision for Sr and Nd analysis was 20 ppm for Sr, and 10 ppm for Nd.

5.7 $^{40}Ar/^{39}Ar$ Geochronology

After crushing in a jaw crusher and sieving, 9 samples were found to contain adequate phenocrysts for $^{40}Ar/^{39}Ar$ dating. Mineral separates of sanidine, plagioclase and biotite were handpicked. All crystals which were used for single crystal laser analysis were washed in an ultrasonic bath of 5% HF for three minutes then rinsed with distilled water. Biotite and plagioclase crystals for furnace step heating were washed in an ultrasonic bath of acetone for three minutes. 30 mg of each sample were then packed for irradiation. Samples were wrapped in aluminum foil packets and stacked inside 6 mm (inside diameter) Pyrex tubes. The thicknesses of the packages averaged 3 mm. Every 5 – 10 mm along the tube, Fish Canyon Tuff sanidine crystals were placed as flux monitors. To correct for Ar produced by interfering nuclear reactions with potassium and calcium, K-glass and optical grade CaF_2 were irradiated along with the samples. The tubes were then loaded into aluminum containers and irradiated at the Oregon State University Radiation Center In-Core Irradiation Tube (ICIT) of the 1 MW TRIGA-type reactor.

For single crystal laser fusion analysis, the CaF_2 crystals, along with the samples, were then loaded into a copper sample tray which was placed in a high vacuum line and analyzed using a MAP – 215-50 Mass spectrometer. The samples were fused using a 20W CO_2 manually controlled laser. Each sample was fused for approximately 30 seconds. Crystals for fusion were positioned using a motorized sample stage and the samples were observed during fusion using a video camera. Samples which were analyzed using the furnace step heating method were placed in a double vacuum resistance furnace.

Reactive gases were removed from both laser fusion and furnace step heating samples prior to introduction into the mass spectrometer by using three GP-50 SAES getters. Sample gases were introduced into the mass spectrometer by expansion; 76% of the gas was admitted from furnace step heating, and 80% from laser fusion. A Balzers electron multiplier was used to determine peak intensities by peak hopping through seven cycles. Initial peak heights were determined by linear regression to the time of admission of the gas. In order to correct for discrimination of the mass spectrometer and monitor its sensitivity, atmospheric argon was sampled repeatedly during analysis. Atmospheric $^{40}Ar/^{36}Ar$ during this analysis was measured as $286.83 \pm 0.37\%$. A discrimination correction of 1.0325 (4 AMU) was applied to the measured Ar ratios. Sensitivity was measured as $\sim 6 \times 10^{-17}$ mol mV^{-1} with the multiplier operated at a gain of 36 over the Faraday. Laser fusion line blanks averaged 4.5 mV for mass 40 and 0.15 mV for mass 36. For furnace step heating, the line blanks averaged 23.4 mV for mass 40 and 0.10 mV for mass 36. Discrimination, line blanks and sensitivity remained stable throughout this analysis.

LabSPEC software written by B. Idelman (Lehigh University) was used for automation of the sample stage, laser, extraction line and mass spectrometer. LabSPEC software was also used for final data reduction and age calculations.

Measured $(^{40}Ar/^{39}Ar)_K$ values were 4.667 ($\pm$ 53.93%) x 10^{-3}. Ca correction factors were $(^{36}Ar/^{37}Ar)_{Ca}$ = 3.059 ($\pm$ 2.45%) x 10^{-4} and $(^{39}Ar/^{37}Ar)_{Ca}$ = 6.8823 ($\pm$ 1.84%) x 10^{-4}. J factors were determined by fusion of 4-8 individual crystals of neutron fluence monitors (K-glass and CaF_2 fragments). The reproducibility at each standard position was 0.04% to 0.6%, which indicated the absence of any significant flux gradient within packages. An age of 27.9 Ma was used for the Fish Canyon Tuff sanidine flux monitor in calculating ages for samples. Results of these analyses are listed in Appendix B.

CHAPTER 6

PETROGRAPHY

Canovas Canyon Rhyolite is highly variable petrographically, ranging from aphyric obsidian to porphyritic rhyolite. Most samples are sparsely porphyritic, containing <5% phenocrysts of quartz, plagioclase, biotite and sparse sanidine. Samples from Borrego Dome and Bear Springs Peak are distinctly porphyritic, containing ~15-20% phenocrysts of quartz, sanidine and biotite. Whole rock percentages for phenocrysts for all samples are included in Table 6.01. Phenocrysts are presented in modal abundance in Table 8.02.

6.1 Bear Springs Canyon

BSC0605 contains glomerocrysts of biotite and plagioclase with occasional sanidine overgrowths. It contains 19.2% phenocrysts in altered groundmass of plagioclase microliths. Phenocrysts include sanidine, quartz, plagioclase and biotite. Plagioclase forms glomerocrysts, and sanidine is euhedral to subhedral, occasionally embayed, and up to 3 mm in length. Biotite is light to reddish brown, tabular, and up to 1 mm. Quartz is sub to euhedral, and up to 2 mm in length. Sanidine is tabular, 0.02 to 0.30 mm, some with oscillatory zoning. Biotite is reddish brown in thin section, bronze in hand specimen. There appeared to be two populations of biotite, the first consisted of small phenocrysts, from 0.01 to 0.05 mm in size, and the second population consisted of crystals from 0.5 to 2 mm crystals. Plagioclase is extensively altered, and is from 0.01 to 0.02 mm in size, quartz is sub- to euhedral.

34
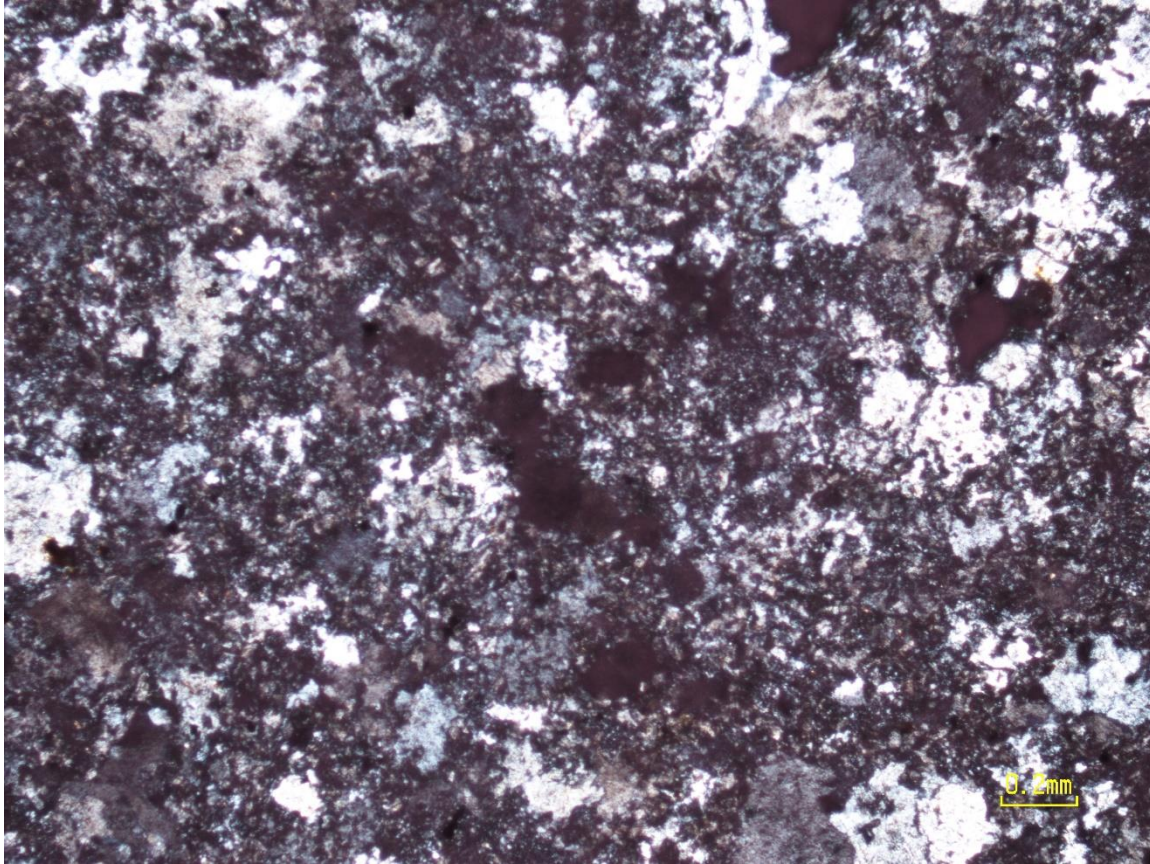
Figure 6.01. Sample CCHC0305 40X's magnification, crossed Nichols showing silicification.

CCBSC0601 is perlitic and aphyric. CCBSC0602, sampled from a nearby dome, is nearly aphyric, CCBSC0105 is aphyric as well. CCHC0305 is an aphyric tuff with less than 0.1% phenocrysts. This sample appears to be nearly completely silicified, (Figure 6.01) Biotite shows bird's eye extinction. CCBSC0606 (Figure 6.02) shows magma flow banding in thin section.
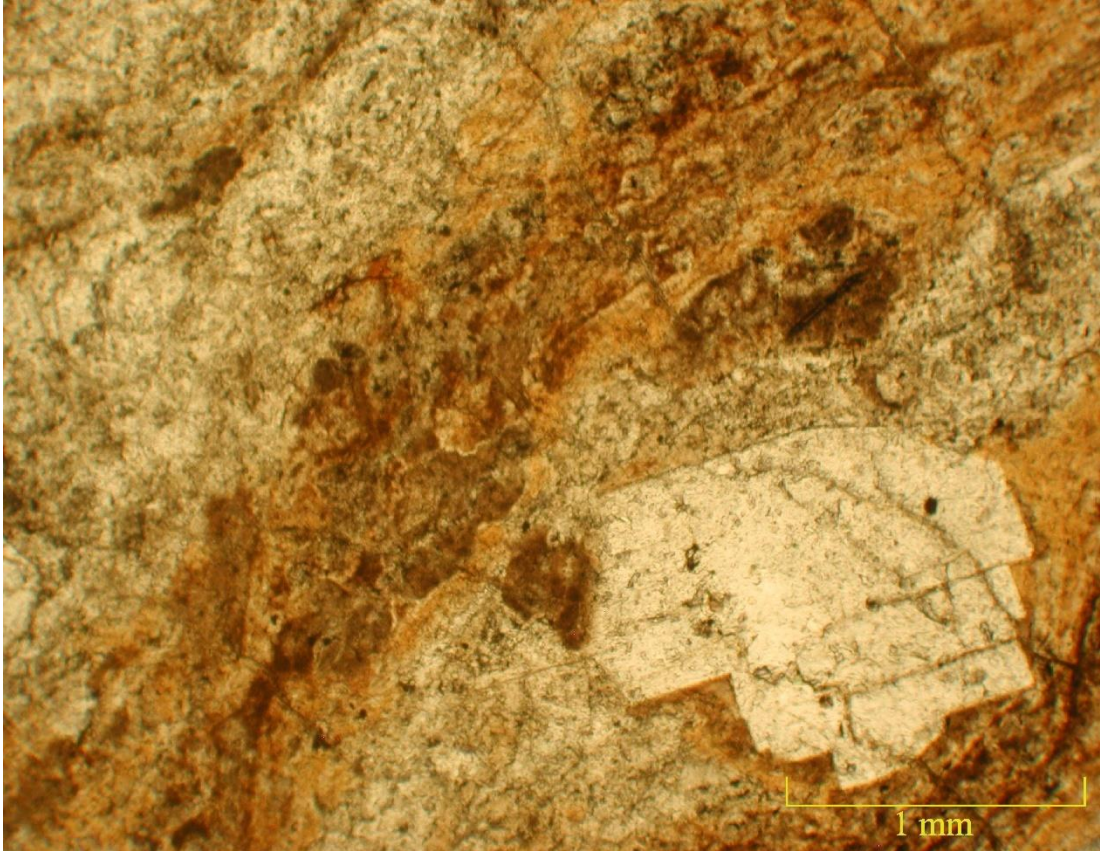
Figure 6.02. CCBSC0606 100X magnification. Plagioclase phenocryst is in the lower right hand corner. Flow banding is evident.

6.2 Bear Springs Peak

The biotite in sample CCBSP0105 is needle-like and skeletal, and is up to 1 mm in length. The sample also contains clinopyroxne glomerocrysts, up to 3 mm in size. Quartz is rounded, and up to 0.5 mm, sanidine up to 0.7 mm, and plagioclase which is tabular, is up to 0.5 mm on size. CCBSP0405 is flowbanded and contains mantled plagioclase (Figure 6.03). Plagioclase shows oscillatory zoning and some sanidines are zoned, with heavily resorbed cores. Quartz is rounded.
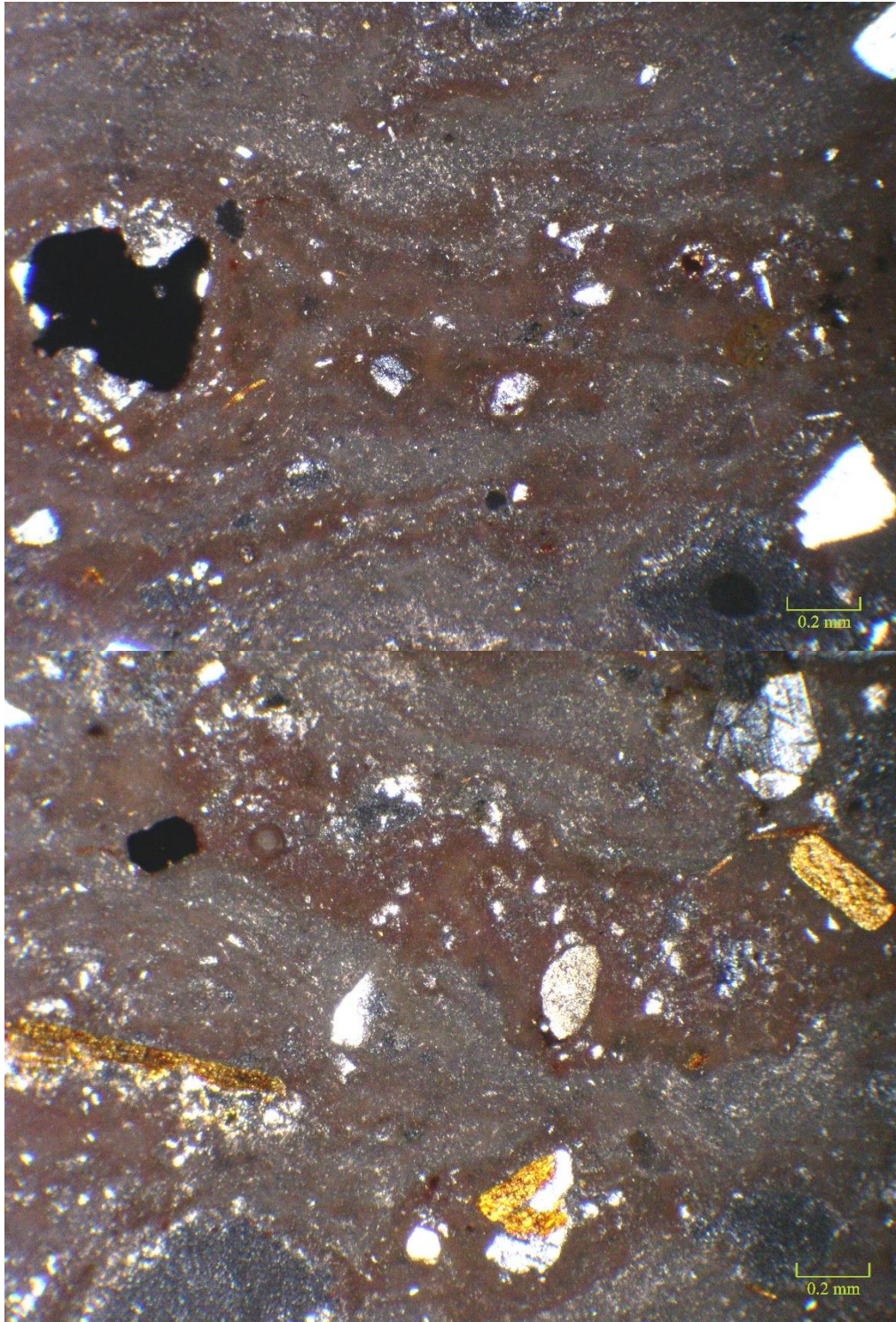
Figure 6.03 a. and b. CCBSP0405, showing flow banding. Plane polarized light, with crossed Nichols, 40X magnification. Large phenocryst at left in figure a is a mantled plagioclase.

6.3 Borrego Dome

Sample BD0205 from Borrego Dome contains 22.8% phenocrysts consisting of plagioclase, sanidine, quartz, biotite and hornblende in an extensively altered groundmass. Plagioclase is blocky and tabular, with albite twinning, some resorbed and embayed, often as glomerocysts. Tabular sanidine is pitted along cleavage, 1 to 1.5 mm in length, rounded to euhedral. Approximately 1/3 of sanidines exhibit zoning. Occasional sanidine is also found with anti-rapikivi texture. Hornblende, up to 0.5 mm in length, is brownish green, fractured, and resorbed. One population of biotite is skeletal, and reddish brown. It occurs as 0.5 - 0.75 mm lathes, occasionally completely replaced by oxides. Other biotite phenocrysts are light to dark brown, hexagonal, and exhibit birdseye extinction and high interference colors.

6.4 Borrego Mesa

BM0305, from Borrego Mesa, was the westernmost sample collected in this study. It contained 7.3% phenocrysts comprised of plagioclase, sanidine, and rare quartz, set in a groundmass of plagioclase microliths. Plagioclase phenocrysts are up to 1.5 mm in length, some resorbed and embayed. Sanidine, 1 to 1.5 mm, is subangular and pitted along cleavage. Biotite forms two populations, one of which is pseudo-hexagonal, light to dark brown and tabular. The second is skeletal, and partially to nearly completely replaced with oxides.
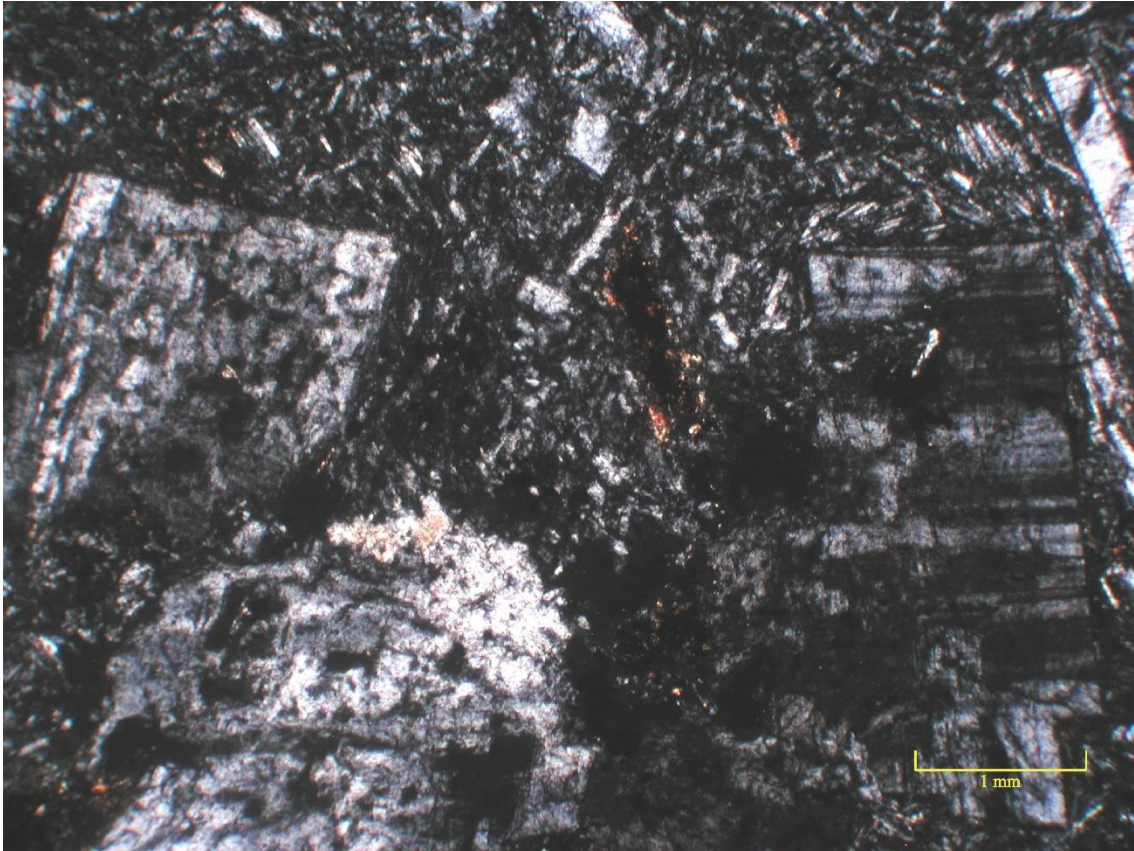
Figure 6.04. Borego Mesa. Plagioclase at right exhibits rolling extinction. 100 X magnification.

6.5 Hondo Canyon

Sample HC0105 is flow banded, with a brown glassy groundmass. About 25% of the groundmass consisted of plagioclase and other mineral microlites. Quartz is 0.005- 0.01 mm, and subhedral. Plagioclase is up to 2 mm in length, with albite law twinning. Plagioclase has heavily resorbed cores zoned, subhedral to euhedral, with occasional anti-rapikivi texture.

Sample HC0106 is a sedimentary rock apparently sourced from volcanic rocks. It was sent to Shari Kelley at the New Mexico School of mines to be used in updating geological mapping of the area.

Sample HC0305 has a devitrified groundmass of plagioclase microlites which, in plane

polarized light, appears to have a leopard spotted pattern of alteration. The sample contains filled

vesicles, sphericules, oxide staining, and is aphyric.
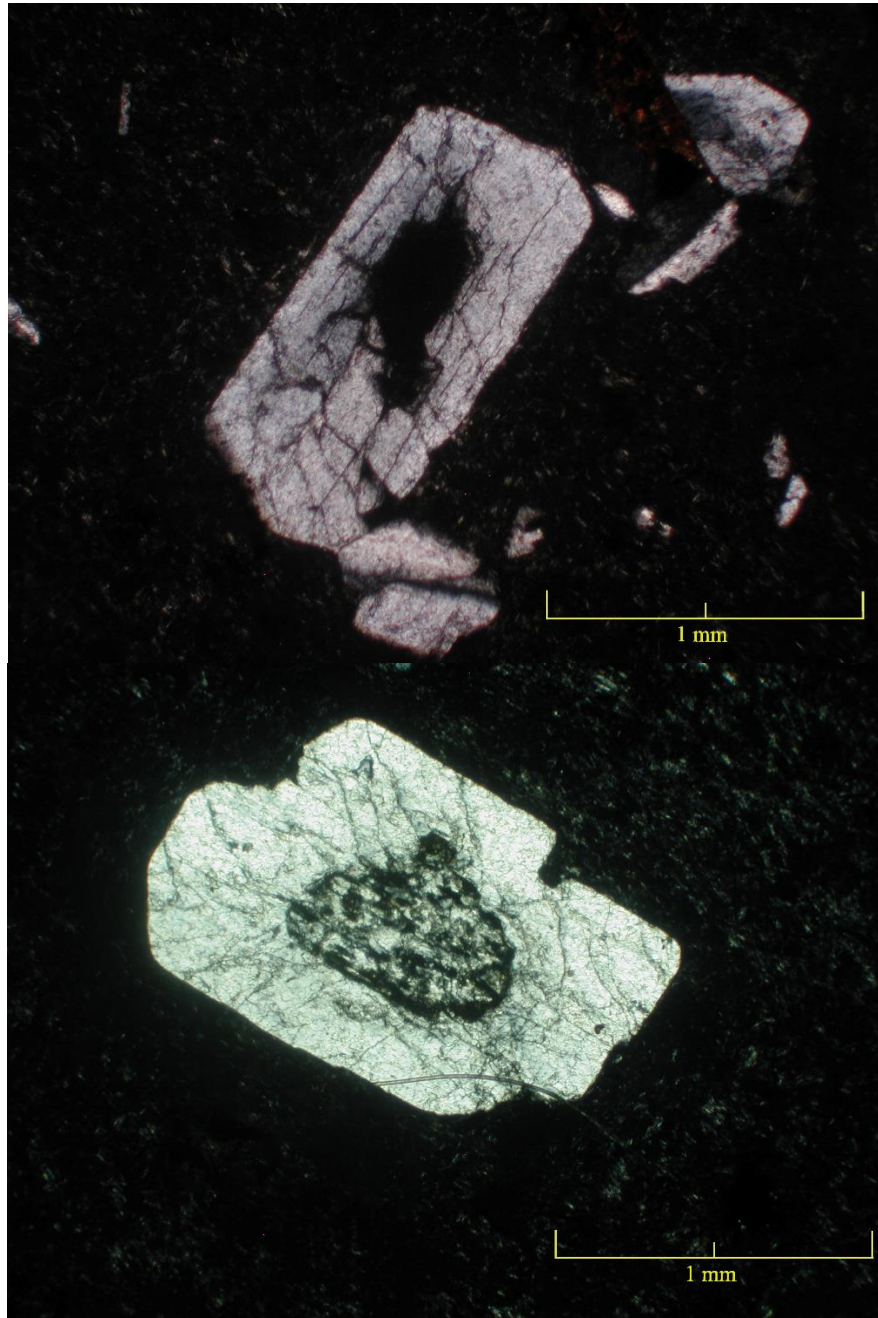
Figure 6.05 a. and b. Two plagioclase phenocrysts with resorbed cores from sample HC0105. 100 X magnification, under plane polarized light with crossed Nichols. Plagioclase in upper right hand corner of a exhibits rolling extinction.

6.6 Tres Cerros

Sample TC0105 contained 18.9% phenocrysts. The groundmass consisted of seritized plagioclase microlites. Plagioclase and sanidine phenocrysts are intergrown, and some sanidine is embayed. Quartz is sub- to euhedral. Biotite is light to reddish brown and tabular.

All of the samples displayed evidence of some alteration, although a few of them had been extensively altered. Two of the samples cut for thin sections show evidence of hydrothermal alteration: BSC0602 which appears to have been extensively silicified and BD0205 which appears to have been sericitized. BSC0604 is spherulitic.

Sample #	Plagioclase	Sanidine	Quartz	Horn-blende	Biotite	oxides	OPX	Matrix	TOTAL
BM0305	1.0%	1.3%	0.2%	0.0%	2.7%	2.1%	0.0%	92.8%	100.1%
CCBD0205	4.7%	12.8%	1.2%	0.5%	3.6%	0.0%	0.0%	77.2%	100.0%
CCBSC0105	5.1%	0.0%	0.0%	0.0%	0.0%	0.0%	0.0%	94.7%	99.8%
CCBSC0205	0.5%	2.5%	0.0%	0.0%	1.5%	0.0%	0.0%	95.4%	99.9%
CCBSC0601	0.0%	0.0%	0.0%	0.0%	0.0%	0.0%	0.0%	100.0%	100.0%
CCBSC0602	0.0%	0.0%	0.0%	0.0%	0.0%	0.0%	0.0%	100.0%	100.0%
CCBSC0604	0.0%	0.0%	0.0%	0.0%	0.0%	0.0%	0.0%	99.0%	99.0%
CCBSC0605	0.8%	3.4%	0.2%	0.0%	1.4%	0.0%	0.0%	94.0%	99.8%
CCBSP0405	6.4%	2.0%	3.3%	0.0%	2.2%	0.0%	0.0%	86.3%	100.2%
CCBSP0105	0.3%	1.3%	0.3%	0.0%	1.0%	0.0%	0.8%	96.2%	99.9%
CCBSP0205	0.0%	1.1%	0.0%	0.0%	0.3%	0.0%	0.0%	98.5%	99.9%
CCBSP0505	3.5%	7.6%	0.2%	0.0%	1.5%	0.0%	0.0%	87.0%	99.8%
CCHC0105	0.1%	2.5%	0.4%	0.0%	0.5%	0.0%	0.0%	97.1%	99.8%
CCHC0106	0.0%	0.0%	0.0%	0.0%	0.0%	0.0%	0.0%	96.5%	100.0%
CCHC0305	0.0%	0.0%	0.0%	0.0%	0.0%	0.0%	0.0%	100%	100%
CCTC0105	1.5%	10.8%	5.1%	0.0%	1.5%	0.0%	0.0%	100.0%	100.0%

Table 6.01. Point counting thin sections results.

Sample #	Plagioclase	Sanidine	Quartz	Horn-blende	Biotite	oxides	OPX	Total
BM0305	13.7%	17.8%	2.7%	0.0%	37.0%	28.8%	0.0%	100%
CCBD0205	20.6%	56.1%	5.3%	2.2%	15.8%	0.0%	0.0%	100%
CCBSC0105	100.0%	0.0%	0.0%	0.0%	0.0%	0.0%	0.0%	100%
CCBSC0205	11.1%	55.6%	0.0%	0.0%	33.3%	0.0%	0.0%	100%
CCBSC0601	---	---	---	---	---	---	---	---
CCBSC0602	---	---	---	---	---	---	---	---
CCBSC0604	---	---	---	---	---	---	---	---
CCBSC0605	13.8%	58.6%	3.4%	0.0%	24.1%	0.0%	0.0%	100%
CCBSP0405	46.0%	14.4%	23.7%	0.0%	15.8%	0.0%	0.0%	100%
CCBSP0105	8.1%	35.1%	8.1%	0.0%	27.0%	0.0%	21.6%	100%
CCBSP0205	0.0%	78.6%	0.0%	0.0%	21.4%	0.0%	0.0%	100%
CCBSP0505	27.3%	59.4%	1.6%	0.0%	11.7%	0.0%	0.0%	100%
CCBSC0606	29.6%	22.2%	11.1%	0.0%	37.0%	0.0%	0.0%	100%
CCHC0105	2.9%	71.4%	11.4%	0.0%	14.3%	0.0%	0.0%	100%
CCHC0106	---	---	---	---	---	---	---	---
CCHC0305	---	---	---	---	---	---	---	---
CCTC0105	7.9%	57.1%	27.0%	0.0%	7.9%	0.0%	0.0%	100 %

Table 6.02. Modal percentages of phenocrysts.

CHAPTER 7

GEOCHRONOLOGY RESULTS

A total of nine samples were chosen for geochronology, based on the presence of

phenocrysts suitable for ^{40}Ar/^{39}Ar analysis. Individual plagioclase and sanidine crystals were

laser fused, with the exception of one plagioclase and one biotite sample which were analyzed

using conventional furnace step heating. The results are summarized in Table 7.01

7.1 CCBSC0602 Plagioclase

The results of furnace step heating analysis yielded a very discordant age spectrum, with

ages generally decreasing as more gas was released. During the first step, when the sample was

heated to 650 °C, 44% of the total ^{39}Ar was released, as shown in Figure 7.01. The Ca/K values

increased during the first 3 steps and then stabilized at steps 9 through 10. The Ca/K values,

particularly during the first heating step, are not representative of plagioclase. The generally low

radiogenic yield, Ca/K values in the initial steps as well as the disproportionate amount of argon

released initially suggest that this sample is altered, impure, and/or contains excess argon.
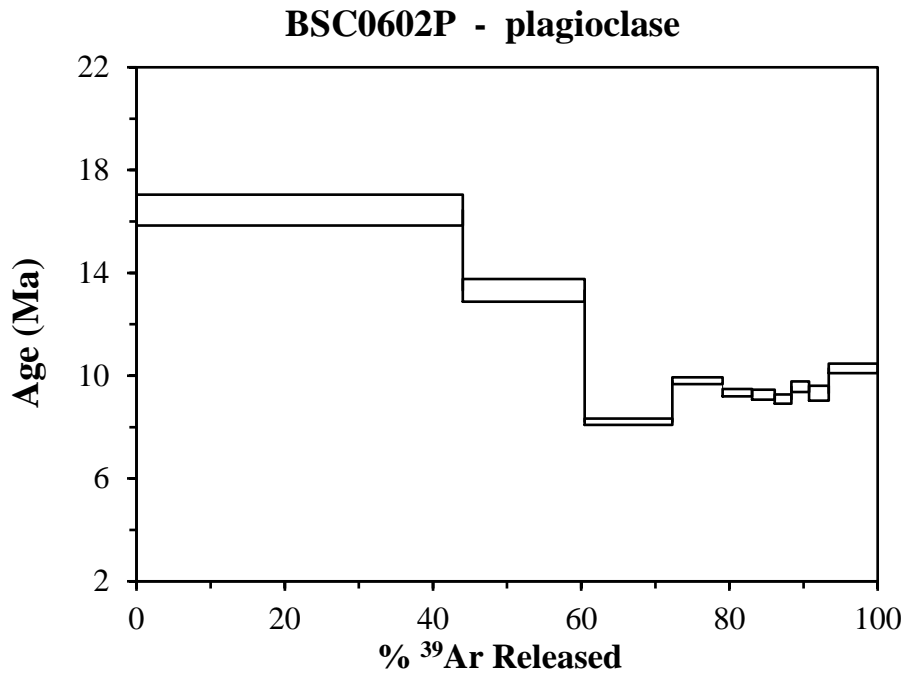
Figure 7.01. Age spectrum for Sample CCBSC0602, furnace step heating. Note the large amount of ^{39}Ar released during the initial three steps, especially the first.
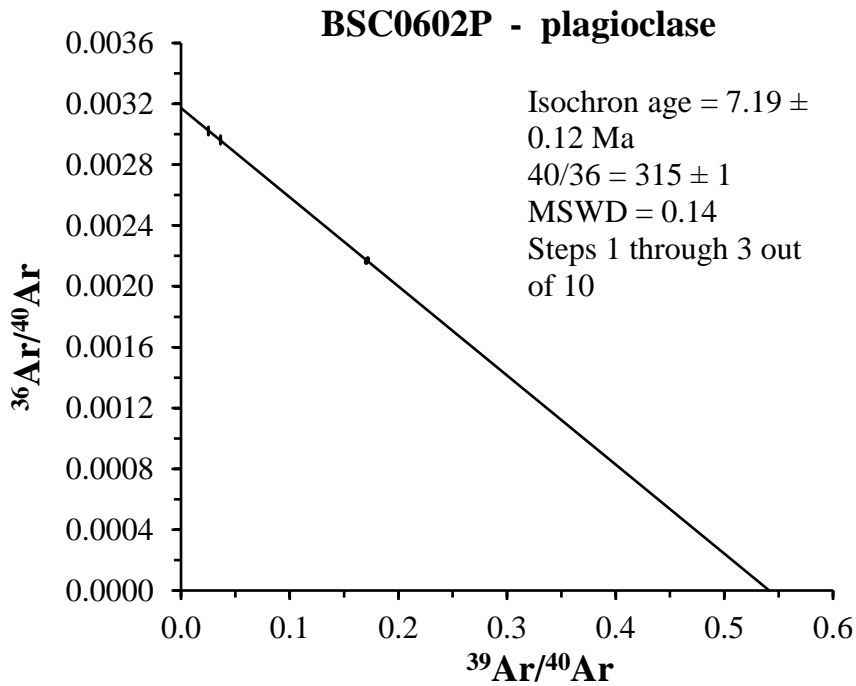
Figure 7.02. Isochron for Sample CCBSC0602, furnace step heating. This is a three point isochron which can not be considered reliable.

While there is no plateau age defined for this sample, an isochron age is defined the first 3 steps (Figure 7.02). Because two of the three points are very close together, it is not considered reliable. The isochron is also considered unreliable since the three points because they represent the first 3 steps, which yielded anomalous Ca/K.

The total gas age is 13.1 ± 0.2 Ma, which is suspect because of the aforementioned issues. The isochron suggests excess argon ($^{40}Ar/^{36}Ar = 315 \pm 1$) as does the discordant age spectrum. The most reliable age for this sample would be based on using the minimum age on the age spectrum as the maximum age for the sample, which would be <8.2 Ma.

7.2 CCBSC0605 Biotite

This sample was also analyzed using furnace step heating analysis. It produced a moderately discordant age spectrum with no plateau defined and a total gas age of 13.1 ± 0.2 Ma. While an isochron is defined by steps 5-8 (48% of the total ^{39}Ar released), the 4 points are very close to each other, resulting in a less reliable line fit (Figures 7.03 and 7.04). $^{40}Ar/^{36}Ar$ is unrealistically low; 234, compared to standard atmospheric argon (295.5), indicating an unreliable isochron. The spectrum data yielded anomalously old ages in the first two steps, which may be the result of ^{39}Ar recoil during irradiation which would leave the margins of the biotite depleted in ^{39}Ar. The data from the two initial heating steps for this sample should be omitted based on this. The most reliable result for the age of this sample would be from taking the average of steps 3-12, which is 9.47 ± 0.16 Ma.
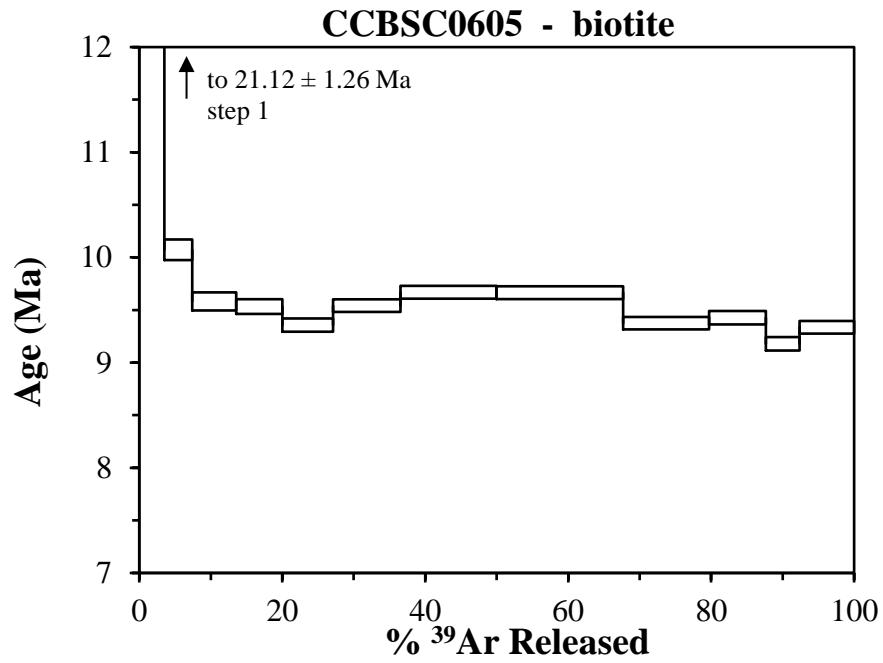
Figure 7.03. Age spectrum for Sample CCBSC0605, biotite furnace step heating. There is no plateau defined.
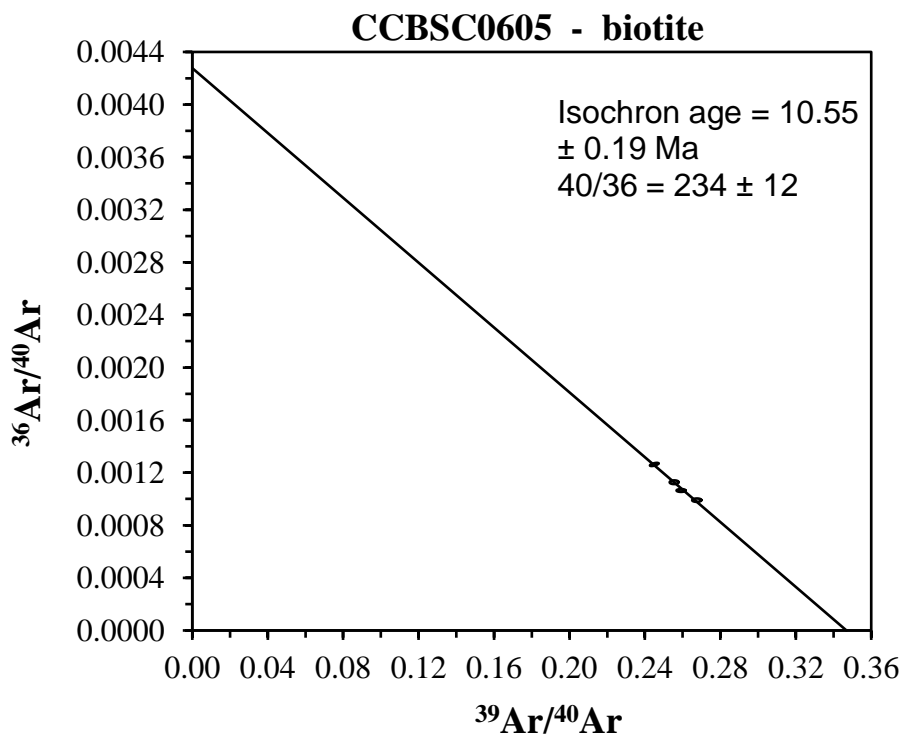
Figure 7.04. Four point isochron for sample CCBSC0605, biotite. Due to the similarity of the data points, this is not considered a reliable isochron.

7.3 CCTC0105 Sanidine

This sample was analyzed using single crystal laser fusion analysis. Eleven analyses yielded ages which were indistinguishable within analytical uncertainty, with a mean age of 6.26 ± 0.03 Ma. Since all analyses were indistinguishable in age, none were rejected as outliers. Thus, a weighted mean age can be calculated on all 11 analyses which results in an identical age of 6.26 ± 0.01 Ma. Nine out of the 11 analyses define a statistically valid isochron age of 6.27 ± 0.02 Ma and indicates that no significant excess argon is present ($^{40}Ar^{/36}Ar = 304 \pm 13$; within uncertainty of atmospheric argon). The most reliable age for this sample would be the isochron age.

7.4 CCHC0105 Plagioclase

This sample was analyzed using single crystal laser fusion, producing data which ranged in age from ~5.1 Ma to ~14 Ma. The high Ca/K ratios are indicative of plagioclase. Of the data points, five were rejected by using the weighted mean method for rejecting outliers based on the MSWD of the population, yielding a weighted mean age of 12.4 ± 0.6 Ma. The younger analyses which were rejected had radiogenic yield ($\%^{40}Ar*$), possibly indicating that these crystals were altered. While four of the analyses did define an isochron, it is not reliable. Since two of the data points are nearly coincident, it is actually a 3-point isochron. The initial $^{40}Ar/^{36}Ar$ of 266 ± 23 is well below the atmospheric value of 295.5. Although the isochron age is within uncertainty of the mean age (11.4 ± 3.3 Ma), the weighted mean age of 12.4 ± 0.6 Ma is likely the most reliable age, due to rejection of the younger, lower $\%^{40}Ar*$ analyses.

7.5 CCBSP0405 Plagioclase/Sanidine

The analysis of this sample using single crystal laser fusion produced data from individual crystals which appear to be either sanidine or plagioclase, which are identified by the Ca/K ratio; Ca/K <1 indicates sanidine, and Ca/K > 1 indicates plagioclase. Combining the two sets of data into one data set yields a mean age of 12.0 ± 3.3 Ma. Weighted mean analysis would reject 7 of the 12 analyses, with the remaining 5 analysis defining a weighted mean age of 9.97 ± 0.11 Ma. Isochron analysis rejects 5 analyses, with the remaining 7 defining an isochron age of 9.32 ± 0.11 Ma. Isochron analysis would indicate an initial argon with $^{40}Ar/^{36}Ar = 314.6 ± 4.7$, thus indicating that these crystals contain excess argon. Since both sanidine and plagioclase analyses fall on this isochron, it suggests that these minerals both crystallized together in the presence of excess argon. The plagioclase ages appear, on average, to be older than the sanidine

but this could be the result of by excess argon. Since plagioclase has a lower radiogenic yield, it will be more affected by the excess argon in terms of anomalously old ages calculated. The isochron age is considered the most reliable for this sample.

7.6 BM0305 Plagioclase

The single crystal laser fusion analysis of this sample produced ages from ~8.9 Ma to ~13.7 Ma, with a mean age is 10.2 ± 1.3 Ma. Weighted mean analysis rejects 4 analyses, with the remaining 6 defining an age of 9.52 ± 0.12 Ma. An isochron is defined by 8 of the analyses, and yields an age of 9.21 ± 0.22 Ma indicating a small amount of excess argon is present with $^{40}Ar/^{36}Ar = 305 \pm 5$. Because the data are spread out along the isochron, both the age and initial argon isotopic composition is well defined, making the isochron age the most reliable for this sample.

7.7 BSP0105 Plagioclase

Single crystal laser fusion analysis produced ages which ranged from ~7.8 Ma to ~19.3 Ma, with a mean of 12.6 ± 2.8 Ma. Weighted mean analysis rejects 5 analyses, with the remaining 5 defining an age of 11.7 ± 0.3 Ma. An isochron is defined by 7 of the analyses, yielding an age of 7.6 ± 1.0 Ma. Excess argon is present since $^{40}Ar/^{36}Ar = 484 \pm 55$. As a result of the very small amounts of gas released, the individual data points have large uncertainties. Therefor, even though the isochron is statistically valid, the line itself as well as the age and initial argon composition are poorly constrained, and so the isochron itself can not be considered

reliable. The weighted mean age is the only useful method to use for this sample, however, the sample itself is of low reliability.

7.8 CCBD0205 Sanidine

Single crystal laser fusion produced data which ranged from ~9.6 Ma to 10.3 Ma, with a mean age of 9.92 ± 0.19 Ma. By using weighted mean analysis, 1 data point is rejected, with the remaining 8 defining an age of 9.87 ± 0.07 Ma. Seven of the analyses define an isochron, yielding an age of 9.88 ± 0.07 Ma, with no excess argon present ($^{40}Ar/^{36}Ar = 296 \pm 8$). The ages all overlap within uncertainty, indicating a highly reliable result. In this case, the most reliable age is the isochron age.

7.9 CCBSC0606 Plagioclase

Single crystal laser fusion analysis was used for this sample which produced data rang in age from ~7.9 Ma to ~13.3 Ma, with a mean age of 10.6 ± 1.4 Ma. Three data points are rejected by weighted mean analysis, with the remaining five defining an age of 10.16 ± 0.30 Ma. No reliable isochron is defined by these data, and the weighted mean age is the only useful result. In this case, the weighted mean approach appears to have successfully removed outliers. Three of the older and younger analyses were rejected, leaving the coherent population of 5 analyses at 10.16 Ma, see Figure 6.05. This sample result should be considered only moderately reliable.

CCBSC0606 - plagioclase

Mean = 10.16 ± 0.3 Ma
[5.8%] 95% conf.
Wtd by data-pt errs only, 0 of 5 rej.
MSWD = 2.3,
probability = 0.055
5 crystals out of 8
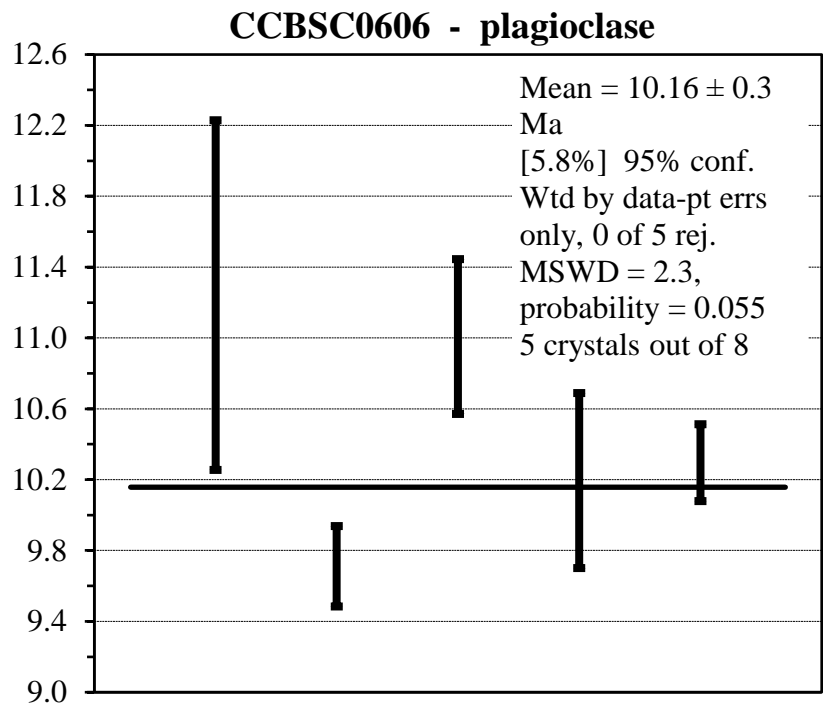
Figure 7.05. Weighted mean age for sample CCBSC0606.

Sample ID	^{40}Ar/^{39}Ar (ma ±2σ) Laser Fusion			^{40}Ar/^{39}Ar (ma ±2σ) Furnace Step Heat		
	Mean	Weighted Mean	Isochron	Total Gas	Plateau	Isochron
CCTC0105 (Sanidine)	6.26 ± 0.03	6.26 ± 0.01	**6.27 ± 0.02**			
BM0305	10.2 ± 1.3	9.5390 ± 0.0640	**9.21 ± 0.22**			
CCBSC0602	**Minimum age on age spectra = maximum age for sample. Sample is <8.2 Ma**			13.1 ± 0.2	NO RESULT	7.19 ± 0.12
CCBSC0605 (Biotite)	**Average of steps 3-12: 9.47 ± 0.16**			9.93 ± 0.04	NO RESULT	10.55 ± 0.19
CCBD0205	9.92 ± 0.19	9.87 ± 0.07	**9.88 ± 0.07***			
CCBSC0606 (plagioclase)	10.6 ± 1.4	**10.16 ± 0.30***	NO RESULT			
CCBSP0405	12.0 ± 3.3	9.97 ± 0.11	**9.32 ± 0.11**			
CCHC0105	11.4 ± 3.3	**12.4 ± 0.6**	NO RESULT			
CCBSP0105	12.49 ± 3.09	11.7 ± 0.3	7.6 ± 1.0			

Table 7.01. Summary of ^{40}Ar/^{39}Ar geochronology results. Data in bold typeface indicates most reliable result for each sample.

CHAPTER 8

GEOCHEMISTRY

Sixteen samples were chosen for geochemical analysis. Sample preparation was

described in Chapter 5. Loss on Ignition results are presented in Table 8.01. Unbound water

ranged from 0.20 percent to 0.86 weight percent. Water bound in minerals ranged from 0.11

percent to 3.81 weight percent. The sample with the greatest mass of volatiles released from

minerals was CCBSC0601, which also showed extensive alteration in thin section.

8.01 Major Element Chemistry and Classification and Loss on Ignition

Sample #	unbound H_2O	Bound H_2O
BM0305	0.39%	0.43%
CCBD0205	0.22%	0.22%
CCBSC0105	0.31%	0.30%
CCBSC0205	0.81%	2.84%
CCBSC0601	0.47%	3.81%
CCBSC0602	0.24%	0.77%
CCBSC0604	0.26%	0.30%
CCBSC0605	0.20%	0.11%
CCBSC0606	0.46%	1.57%
CCBSP0105	0.28%	0.43%
CCBSP0305	0.38%	0.51%
CCBSP0405	0.86%	0.49%
CCBSP0505	0.44%	2.85%
CCHC0105	0.41%	0.50%
CCHC0305	0.32%	0.29%
CCTC0105	0.24%	1.12%

Table 8.01. Loss on ignition for all tested samples, also in weight percent.

All major elements are normalized to 100% volatile free and are used to classify the type of igneous rock after LeBas, et al., (1986) Figure 8.01 illustrates the classification of the CCR. All samples analyzed in this study are rhyolites, (>69 % SiO_2), with the exception of BM0305, a trachydacite, with a SiO_2 content of 67.3%. All other samples are classified as rhyolites, with between 70.9 to >78% SiO_2, with most samples containing between ~73% to 78% SiO_2. Sample CCBSC0205 has an SiO_2 content of 70.9% and CCBSC0604 has an SiO_2 content in excess of 78.0%, indicating alteration. Major and trace element data is listed in Appendix C.
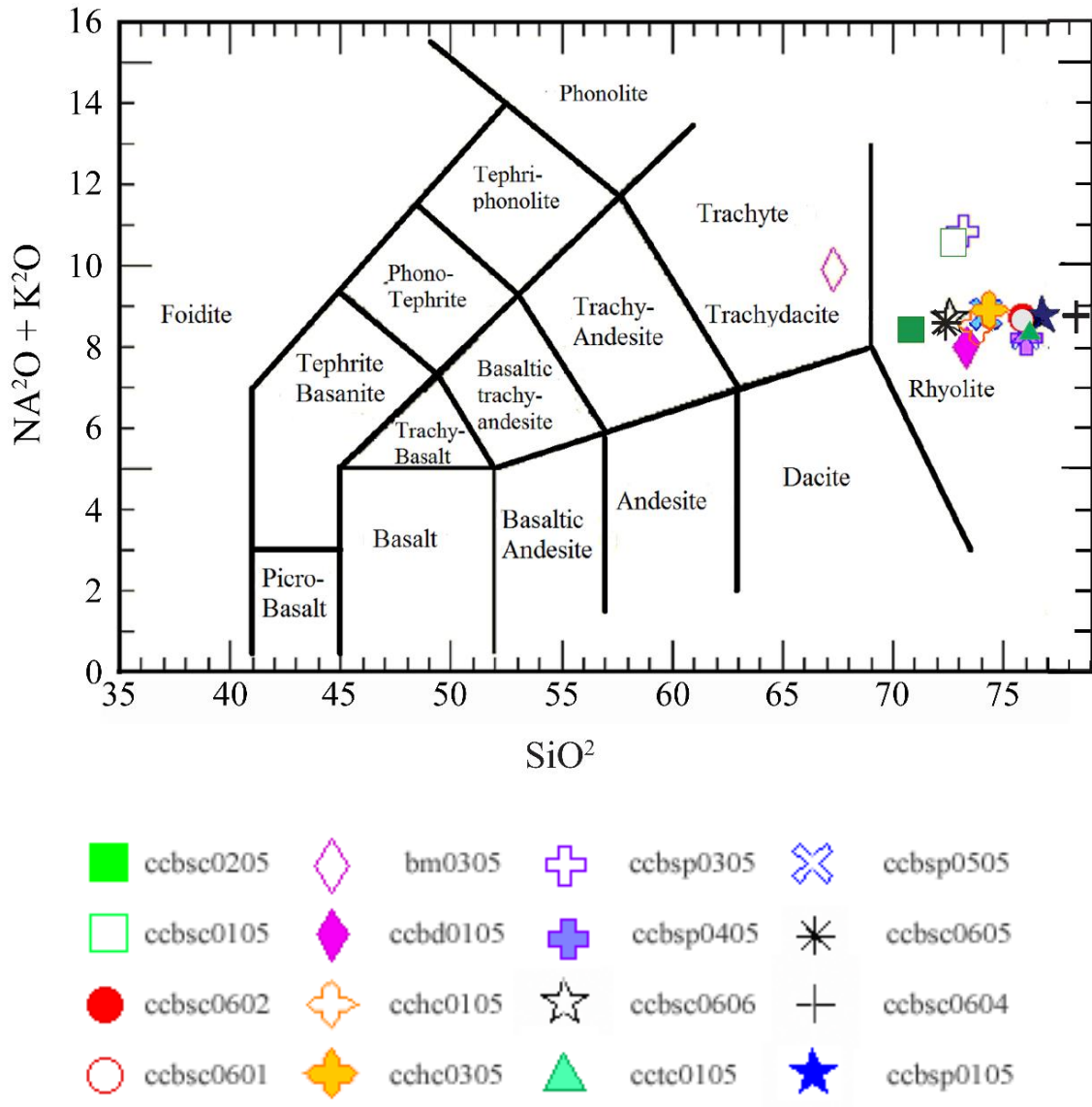
Figure 8.01. Classification based on total alkalis vs. SiO$_2$ (after LeBas et al., 1986), with sample number/symbol key. Major elements are normalized to 100% anhydrous and expressed as weight %. All samples are classified as rhyolite, with the exception of BM0305, which is a trachydacite.
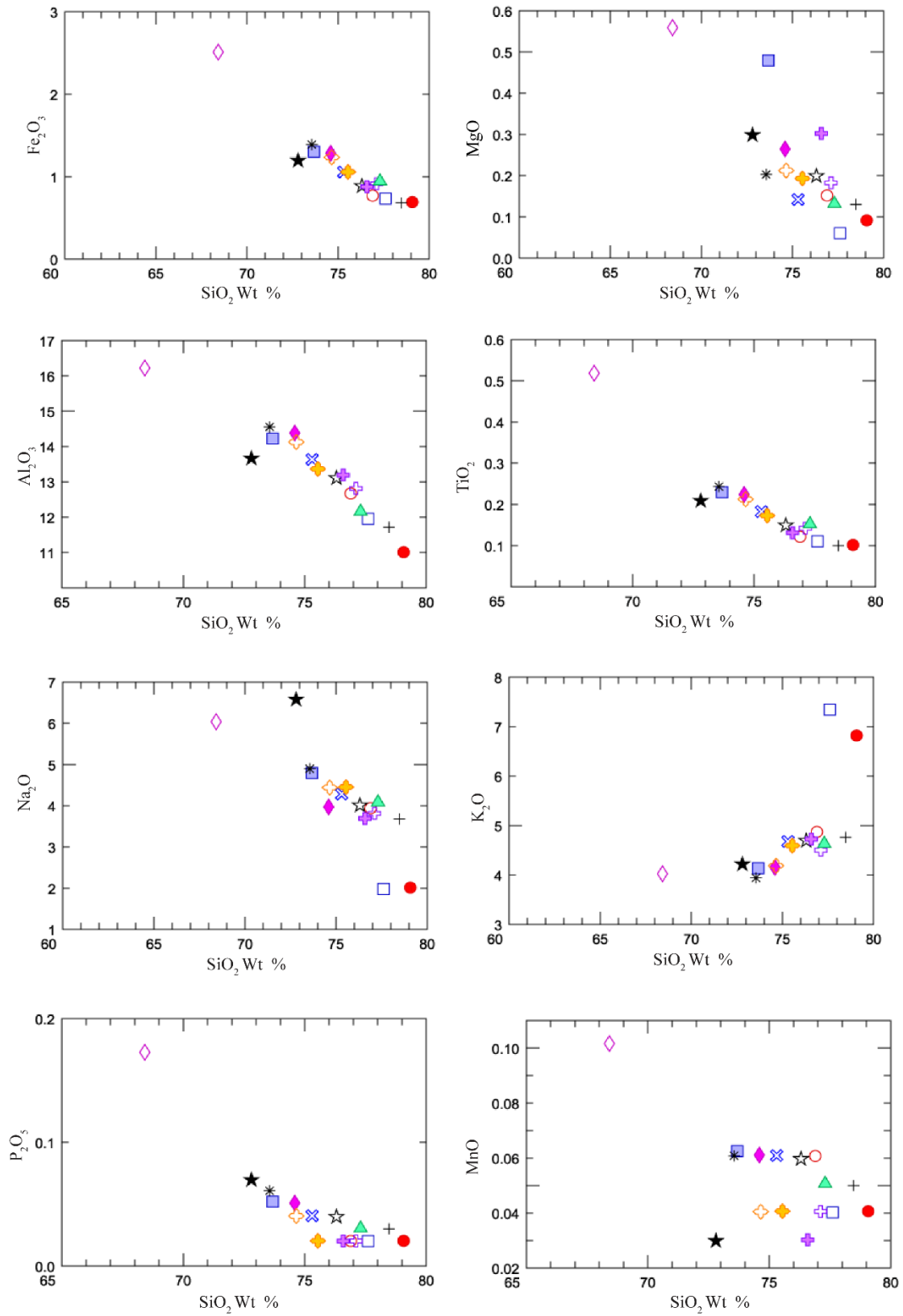
Figure 8.02. Major and minor element Harker diagrams. Samples keyed as in Figure 8.01.

Major element oxides appear to show systematic variation relative to increasing SiO_2. Of the rhyolites, CCBSC0605 (solid star) appears to be the most primitive. Na_2O, Al_2O_3, Fe_2O_3, MgO and P_2O_5 all decrease with increasing SiO_2, while K_2O increases. The data plot in a roughly linear fashion, with the exception of MgO. The scatter in this data may be due to the concentrations approaching the lower detecting limit of the analytical method. K_2O varies from 3.89 to 6.71 wt %. Al_2O_3 varies from 10.85 to 15.95 wt %. Na_2O ranges from 1.98 to 6.61 wt %, inversely proportional to increasing SiO_2.

8.2 Trace Element Chemistry

Selected trace elements are plotted against Nb to identify covariations or trends. Nb is an ideal element to use as an index of differentiation because of its incompatibility and immobility. In addition, the range in concentration of the highest Nb content to the lowest is more than three-fold. Figure 8.03 shows several incompatible trace elements plotted against Nb. The only element that does not generally increase with increasing Nb is Sr. Figure 8.04 shows that there are some similarities among incompatible trace element ratios, for samples CCBSP0405 and CCBSP0505 CCBSP0105 and CCHC0305 CCBSC0606, however, overall there is a great deal of variation among CCR samples.
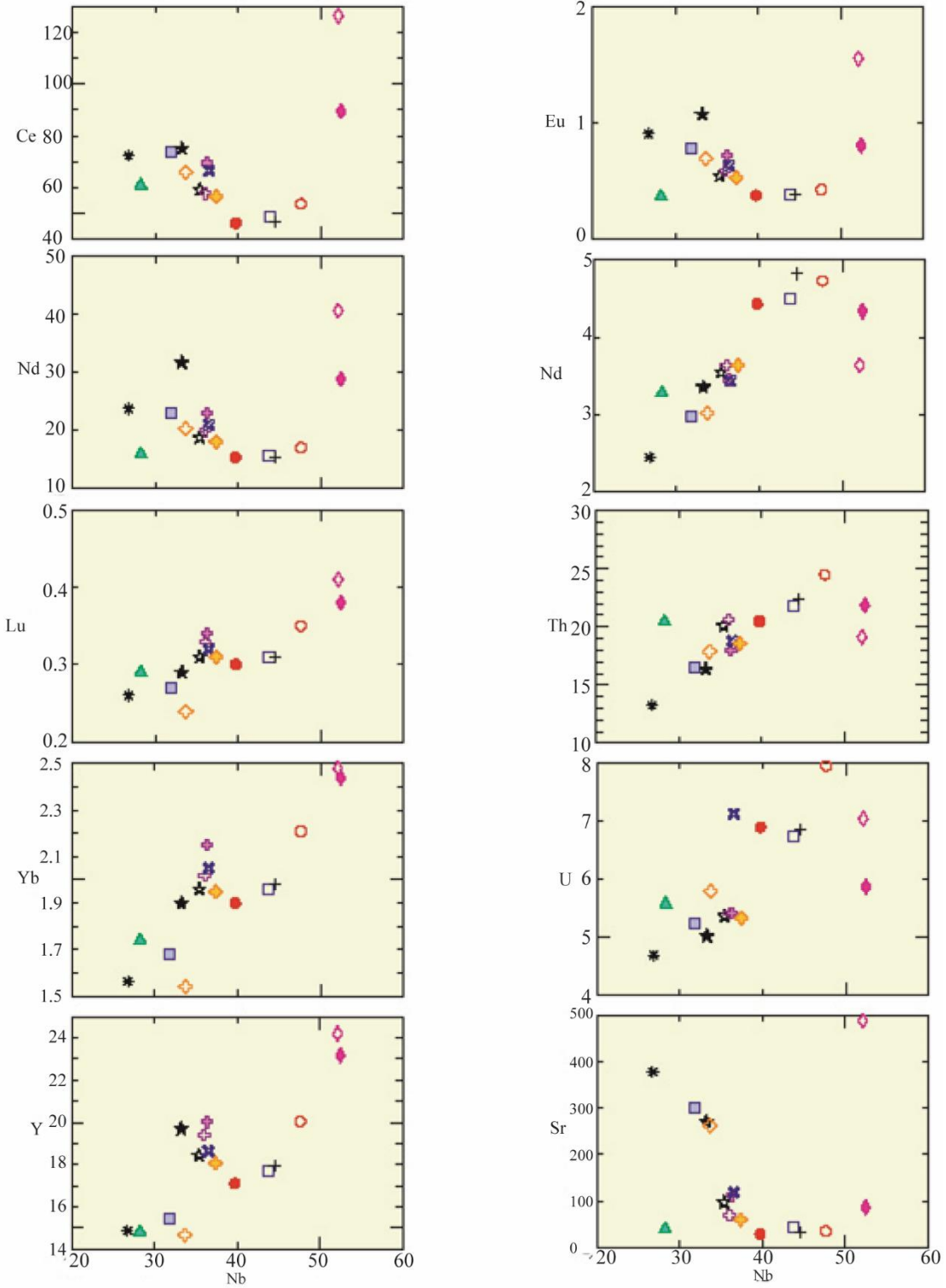
Figure 8.03. Selected trace element concentrations versus Nb. Values are in parts per million.

58
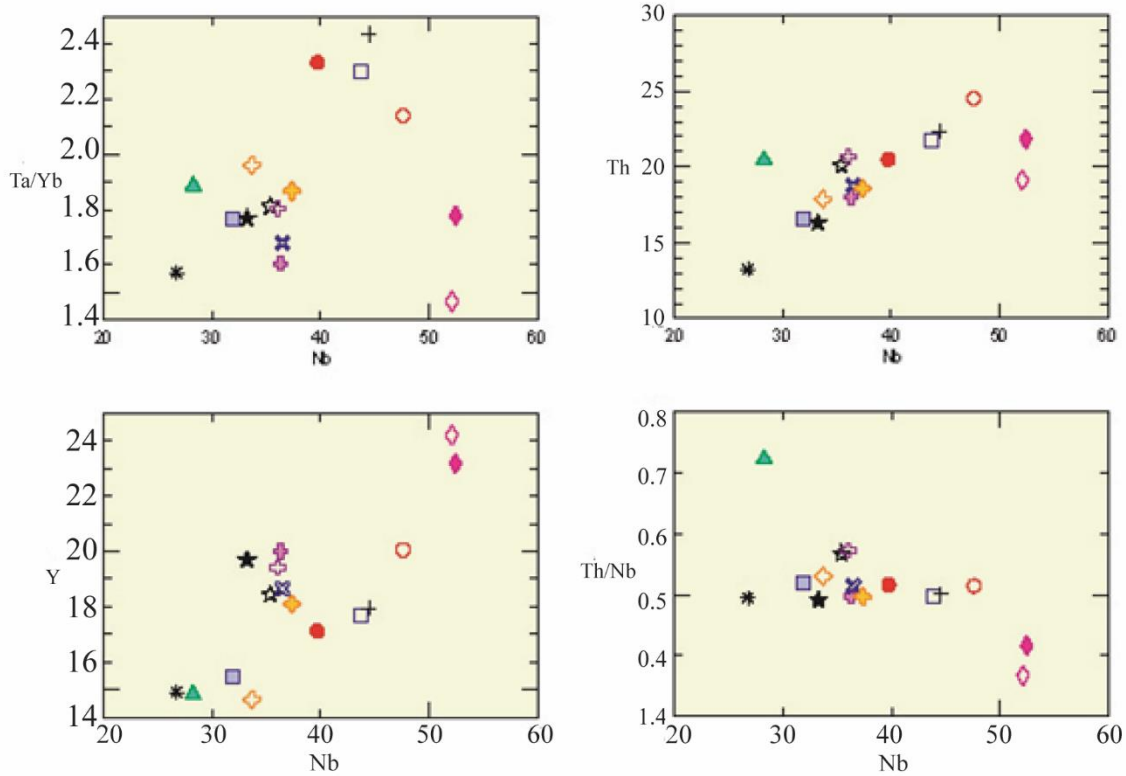
Figure 8.04. Incompatible trace elements and ratios of incompatible trace elements plotted against Nb. All values in ppm.

8.3 Rare Earth Elements

With the exception of BM0305, all samples demonstrate a slight decrease in the amount of Eu compared to chondrites (Figure 8.05). The results also show a negative slope for the LREE's (Light Rare Earth Elements; those which appear to the left of Eu) and an HREE (Heavy rare earth element; those plotted to the right of right of Eu.) slope approaching 0. HREE's are only enriched over chondrite values by one order of magnitude, where as LREE are enriched 2 orders of magnitude.
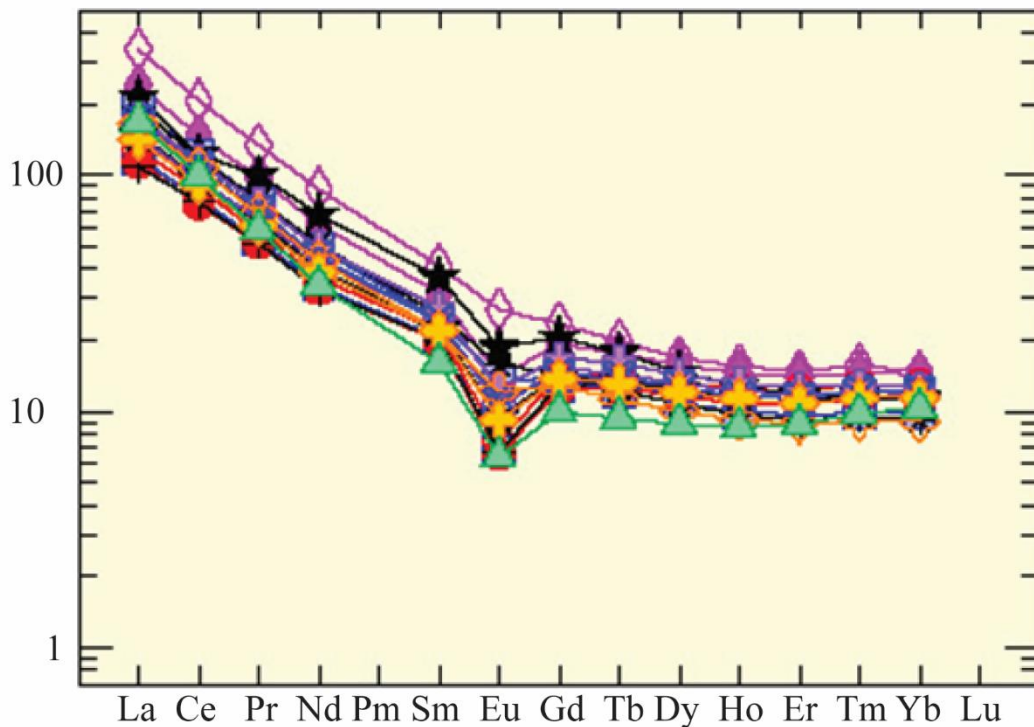
Figure 8.05. Rare Earth Elements (REE), normalized to chondrite, after Sun and McDonough 1989. Logarithmic Y axis indicates enrichment/ depletion of REE in Canovas Canyon Rhyolite versus chondrite.

8.4 Isotope Geochemistry

The ^{87}Sr/^{86}Sr ratios range of the CCR range from 0.704684 to 0.709791. ^{87}Sr/^{86}Sr ratios tend to increase with decreasing Sr content. ^{143}Nd /^{144}Nd ratios for the CCR range from 0.51242 to 0.512613, and εNd values range widely from -4.17 to -0.49 (Figure 8.06). There are no trends apparent between ^{87}Sr/^{86}Sr and increasing ^{143}Nd /^{144}Nd. Lead isotope ratios of the CCR are shown in Figures 7.07 and 7.08. The ^{208}Pb/^{204}Pb values range from 37.637 to 37.098. ^{206}Pb/^{204}Pb ratio ranges from 17.830 to 18.315, ^{207}Pb/^{204}Pb varies from 15.510 to 15.553, and ^{208}Pb/^{204}Pb varies from 15.510 to 15.553. Both ^{208}Pb/^{204}Pb and ^{207}Pb/^{204}Pb generally increase with increasing ^{206}Pb/^{204}Pb.
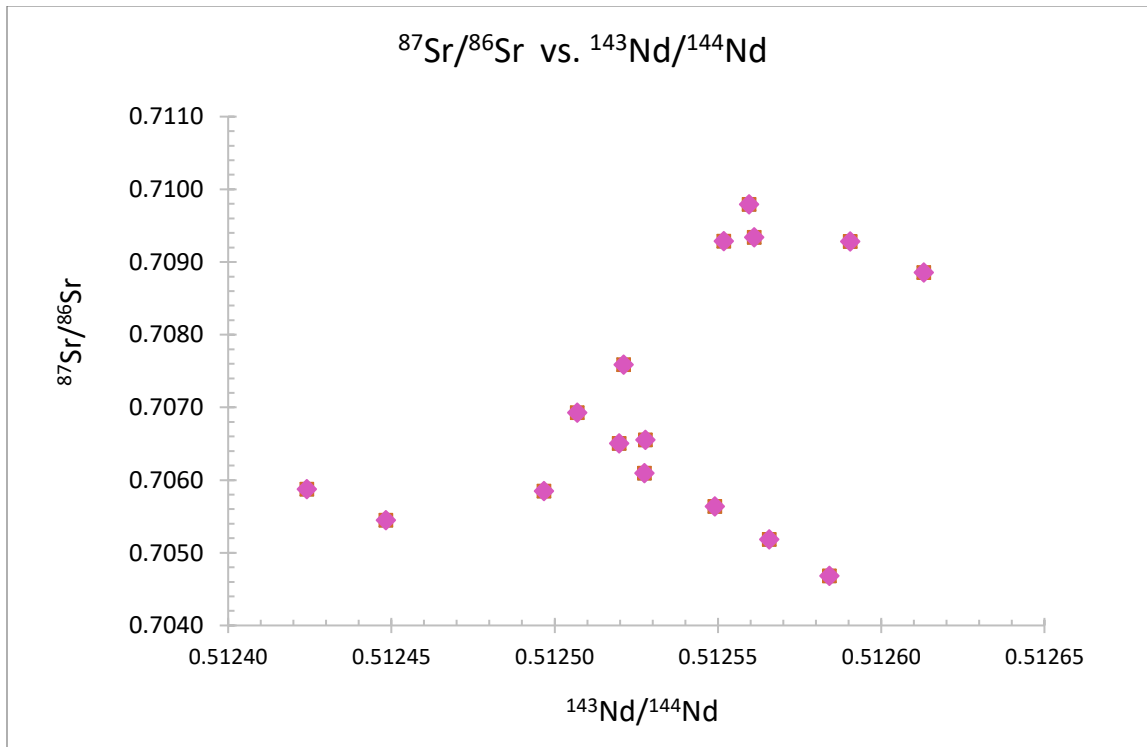
Figure 8.06. ^{87}Sr/^{86}Sr versus ^{143}Nd/^{144}Nd, Canovas Canyon Rhyolite.

PB Isotopic Data
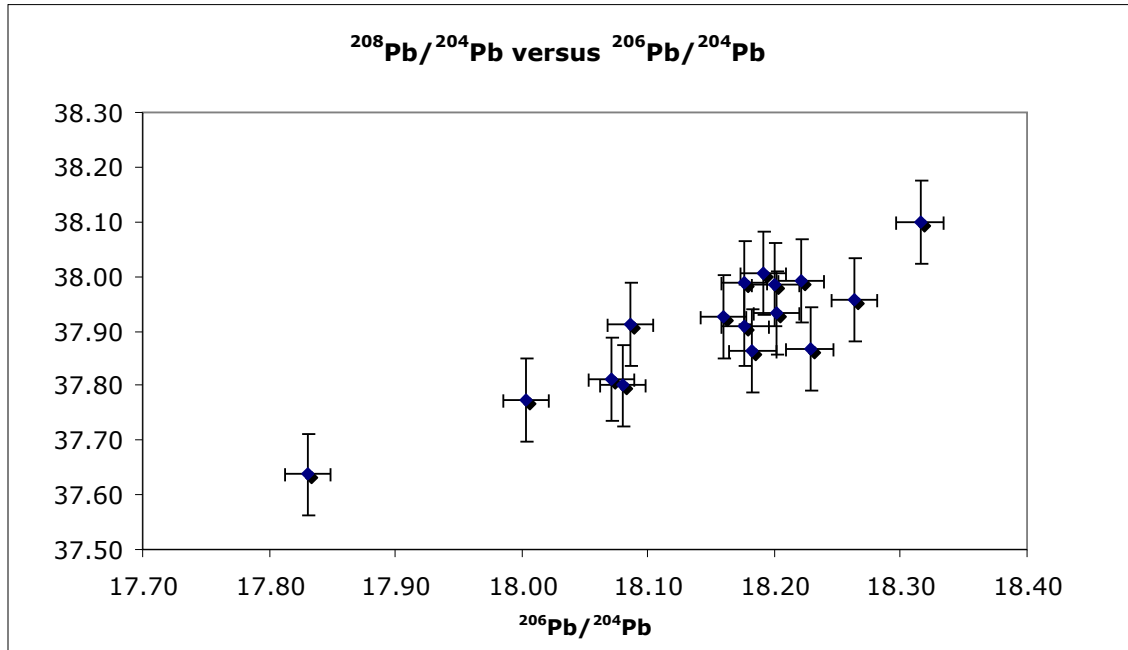
Figure 8.07. $^{208}Pb/^{204}Pb$ (Y-axis) ranges from 37.637 to 37.098. $^{206}Pb/^{204}Pb$ ratio ranges from 17.830 to 18.315. Uncertainties are 0.2% for $^{208}Pb/^{204}Pb$, and 0.1% for $^{206}Pb/^{204}Pb$. and 0.15% for $^{207}Pb/^{204}Pb$.
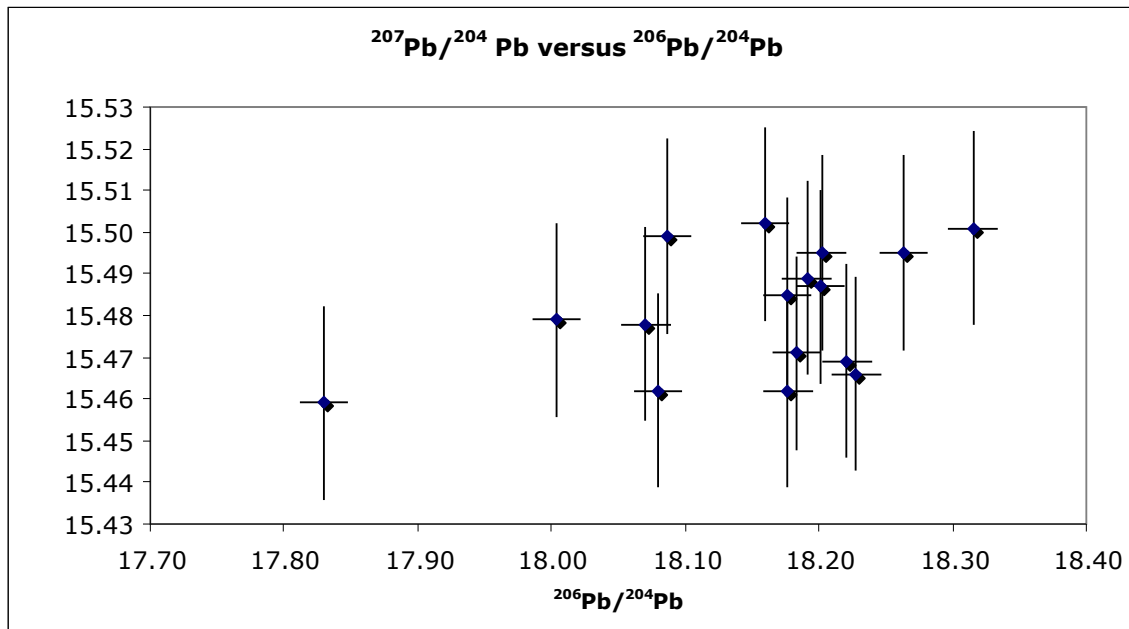
Figure 8.08. $^{207}Pb/^{204}Pb$ (Y axis) versus $^{206}Pb/^{204}Pb$. $^{208}Pb/^{204}Pb$ varies from 15.510 to 15.553. Uncertainties are 0.1% for $^{206}Pb/^{204}Pb$. and 0.15% for $^{207}Pb/^{204}Pb$.

CHAPTER 9

DISCUSSION

The origin of each of the Canovas Canyon Rhyolite (CCR) eruptive units exists somewhere on a spectrum between a being a product of fractional crystallization of a basalt, and a pure crustal melt. The timing among the eruptions over an ~4 Ma period as indicated by the $^{40}Ar/^{39}Ar$ dating (Chapter 6) most likely precludes the CCR having been produced by one single magma system. In addition, the extent of the area (50 km^2), over which the CCR was erupted makes it unlikely that it could have come from one system. Radiogenic isotopes can be used to constrain whether the CCR is a direct fractionate from basalt, a pure crustal melt, or whether it is the product of mixing between two or more separate isotope reservoirs. Models for the petrogenesis of the CCR are presented below.

9.1 Petrography

In thin section, disequilibrium textures such as resorbed and embayed phenocrysts, and overgrowth textures such as anti-rapikivi feldspars. The CCR varies from aphyric obsidian to crystal rich rhyolite. While most samples were sparsely porphyritic, the average of phenocryst abundance among the samples was 6.4%, with values as high as 22.8%, and three samples were aphyric. No trends in either changes in types of phenocrysts, or their abundances over time were apparent.

9.2 ^{40}Ar/^{39}Ar Geochronology

Nine of the samples yielded phenocrysts suitable for ^{40}Ar/^{39}Ar analysis. Of these, seven produced reliable data, and six of those were samples of the CCR. Figure 9.01 shows a probability distribution diagram of the timing of eruptions of the CCR based on these results. The timing of the eruptions, spanning more than 4 Ma, appears to answer the question of whether or not a single, long-lived magma system gave rise to all of the CCR eruptions. A single, stable magma chamber with chemical and thermal gradients as well as convection currents is unlikely to remain in a state where its melt fraction is high enough to sustain convection and compositional layering for a period as long as 4 Ma. It is unusual to find a magma system which exists in the crust for longer than 1 Ma (Reid, 2008). This is especially true in an extensional terrane where magma bodies tend to form higher up in the crust, where they are likely to cool faster (Lee, et al., 2014). In the Jemez, and active hydrothermal system would also tend to shorten the life span of magma bodies. Such a thermal equilibrium would only be possible if the influx of heat and material from basalt underplating occurred at a constant rate. The heat input from beneath would have to exactly balance heat loss from the upper parts of magma chamber for the system to remain active. The influx of basaltic magma would need to be just enough to cause melting and convection, but not enough to disrupt the system and cause a caldera forming, chamber emptying eruption such as the ones which created the Bandelier Tuff. It can be argued, based on the large uncertainties of the ^{40}Ar/^{39}Ar data, as well as the small probability of the oldest eruption (Figure 9.01), that the age range of the CCR is disputable, and it is possible, based on this study alone, to argue that all of the CCR units were produced in a much shorter span, approaching 1 Ma (Dr. Shichun Huang, personal communication, November 18, 2016). However, when combined with the data from other research, the time span of more than 4 Ma is

robust (Gardner, et al., 1986; Justet, 2003).
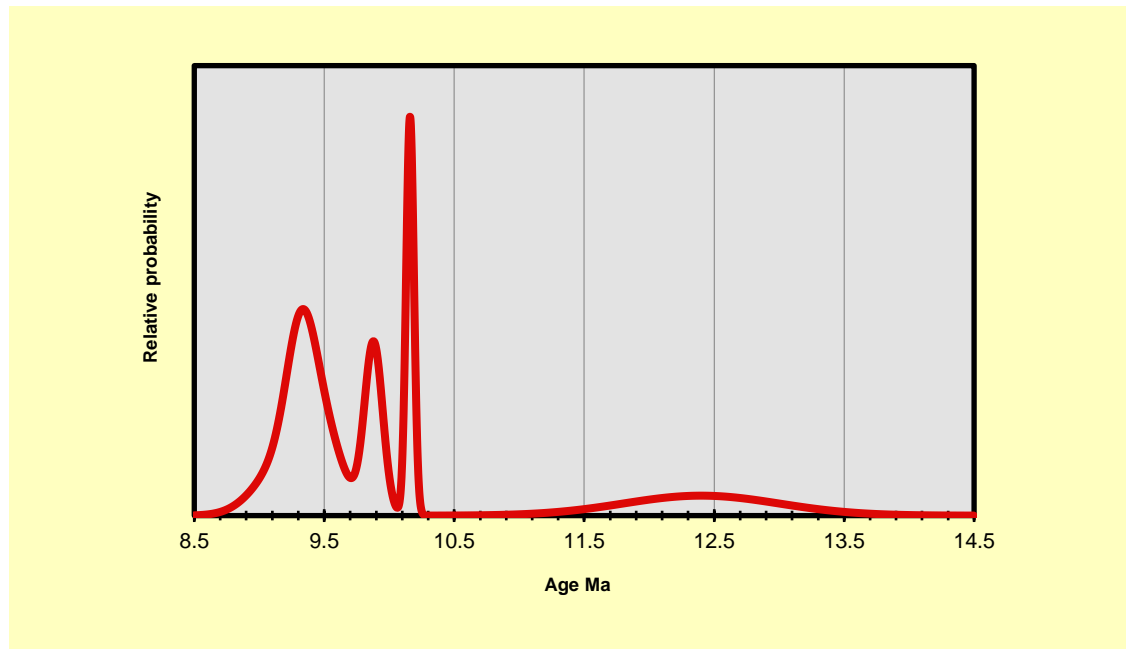
Figure 9.01. Probability distribution plot for the Canovas Canyon Rhyolite, showing the timing of eruptions. Not included in this figure are results from sample CCTC0105, which is 6.26 ± 0.03 Ma, placing it within the age range of the Bearhead Rhyolite.

There are three CCR samples which have ages that overlap within analytical uncertainty, and could potentially have been produced by the same magma system. These are CCBSC0605 at 9.47 ± 0.19 Ma, CCBSP0405, at 9.32 ± 0.11 Ma, and BM0305 at 9.21 ± 0.22 Ma. In order to determine whether these could be the product of a single, evolving magma chamber, it is necessary to compare their isotopic composition, as well as their major and trace element chemistry.

9.3 Major and Trace Element Chemistry

During the 4 Ma period of CCR eruptions, there are no consistent trends in major or trace element chemistry (Figure 9.02) This indicates that no simple petrogenic process, such as closed system fractional crystallization in one single magma chamber, or progressive crustal melting, was responsible for the generation of the CCR.

Niobium is, for the most part, an incompatible element in most rhyolite minerals, with the exception of zircon, biotite and magnetite. Based on the mineralogy present in the CCR, it is expected that with continuing fractional crystallization of a single magma batch, the concentration of Nb should increase in the magma with time. If the CCR was produced by one evolving magma system, both Nb and SiO_2 concentrations would be expected to increase together. In the end member models in which rhyolites like the CCR are produced by small eruptions which tap the apex of a long lived magma system, as long as there is sufficient influx of heat to produce convection, crystallization should continue, and the high silica rhyolite should continue to evolve.

Figure 9.02a shows that there is a lack of a clear, linear and positive correlation between Nb and SiO_2. Figure 9.02b shows the change in SiO_2 over time. If the CCR was the product of one, long lived magma system, as the system evolved by fractional crystallization, the amount of silica should increase with time. Also, if one system produced the CCR, longer time intervals between eruptions would produce more evolved magmas, as they would have had a longer time to reside in the crust and fractionate. No such trends are apparent. Figure 9.03 shows that the ratio between the two incompatible elements, the La and Yb ratio is different for each unit with respect to time, indicating that these rhyolites did not erupt from the same system. AFC modeling among the CCR units themselves was unsuccessful, indicating that the rhyolites are not related.
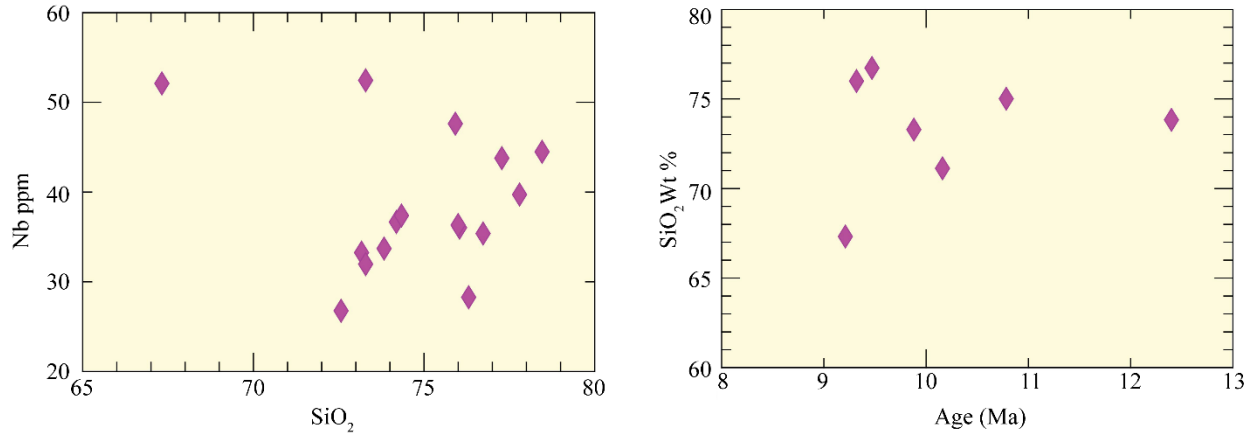
Figure 9.02 a. and b. a. Nb (ppm) versus SiO$_2$ weight %. b. SiO$_2$ weight % versus age, for CCR samples only. The CCR does not show any trend between increasing SiO$_2$ (weight %) and increasing Nb (ppm). There is also no systematic change in SiO$_2$ with respect to time.

The three samples close in age: CCBSC0605, CCBPS0405, and BM0305 (from oldest to youngest), do not show any major or trace element trends indicating that they were produced by a single evolving magma system. The youngest of the three, BM0305, is actually a trachydacite, and could not have evolved from either of the older two units, which are rhyolites. There is a distance of between 6 and 7 kilometers between BM0305 and the other two units, making it unlikely that they could have erupted from the same magma chamber. While magma chambers of such large sizes are known, they are less likely in extensional regimes (Lee et al., 2014). The Sr concentrations between CCBSC0605 and CCBPS0405 increase, although SiO$_2$ decreases along with several other incompatible elements such as La, Eu, Ba, Sr and Zr. While Lu and Y do behave incompatibly and increase with time, Rb, which is also incompatible decreases. All of these data, taken together indicate that these three samples could not have been produced from the same magma system by a simple process such as closed system fractional crystallization.
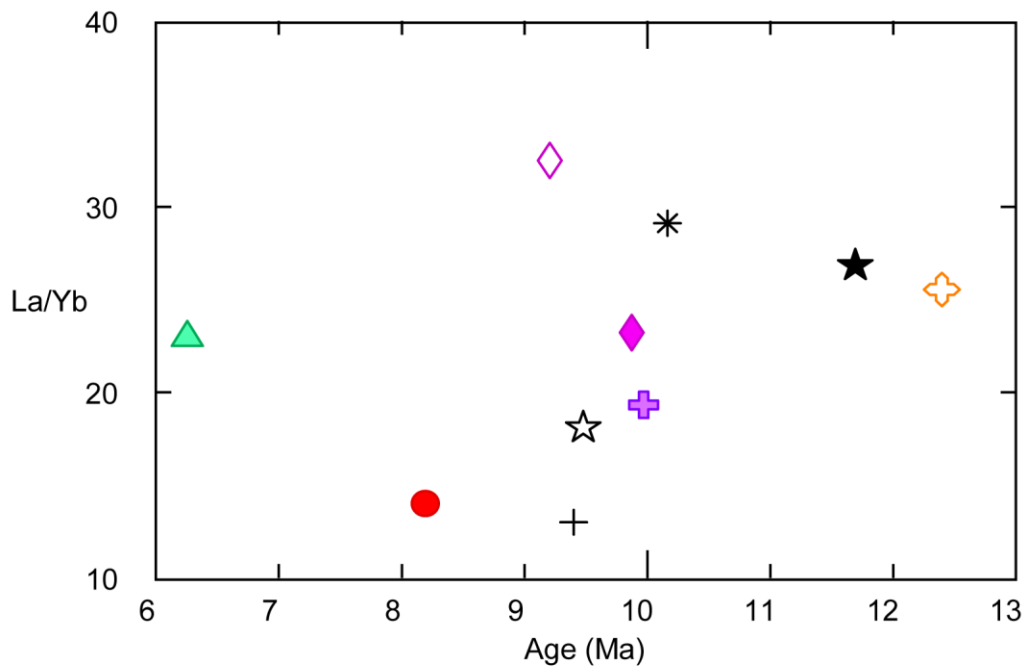
Figure 9.03. La/Yb versus age. There appears to be no systematic variation with time in the relationship between the two incompatible elements.

9.4 Isotope Geochemistry

Radiogenic isotope ratios are not modified by processes such as partial melting or fractional crystallization and therefore these may provide information on crustal vs. mantle sources. The Nd and Sr isotope compositions of some CCR very closely resemble, and in some cases, overlap, with those of associated Jemez basalts. Figure 9.04 shows the Nd versus Sr isotope signatures of the CCR and associated basalts as well as the upper, middle and lower crust.
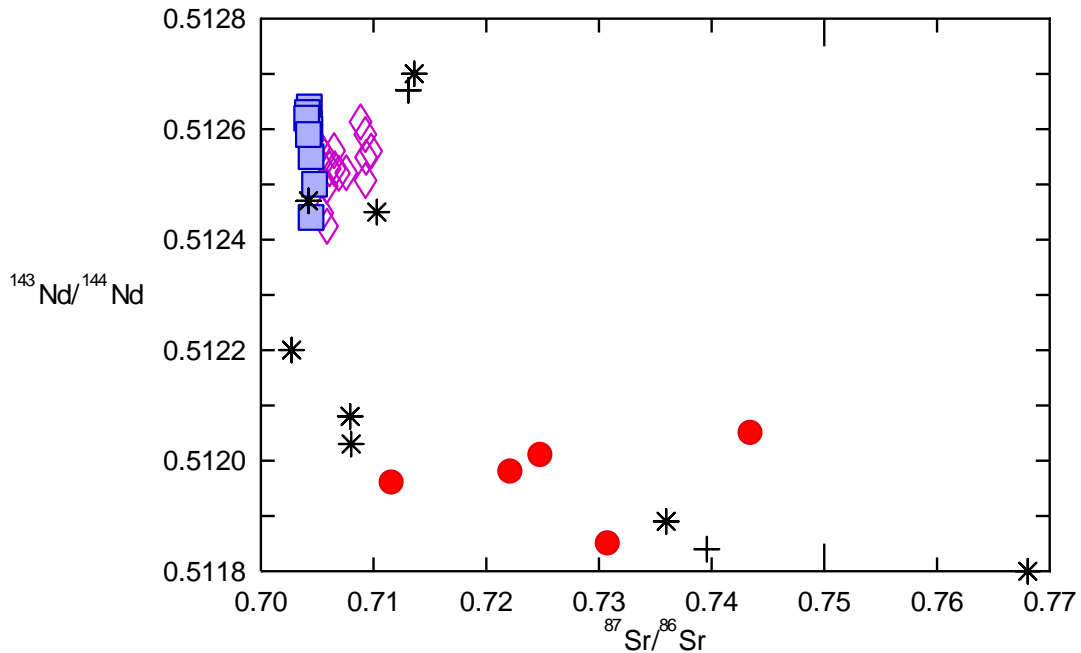
Figure 9.04. Nd isotope versus Sr isotope compositions for the CCR, Jemez mafics, upper- middle- and lower- crust. Open diamonds are CCR, Square represent Jemez mafic magmas, asterisks represent middle crust, crosses are upper crust, and circles are lower crust. Data from this study, Wolff et al, 2005, and Justet, 2007.

The Sr and Nd isotope ratios of the lower and upper crust beneath the Jemez show a wide array of values. In order to model mixing, the end members chosen include basalts which are contemporaneous with the CCR, and samples of lower and middle crust. The crustal and mafic end members which are used are from Wolff et al. (2005). Crustal xenoliths are from the Santa Fe Range, the Taos Range, and lithic fragments recovered from the Bandelier Tuff. Figure 9.05 shows mixing modeling using the most primitive basalt as the mafic end member, with three possible crustal assimilants. Some of the mafic end members have lower radiogenic Nd ratios than the most primitive mafic endmembers, possibly as a result of crustal contamination,
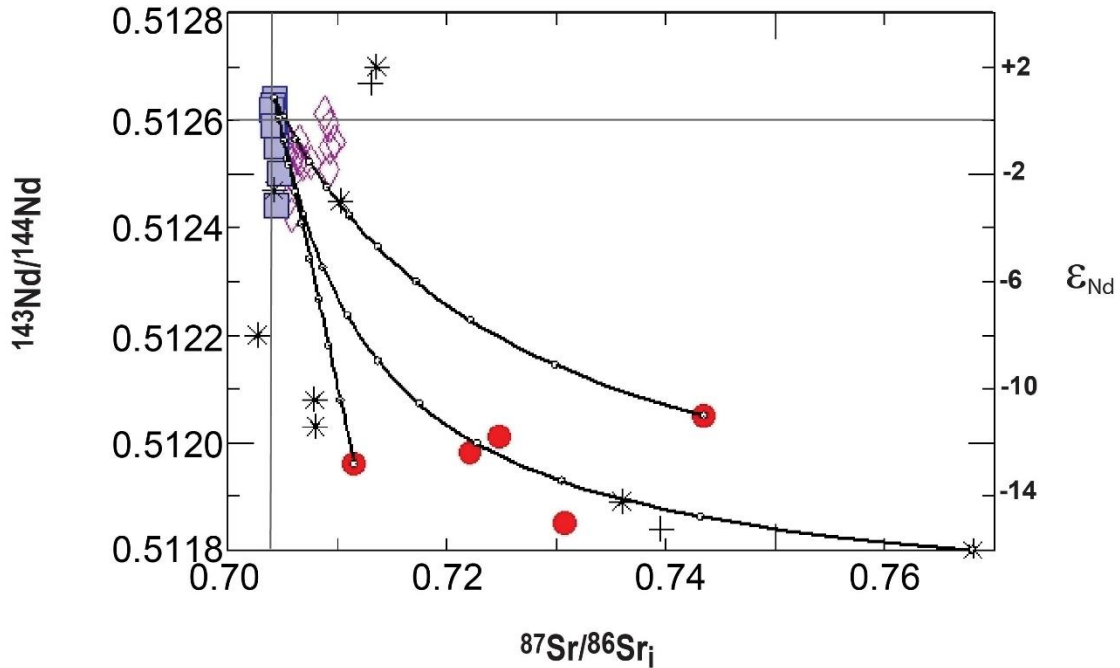
Figure 9.05. Three examples of calculated mixing lines between the most primitive Jemez mafic endmember and three selected crustal lithologies. Squares represent Jemez mafic lavas, circles are upper crustal xenoliths, asterisks/ crosses are lower crustal xenoliths, and open diamonds are CCR data from this study. Open circles along the mixing lines indicate amount of mixing between possible end members in 10% increments. Solid horizontal and vertical lines represent bulk earth values. Mafic and crustal data from Wolff, et al., (2005). Not all of the CCR isotope ratios can be accounted for by using these particular endmembers.

The Nd and Sr isotope data indicate that the all CCR units are either: 1) A direct product of fractional crystallization of basalt, or 2) a product of fractional crystallization of basalt with some assimilation of continental crust. Depending upon which crustal end member is chosen, they are explainable as Jemez basalt with up to 50% crustal material (Figure 9.05). Some of the basalts produced by the Jemez have lower Nd and higher Sr ratios than the most primitive samples, and could have undergone crustal contamination.

The Nd and Sr isotope ratios of CCR, while defining a fairly narrow range, can be only

be produced by contributions from basalt and crust isotope reservoirs. It is possible that the crustal contamination is not from melting of the crust, but from interaction between a rhyolite produced by basalt fractionation and hydrothermal fluids. However, there is no correlation between the weight percent of water in the rock and Sr isotope signatures. Both upper and lower crust appear to contribute material. The isotope signature of some of the CCR units are similar to the least evolved basalts, whereas other units resemble basalts which show evidence of crustal contamination. While the resemblance of the Sr isotope signature to the associated mafic endmembers is not expected for the products of smaller, ephemeral magma systems, there is a possible explanation for why the Sr isotope signature of the rhyolites was inherited rather than overwritten by crustal values. Basalt fractionation in the presence of water crystallize amphiboles and titanite, while plagioclase formation is suppressed. This results in rhyolites which have higher Eu and Sr contents, so that it would require more crustal contamination to alter the Sr isotope signature of a "cool, wet" rhyolite than a "hot, dry rhyolite." With regards to the three samples CCBSC0606, CCBSP0405, and BM0305, the oldest two have εNd values of -2.05 and -2.19 respectively, while BM0305 has an εNd of -0.94. The initial Sr of the oldest two units, are 0.706549 and 0.707582, whereas the youngest, BM0305, has an initial Sr isotope ratio of 0.704680, indicating that while CCBSC0606 and CCBSP0405 could be related, BM0305 is not.

The $^{208}Pb/^{204}Pb$ versus $^{206}Pb/^{204}Pb$ isotopes ratios of the CCR are virtually identical to those of the associated basalts, however, there is little difference between the ratios of the Jemez basalts and some of the crustal rocks. $^{207}Pb/^{204}Pb$ versus $^{206}Pb/^{204}Pb$ for the basalt and crust and CCR are for the most part, indistinguishable (Figure 9.07 a. and b). The Pb content of the crust tends to be lower than that of the CCR, so that the crustal isotope signature would be less likely to dominate a rhyolite which it had contaminated.
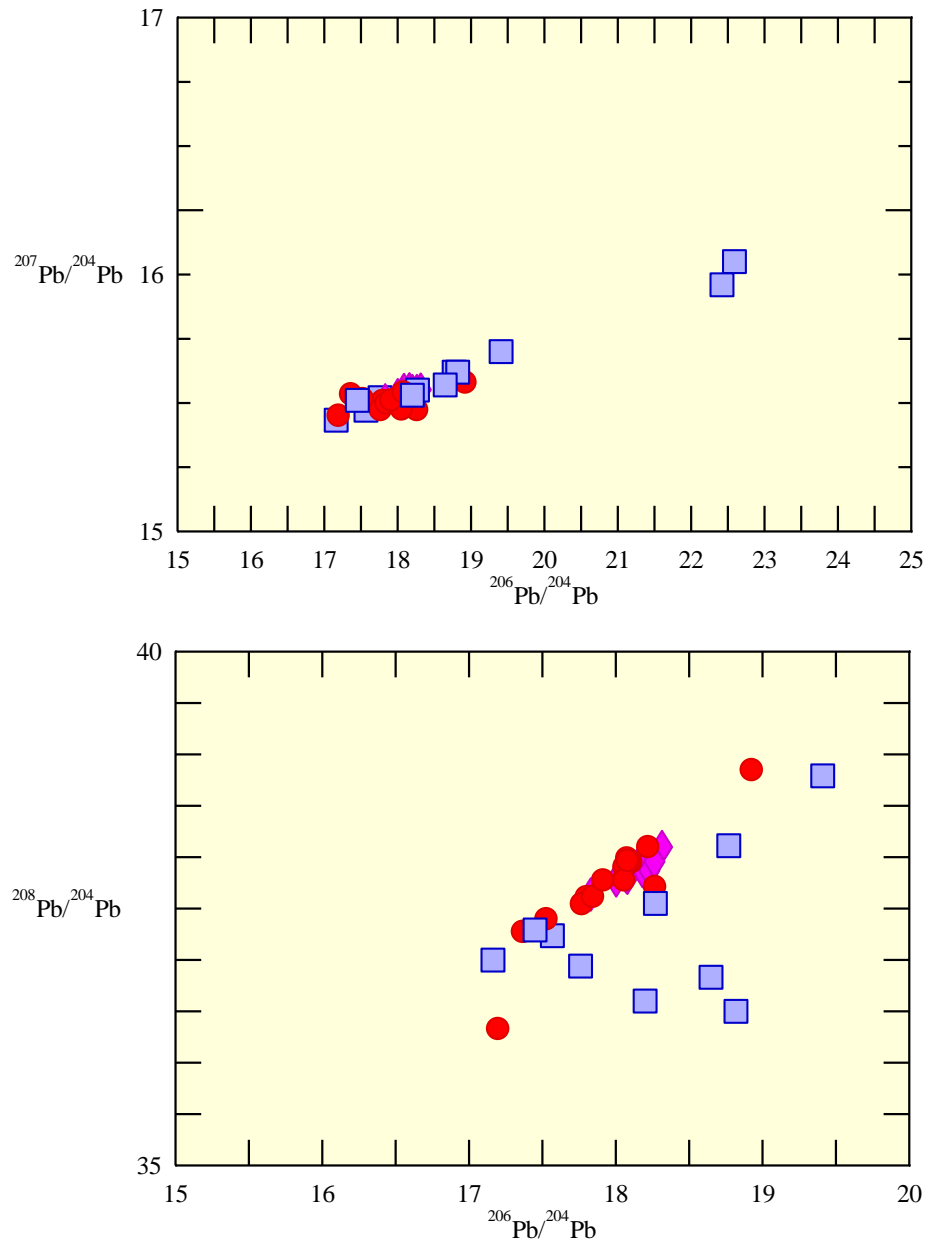
Figure 9.06 a and b. a. $^{207}Pb/^{204}Pb$ versus $^{206}Pb/^{204}Pb$. b. $^{208}Pb/^{204}Pb$ versus $^{206}Pb/^{204}Pb$. Circles represent Jemez basalts, squares represent crustal values and diamonds represent CCR. Data from Wolff, et al., 2005 and this study.

9.5 Models for the Canovas Canyon Rhyolite

$^{40}Ar/^{39}Ar$ data indicate that CCR eruptions occurred over an ~4 Ma period, from about 12.4 to 7.6 Ma (Figure 9.01). It would be extremely unlikely that one magma chamber could exist in the crust for that length of time. The Canovas Canyon Rhyolite exhibits significant variability in phenocryst assemblages, and range from aphyric to porphyritic. The samples display a variety of textures, suggesting that the processes which produced the CCR varied from unit to unit. Aside from the unlikelihood of a magma system remaining stable in the crust for such a prodigious length of time, there are no major or trace element geochemistry trends which would indicate one long lived magma system. There are also no temporal trends in major and trace element chemistry which suggest a simple process such as pure fractional crystallization. Epsilon Nd ranges widely from a low of -4.17 to a high of -0.49. $^{87}Sr/^{86}Sr$ ratios range from 0.704684 to 0.709791(See Figure 7.06). Pb isotope signatures are very similar to related basalts, with some overlap of crustal values as well (see figures 9.08a and b).
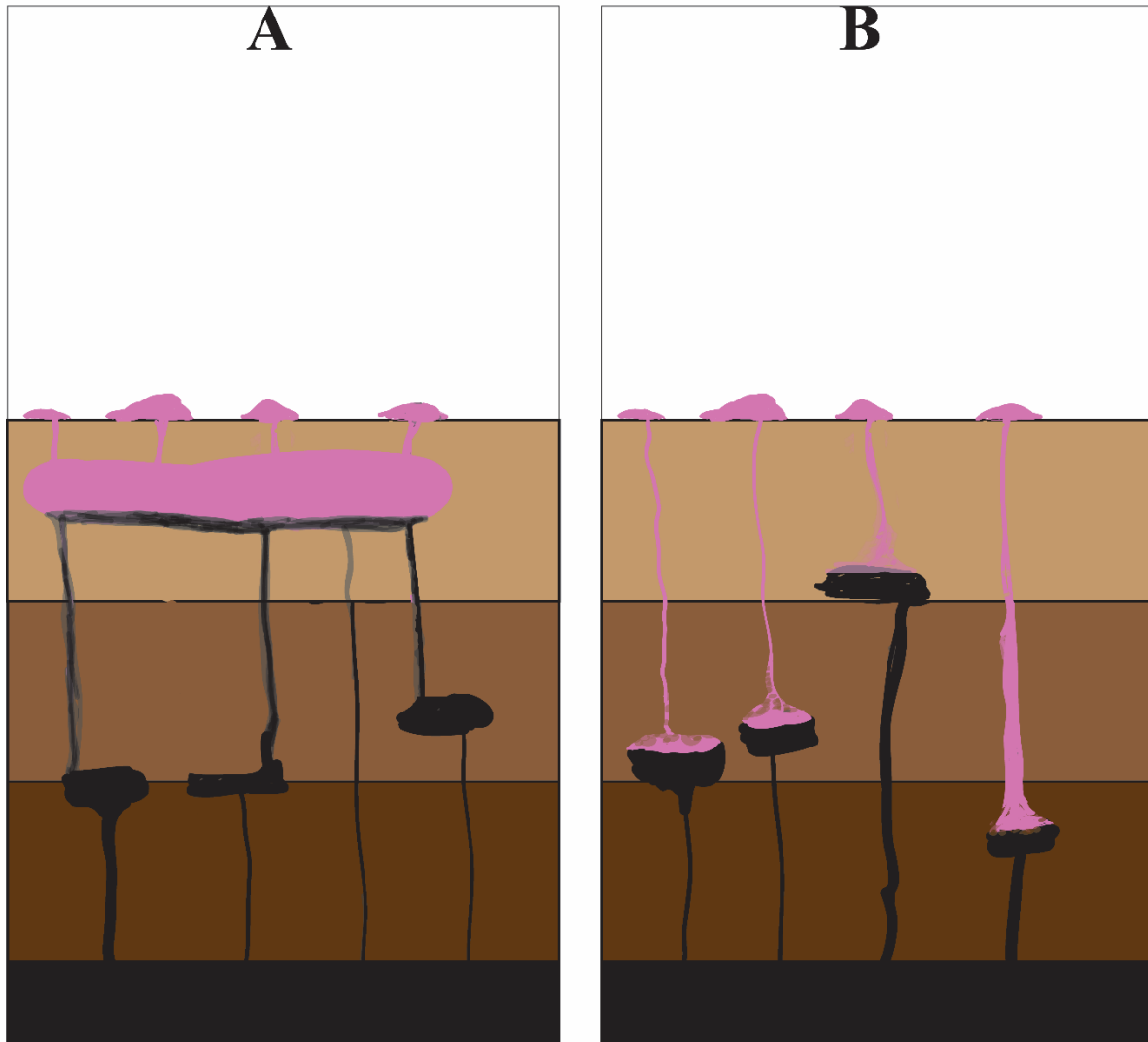
Figure 9.07 A and B. End member models for the Canovas Canyon Rhyolite. A. illustrates repeated basalt injection at the lower crust resulting in one long lived magma system, producing a series of relatively small silicic eruptions. B. shows basalt injections which evolve independently, producing small ephemeral magma chambers and rhyolitic eruptions which are not related to one another.

Based on the results of this study, no simple petrogenetic relationships among these rhyolites can be identified. Instead it appears that the CCR was produced by a series of small, ephemeral, unrelated silicic magma systems. Figure 9.07 A and B above show the two end member models for the production of silicic magmas in extensional terranes, where basalt

underplating drives magma formation in the crust. Model A depicts the establishment and evolution of a single magma system which may have substantial (>1 Ma) longevity. Model B shows a number of more ephemeral silicic magma chambers, each of which produces eruptions and crystallizes on a brief interval of time (<100's ka). Canovas Canyon Rhyolites appear to best fit the second model.

CHAPTER 10

CONCLUSIONS

The separate eruptive units of the CCR most likely were not produced by a single long-lived magma chamber. Although the CCR exhibits significant variability in phenocryst assemblages, there are no progressive changes in phenocryst abundances or assemblages with respect to time. There are no geochemical trends, either in major elements, such as SiO_2, or in incompatible trace elements such as La/Yb versus time which would suggest a simple process such as fractional crystallization.

REE abundances show a strongly negative LREE slope, an HREE slope close to 1, and a lack of a significant Eu anomaly. Both the negative LREE slope and the HREE slope approaching 0 are indicators of fractional crystallization. The lack of a pronounced Eu anomaly does not indicate magmas which have undergone extensive fractionation of plagioclase dominated crystal assemblages. The lack of a strong Eu anomaly could be an indicator that the end member magma crystallized in a water-rich environment, where plagioclase crystallization was suppressed (Bachman and Bergantz, 2008). Instead, titanite and amphibole may have formed, two minerals which do not sequester Sr and Eu. Based on the relative REE abundances, the CRR most likely formed as a "cool, wet" rhyolite (Bachman and Bergantz, 2008). Other rhyolites in the Jemez, for instance, the El Rechuelos Rhyolite has a REE pattern typical of a "hot, dry" rhyolite, with a more pronounced Eu anomaly (Loeffler, 1988).

Also indicating that the units were most likely not produced by the same system is the

distribution of the eruptions in space and time. New $^{40}Ar/^{39}Ar$ data indicate that the CCR was produced over a period of ~ 4 Ma, which is in agreement with existing data (Gardner, et al., 1986). In addition, the CCR was erupted over an area that covered more than 50 km^2, making it highly unlikely a single magma chamber produced the CCR (Spell, written communication, 2016). Except for samples CCBSC0605 and CCBSC0606, which were approximately 0.5 km, apart, even units which are relatively close together in age do not exhibit any major or trace element trends which would indicate that they could have evolved in the same system. Units of similar ages are found in different parts of the field area as well, which would make their having developed from the same magma chamber even more unlikely. $^{144}Nd/^{143}Nd$ and $^{87}Sr/^{86}Sr$, and Pb isotope data indicate that the CCR was the product of a mantle component with between 0% to 50% crustal contamination. Pb isotope ratios of the CCR are virtually identical to those of coeval basalts. Taken together, these relationships preclude any simple petrogenetic relationships among these rhyolites. Instead they appear to have been produced by ephemeral, unrelated silicic magma systems.

Of the two end member models for the production of silicic magmas, the model of more ephemeral silicic magma chambers fits the CCR (Figure 9.08 b.). In this model, individual magma systems produce eruptions and crystallize during brief intervals of time (<100's ka). It appears that the Canovas Canyon Rhyolite is an excellent example of this type of model.

^{39}Ar/ ^{40}Ar DATA

Table A01. Sample #CCBSC0602 ^{39}Ar/ ^{40}Ar Data

Padmore-UNLV, BSC0602P, plagioclase, 19.66 mg, J = 0.00216218 ± 1.0008%

4 amu discrimination = 1.03025 ± 0.37%, 40/39K = 0.004667± 0.53927%, 36/37Ca = 0.0003059 ± 2.45%, 39/37Ca = 0.00068823 ± 1.84%

step	T (C)	t (min.)	36Ar	37Ar	38Ar	39Ar	40Ar	%40Ar*	% 39Ar rlsd	Ca/K	37d	start d
1	650	12	35.718	5.848	15.409	290.720	11456.72	10.7	44.0	0.6	13.17	13.14
2	730	12	9.128	7.568	4.584	108.592	2973.54	12.5	16.4	2.08		
3	810	12	1.117	13.820	1.715	78.113	461.653	36.1	11.8	5.29		
4	890	12	0.418	13.503	0.702	44.781	209.710	55.7	6.8	9.02		
5	960	12	0.481	8.610	0.450	26.262	186.465	36.7	4.0	9.81		
6	1020	12	0.539	6.453	0.480	20.180	190.720	27.3	3.1	9.57		
7	1080	12	0.426	4.695	0.359	14.853	147.105	26.3	2.2	9.46		
8	1140	12	0.616	4.973	0.368	15.753	207.712	21.0	2.4	9.45		
9	1210	12	0.742	5.576	0.454	17.520	246.314	18.7	2.7	9.52		
10	1400	12	1.399	14.006	1.027	43.604	496.688	26.5	6.6	9.61		
								Cumulative %39Ar rlsd =	100.0			

note: isotope beams in mV, rlsd = released, error in age includes J error, all errors 1 sigma

(36Ar through 40Ar are measured beam intensities, corrected for decay for the age calculations)

Table A01. Sample #CCBSC0602 ^{39}Ar/ ^{40}Ar Data (continued)

Table A01. Sample #CCBSC0602 ^{39}Ar/ ^{40}Ar Data (continued)

step	40Ar*/39ArK	Age (Ma)	1s.d.	anal err	37/39c	%39ArK	total39	mol 39Ar	Wmdata	WMs	wfactor	WxX
1	4.234882	16.44	0.60	0.58	0.2609	99.98	660.38	0	16.44	0.58	2.99	49.22
2	3.427632	13.32	0.44	0.44	0.9040	99.94		0	13.32	0.44	5.15	68.56
3	2.109268	8.21	0.12	0.12	2.2950	99.84		0	8.21	0.12	66.39	545.03
4	2.520469	9.81	0.13	0.13	3.9114	99.73		0	9.81	0.13	57.71	565.86
5	2.400627	9.34	0.14	0.14	4.2528	99.71		0	9.34	0.14	49.11	458.71
6	2.380527	9.26	0.19	0.19	4.1480	99.71		0	9.26	0.19	26.63	246.66
7	2.336466	9.09	0.18	0.18	4.1003	99.72		0	9.09	0.18	31.29	284.47
8	2.460415	9.57	0.21	0.21	4.0950	99.72		0	9.57	0.21	23.62	226.05
9	2.395215	9.32	0.29	0.29	4.1284	99.71		0	9.32	0.29	11.99	111.69
10	2.644210	10.29	0.19	0.19	4.1666	99.71		0	10.29	0.19	28.99	298.2
	Total gas age =	13.08	0.15						**WtdMean**	**1sd**	**wJ**	
	No plateau								9.39	0.06	0.15	
	Isochron age =	7.19	0.12									
	(steps 1-3)											

Table A01. Sample #CCBSC0602 ^{39}Ar/ ^{40}Ar Data (continued)

step	39/40c	39/40err	36/40c	36/40err	R2	T (C)	36c	39c	40c
1	0.03	0.3727	0	0.3771	0.1229	650	35.64	290.67	11449.46
2	0.04	0.3703	0	0.4000	0.0470	730	9.05	108.52	2964.20
3	0.17	0.3787	0	0.3785	0.4961	810	1.01	77.99	452.46
4	0.22	0.3861	0	0.5879	0.0379	890	0.31	44.66	200.67
5	0.15	0.3841	0	0.4344	0.3417	960	0.38	26.18	170.16
6	0.11	0.4185	0	0.5797	0.0610	1020	0.44	20.12	174.44
7	0.11	0.3901	0	0.5128	0.0194	1080	0.34	14.81	130.85
8	0.08	0.3806	0	0.3963	0.0767	1140	0.53	15.71	191.46
9	0.08	0.4207	0	0.6004	0.0332	1210	0.65	17.47	230.05
10	0.1	0.3910	0	0.3857	0.5643	1400	1.10	43.48	430.17

4AMU	39/40c	37/40c
1.03025	1.00756	1.01513

Table A01. Sample #CCBSC0602 ^{39}Ar/ ^{40}Ar Data (continued)

Blank correction beam errors

step	%36err	%39err	%40err	36err	40err	%36err	%40err	WtdAge39Ar		Age (Ma) ± 2 sig err	
1	0.070	0.040	0.020	0.0250	2.2969	0.07	0.02	7.24	1	15.29	17.60
2	0.150	0.010	0.010	0.0137	0.3373	0.15	0.01	2.19	2	12.44	14.20
3	0.020	0.060	0.040	0.0006	0.2438	0.06	0.05	0.97	3	7.96	8.45
4	0.310	0.070	0.030	0.0014	0.1711	0.45	0.09	0.66	4	9.54	10.07
5	0.110	0.000	0.040	0.0008	0.1757	0.2	0.1	0.37	5	9.05	9.63
6	0.340	0.160	0.060	0.0019	0.1960	0.43	0.11	0.28	6	8.87	9.65
7	0.230	0.020	0.010	0.0011	0.1598	0.33	0.12	0.2	7	8.73	9.45
8	0.040	0.030	0.010	0.0006	0.1605	0.11	0.08	0.23	8	9.16	9.98
9	0.400	0.180	0.050	0.0030	0.2012	0.46	0.09	0.25	9	8.74	9.90
10	0.030	0.090	0.070	0.0007	0.3824	0.06	0.09	0.68	10	9.91	10.66

Table A02. Sample #CCBSC0605 ^{39}Ar/ ^{40}Ar Data

Padmore-UNLV, CCBSC0605, biotite, 5.72 mg, J = 0.00203454 ± 0.1534%

4 amu discrimination = 1.03025 ± 0.37%, 40/39K = 0.004667± 0.53927%, 36/37Ca = 0.0003059 ± 2.45%,
39/37Ca = 0.00068823 ± 1.84%

step	T (C)	t (min.)	36Ar	37Ar	38Ar	39Ar	40Ar	%40Ar*	% 39Ar rlsd	Ca/K	37d	start d	end d
1	750	12	13.297	0.426	4.339	51.565	4104.40	7.2	3.5	0.24	13.00	12.97	13.03
2	800	12	0.837	0.255	1.656	57.230	389.99	41.0	3.9	0.13			
3	850	12	0.798	0.289	2.529	90.282	457.23	52.4	6.1	0.09			
4	900	12	0.613	0.272	2.614	94.818	414.73	60.4	6.5	0.08			
5	940	12	0.620	0.266	2.826	104.132	438.62	67.6	7.1	0.08			
6	980	12	0.696	0.306	3.765	138.467	554.71	66.6	9.4	0.07			
7	1020	12	0.899	0.371	5.335	197.032	771.62	68.4	13.4	0.06			
8	1060	12	1.058	0.488	7.067	260.302	983.14	70.6	17.7	0.06			
9	1090	12	0.733	0.504	4.866	176.535	655.8	70.2	12.0	0.08			
10	1120	12	0.457	0.504	3.333	116.594	427.62	74.0	7.9	0.13			
11	1150	12	0.292	0.354	1.985	69.236	254.749	75.1	4.7	0.15			
12	1400	12	0.675	0.661	3.339	112.017	474.38	69.5	7.6	0.17			

Cumulative %39Ar rlsd = 100.0

note: isotope beams in mV, rlsd = released, error in age includes J error, all errors 1 sigma

(36Ar through 40Ar are measured beam intensities, corrected for decay for the age calculations)

Table A02. Sample #CCBSC0605 ^{39}Ar/^{40}Ar Data (continued)

step	40Ar*/39ArK	Age (Ma)	1s.d.	anal err	37/39c	%39ArK	total39	mol 39Ar	Wmdata	WMs	wfactor	WxX
1	5.786746	21.12	1.26	1.26	0.1058	99.99	1468.21	0	21.12	1.26	0.63	13.37
2	2.752013	10.07	0.10	0.1	0.0570	100		0	10.07	0.1	106.78	1075.57
3	2.617512	9.58	0.09	0.08	0.0410	100		0	9.58	0.08	139.28	1334.55
4	2.604091	9.53	0.07	0.07	0.0367	100		0	9.53	0.07	213.39	2034.29
5	2.555889	9.36	0.06	0.06	0.0327	100		0	9.36	0.06	265.75	2486.6
6	2.606556	9.54	0.06	0.06	0.0283	100		0	9.54	0.06	295.36	2818.29
7	2.641341	9.67	0.06	0.06	0.0241	100		0	9.67	0.06	285.63	2761.78
8	2.640246	9.67	0.06	0.06	0.0240	100		0	9.67	0.06	285.62	2760.49
9	2.560819	9.38	0.06	0.06	0.0366	100		0	9.38	0.06	305.42	2863.31
10	2.575060	9.43	0.06	0.06	0.0553	100		0	9.43	0.06	257.28	2425.34
11	2.507144	9.18	0.06	0.06	0.0655	100		0	9.18	0.06	256.56	2354.96
12	2.550138	9.34	0.06	0.06	0.0756	99.99		0	9.34	0.06	294.56	2750.01
Total gas age =		9.93	0.04						WtdMean	1sd	wJ	
No plateau									9.49	0.02	0.04	
Isochron age =	10.55	0.19										
(steps 5-8)												

Table A02. Sample #CCBSC0605 ^{39}Ar/ ^{40}Ar Data (continued)

step	39/40c	39/40err	36/40c	36/40err	R2	T (C)	Age (Ma) ± 2 sig err	
1	0.01	0.3718	0	0.4420	0.0461	750	18.60	23.63
2	0.15	0.3769	0	0.3803	0.4881	800	9.88	10.27
3	0.2	0.3720	0	0.6207	0.0154	850	9.41	9.75
4	0.23	0.3739	0	0.5132	0.0801	900	9.40	9.67
5	0.24	0.3726	0	0.3864	0.6325	940	9.23	9.48
6	0.26	0.3751	0	0.5076	0.0247	980	9.43	9.66
7	0.26	0.3756	0	0.4023	0.0126	1020	9.55	9.79
8	0.27	0.3705	0	0.5229	0.0288	1060	9.55	9.78
9	0.27	0.3756	0	0.4732	0.1682	1090	9.26	9.49
10	0.29	0.3728	0	1.0264	0.0238	1120	9.30	9.55
11	0.3	0.3784	0	1.2117	0.0328	1150	9.05	9.30
12	0.27	0.3734	0	0.5433	0.0132	1400	9.22	9.45
	4AMU	**39/40c**	**37/40c**					
	1.03025	1.00756	1.01513					

Table A02. Sample #CCBSC0605 ^{39}Ar/ ^{40}Ar Data (continued)

step	36c	39c	40c	%36err	%39err	%40err	36err	40err	%36err	%40err	WtdAge39Ar
							blank corr beam errors				
1	13.25	51.56	4095.33	0.240	0.030	0.020	0.0319	0.8362	0.24	0.02	0.74
2	0.79	57.23	380.89	0.010	0.050	0.030	0.0006	0.1975	0.07	0.05	0.39
3	0.75	90.28	447.98	0.460	0.010	0.010	0.0037	0.1656	0.5	0.04	0.59
4	0.56	94.82	405.46	0.310	0.020	0.030	0.0020	0.2020	0.35	0.05	0.62
5	0.55	104.13	421.96	0.020	0.010	0.020	0.0006	0.1817	0.1	0.04	0.66
6	0.62	138.46	537.88	0.300	0.050	0.020	0.0022	0.1940	0.35	0.04	0.9
7	0.83	197.03	754.51	0.130	0.060	0.010	0.0013	0.1769	0.16	0.02	1.3
8	0.99	260.3	965.74	0.340	0.002	0.010	0.0036	0.1871	0.37	0.02	1.71
9	0.66	176.53	638.79	0.250	0.030	0.050	0.0019	0.3645	0.29	0.06	1.13
10	0.36	116.59	402.48	0.750	0.010	0.020	0.0035	0.1807	0.96	0.04	0.75
11	0.20	69.23	229.84	0.760	0.020	0.030	0.0023	0.1765	1.15	0.08	0.43
12	0.43	112.01	407.55	0.240	0.030	0.010	0.0017	0.1661	0.4	0.04	0.71

Table A03. Sample #CCHC0105 ^{39}Ar/ ^{40}Ar Data

Padmore-UNLV, CCHC0105, single crystal, J = 0.00211863 ± 0.1751%

4 amu discrimination = 1.01784 ± 0.29%, 40/39K = 0.004667± 0.53927%, 36/37Ca = 0.0003059 ± 2.45%, 39/37Ca = 0.00068823 ± 1.84%

Crystal	T (C)	t (min.)	36Ar	37Ar	38Ar	39Ar	40Ar	%40Ar*	Ca/K	37d	start d	end d
1	1600	4	0.145	1.366	0.253	3.422	36.32	33.9	17.05	15.90	15.76	16.03
2	1600	4	0.183	1.174	0.354	3.315	44.58	20.3	15.12			
3	1600	4	0.175	1.171	0.230	3.015	39.62	16.1	16.59			
4	1600	4	0.133	1.215	1.526	3.659	38.04	46.0	14.18			
5	1600	4	0.096	0.590	0.192	1.857	18.04	40.3	13.56			
6	1600	4	0.148	1.066	0.215	2.089	33.72	20.4	21.83			
7	1600	4	0.161	1.404	0.365	2.784	40.92	22.5	21.57			
8	1600	4	0.203	1.473	0.268	3.632	53.01	17.2	17.33			
9	1600	4	0.141	1.459	0.403	4.403	39.3	34.6	14.15			
10	1600	4	0.106	1.060	0.174	2.149	19.35	15.6	21.09			

note: isotope beams in mV rlsd = released, error in age includes J error, all errors 1 sigma

(36Ar through 40Ar are measured beam intensities, corrected for decay in age calculations)

Table A03. Sample #CCHC0105 ^{39}Ar/ ^{40}Ar Data (continued)

Crystal	40Ar*/39ArK	Age (Ma)	1s.d.	anal err	37/39c	%39ArK	total39	mol 39Ar	Wmdata	WMs	wfactor	WxX
1	3.4999	13.33	0.64	0.64	6.288897	99.56	30.33	0	13.33	0.64	2.44	32.58
2	2.6841	10.23	0.58	0.58	5.579411	99.61		0	10.23	0.58	2.96	30.23
3	2.0630	7.87	0.55	0.55	6.118900	99.58		0	7.87	0.55	3.34	26.31
4	4.6563	17.71	3.47	3.47	5.231397	99.64		0	17.71	3.47	0.08	1.47
5	3.6642	13.95	0.92	0.92	5.005459	99.65		0	13.95	0.92	1.18	16.46
6	3.1956	12.17	1.32	1.32	8.039380	99.44		0	12.17	1.32	0.58	7.01
7	3.2541	12.40	0.58	0.58	7.945142	99.45		0	12.40	0.58	2.94	36.39
8	2.4868	9.48	0.47	0.47	6.389409	99.56		0	9.48	0.47	4.55	43.15
9	3.0250	11.53	0.51	0.5	5.220480	99.64		0	11.53	0.5	3.93	45.26
10	1.3407	5.12	0.64	0.64	7.770935	99.46		0	5.12	0.64	2.43	12.46
	Mean ± s.d. =	11.38	3.30									
									WtdMean	1sd	wJ	
									10.2868	0.2023	0.2	

Table A03. Sample #CCHC0105 ^{39}Ar/ ^{40}Ar Data (continued)

Crystal	39/40c	39/40err	36/40c	36/40err	R2	36c	39c	40c	%36err	%39err	%40err	36err
1	0.1	1.0028	0	2.3019	0.5144	0.07	3.41	34.04	0.96	0.51	0.76	0.0015
2	0.08	0.4054	0	1.4046	0.2761	0.11	3.3	42.30	0.74	0.12	0.24	0.0015
3	0.08	0.3565	0	1.2655	0.0199	0.10	3	37.34	0.63	0.20	0.05	0.0013
4	0.1	3.9100	0	4.7256	0.8835	0.06	3.65	35.76	1.25	1.27	3.47	0.0018
5	0.12	1.3918	0	4.6160	0.7593	0.03	1.85	15.77	1.02	0.05	1.19	0.0012
6	0.07	1.1499	0	2.9924	0.3195	0.08	2.08	31.45	1.41	0.78	0.74	0.0022
7	0.07	0.7680	0	1.1596	0.9216	0.09	2.77	38.65	0.28	0.03	0.67	0.0008
8	0.07	0.6659	0	0.8519	0.9637	0.13	3.62	50.73	0.16	0.03	0.57	0.0007
9	0.12	0.8343	0	2.4664	0.5343	0.07	4.39	37.01	1.02	0.24	0.7	0.0016
10	0.12	1.0268	0	2.6555	0.7721	0.03	2.14	17.08	0.54	0.33	0.82	0.0008

									4AMU	**39/40c**	**37/40c**	
									1.01784	1.00446	1.00892	

Table A03. Sample #CCHC0105 ^{39}Ar/ ^{40}Ar Data (continued)

Crystal	40err	%36err	%40err	K/Ca	WtdAge39Ar	% 39Ar rlsd		Age (Ma)
1	0.2764	2.13	0.81	0.06	1.5	11.3	1	13.33
2	0.1079	1.35	0.26	0.07	1.12	10.9	2	10.23
3	0.0204	1.23	0.05	0.06	0.78	9.9	3	7.87
4	1.3185	2.94	3.69	0.07	2.14	12.1	4	17.71
5	0.2145	4.4	1.36	0.07	0.85	6.1	5	13.95
6	0.2495	2.87	0.79	0.05	0.84	6.9	6	12.17
7	0.2746	0.87	0.71	0.05	1.14	9.2	7	12.40
8	0.3038	0.53	0.6	0.06	1.14	12.0	8	9.48
9	0.2751	2.33	0.74	0.07	1.67	14.5	9	11.53
10	0.1583	2.47	0.93	0.05	0.36	7.1	10	5.12
							mean=	11.38
							1s.d.=	3.30
							± 2 s.d. =	4.79
								17.97

Table A04. Sample #CCBSP0405 ^{39}Ar/ ^{40}Ar Data

Padmore-UNLV, CCBSP0405, single crystal, J = 0.00209167 ± 0.1296%

4 amu discrimination = 1.01784 ± 0.29%, 40/39K = 0.004667± 0.53927%, 36/37Ca = 0.0003059 ± 2.45%, 39/37Ca = 0.00068823 ± 1.84%

Crystal	T (C)	t (min.)	36Ar	37Ar	38Ar	39Ar	40Ar	%40Ar*	Ca/K	37d	start d	end d
1	**1600**	**4**	**0.052**	**0.147**	**0.428**	**21.099**	**57.40**	**99.3**	**0.29**	**15.73**	**15.7**	**15.76**
2	1600	4	0.105	0.417	0.089	1.452	20.98	35.2	12.12			
3	1600	4	0.066	0.550	0.100	3.011	12.53	89.2	7.7			
4	1600	4	0.095	0.465	0.118	2.151	15.92	33.0	9.12			
5	1600	4	0.107	0.550	0.149	3.255	26.77	48.4	7.12			
6	**1600**	**4**	**0.085**	**0.169**	**0.642**	**25.067**	**70.2**	**89.3**	**0.28**			
7	1600	4	0.117	0.924	0.203	5.409	33.11	51.1	7.2			
8	1600	4	0.167	0.853	0.297	3.002	41.05	24.1	11.99			
9	1600	4	0.115	0.495	0.148	1.967	22.21	24.5	10.62			
10	**1600**	**4**	**0.150**	**0.219**	**2.879**	**92.835**	**262.48**	**89.9**	**0.1**			
11	1600	4	0.163	1.002	0.316	6.273	46.51	36.3	6.73			
12	1600	4	0.410	1.432	0.376	3.000	115.56	12.6	20.19			

note: isotope beams in mV rlsd = released, error in age includes J error, all errors 1 sigma

(36Ar through 40Ar are measured beam intensities, corrected for decay in age calculations)

Table A04. Sample #CCBSP0405 ^{39}Ar/ ^{40}Ar Data (continued)

Crystal	40Ar*/39ArK	Age (Ma)	1s.d.	anal err	37/39c	%39ArK	total39	mol 39Ar	Wmdata	WMs	wfactor	WxX
1	**2.6483**	**9.97**	**0.06**	**0.06**	**0.108597**	**99.99**	**168.52**	**0**	**9.97**	**0.06**	**271.95**	**2710.23**
2	4.8405	18.17	1.91	1.91	4.476422	99.69		0	18.17	1.91	0.27	4.98
3	3.3414	12.57	0.40	0.4	2.847170	99.8		0	12.57	0.4	6.26	78.66
4	2.2629	8.52	1.04	1.04	3.369567	99.77		0	8.52	1.04	0.93	7.94
5	3.8145	14.34	0.41	0.41	2.633742	99.82		0	14.34	0.41	6.08	87.16
6	**2.4624**	**9.27**	**0.08**	**0.07**	**0.105086**	**99.99**		**0**	**9.27**	**0.07**	**182.46**	**1691.02**
7	3.0263	11.38	0.29	0.29	2.662665	99.82		0	11.38	0.29	12.09	137.61
8	3.2291	12.14	1.07	1.07	4.428941	99.69		0	12.14	1.07	0.87	10.61
9	2.6864	10.11	6.99	6.99	3.922495	99.73		0	10.11	6.99	0.02	0.21
10	**2.5370**	**9.55**	**0.10**	**0.1**	**0.036770**	**100**		**0**	**9.55**	**0.1**	**101.56**	**969.65**
11	2.6339	9.91	0.35	0.35	2.489740	99.83		0	9.91	0.35	8.27	81.96
12	4.8574	18.24	1.40	1.4	7.440178	99.49		0	18.24	1.4	0.51	9.25
	Mean ± s.d. =	12.01	3.17							**WtdMean**	**1sd**	**wJ**
	sanidine mean =	**9.59**	**0.02**							9.7913	0.0411	0.04

Table A04. Sample #CCBSP0405 ^{39}Ar/ ^{40}Ar Data (continued)

Crystal	39/40c	39/40err	36/40c	36/40err	R2	WtdAge39Ar	% 39Ar rlsd		Age (Ma)
1	0.38	0.4406	0	5.5631	0.2277	1.25	12.5	1	9.97
2	0.08	0.4721	0	6.7938	0.1441	0.16	0.9	2	18.17
3	0.29	0.5693	0	26.1190	0.3190	0.22	1.8	3	12.57
4	0.16	0.7250	0	7.4970	0.2738	0.11	1.3	4	8.52
5	0.13	0.6132	0	2.6444	0.5656	0.28	1.9	5	14.34
6	0.37	0.4573	0	6.5963	0.2852	1.38	14.9	6	9.27
7	0.17	0.4515	0	2.7289	0.3315	0.37	3.2	7	11.38
8	0.08	0.9866	0	2.8593	0.4103	0.22	1.8	8	12.14
9	0.1	0.8468	0	26.3938	0.0569	0.12	1.2	9	10.11
10	0.36	0.7542	0	6.0841	0.1891	5.26	55.1	10	9.55
11	0.14	1.0083	0	1.7443	0.5578	0.37	3.7	11	9.91
12	0.03	1.0780	0	1.0974	0.0404	0.32	1.8	12	18.24
								mean=	12.01
	4AMU	**39/40c**	**37/40c**					1s.d.=	3.17
	1.01784	1.00446	1.00892					± 2 s.d. =	5.67

Table A04. Sample #CCBSP0405 ^{39}Ar/ ^{40}Ar Data (continued)

							blank correction beam errors				
Crystal	**36c**	**39c**	**40c**	**%36err**	**%39err**	**%40err**	**36err**	**40err**	**%36err**	**%40err**	**K/Ca**
1	-0.02	21.1	55.03	1.20	0.11	0.3	0.0009	0.1722	-5.55	0.31	3.41
2	0.04	1.45	18.71	2.25	0.04	0.33	0.0024	0.0693	6.78	0.37	0.08
3	0.00	3.01	10.26	1.11	0.11	0.39	0.0010	0.0490	-26.11	0.48	0.13
4	0.03	2.15	13.65	1.92	0.12	0.56	0.0019	0.0892	7.46	0.65	0.11
5	0.04	3.25	24.49	0.70	0.09	0.49	0.0010	0.1307	2.57	0.53	0.14
6	0.02	25.07	67.82	1.12	0.05	0.34	0.0011	0.2373	6.58	0.35	3.52
7	0.05	5.4	30.82	0.91	0.03	0.32	0.0012	0.1063	2.69	0.34	0.14
8	0.10	2.99	38.77	1.52	0.42	0.8	0.0026	0.3268	2.72	0.84	0.08
9	0.05	1.96	19.94	10.45	0.31	0.66	0.0120	0.1462	26.38	0.73	0.09
10	0.08	92.83	259.79	3.28	0.20	0.66	0.0049	1.7324	6.04	0.67	10.07
11	0.09	6.26	44.22	0.77	0.56	0.75	0.0014	0.3479	1.53	0.79	0.15
12	0.34	2.98	113.28	0.84	1.02	0.19	0.0035	0.2196	1.04	0.19	0.05

Table A05. Sample #CCBM0305 ^{39}Ar/ ^{40}Ar Data

Crystal	T (C)	t (min.)	36Ar	37Ar	38Ar	39Ar	40Ar	%40Ar*	Ca/K	37d	start d	end d
1	1600	6	0.202	3.241	0.284	5.706	55.91	36.5	20.2	13.30	13.2	13.4
2	1600	3	0.428	2.990	0.290	6.178	116.7	11.0	17.2			
3	1600	3	0.092	1.052	0.129	2.521	17.17	45.8	14.82			
4	1600	3	0.135	2.426	0.206	5.443	34.29	41.4	15.83			
5	1600	3	0.166	3.527	0.245	5.974	45.24	38.7	21			
6	1600	3	0.127	1.967	0.245	4.026	29.9	38.0	17.36			
7	1600	3	0.198	5.532	0.539	13.316	73.19	53.5	14.75			
8	1600	3	0.369	5.546	0.369	11.974	55.41	58.9	16.45			

note: isotope beams in mV rlsd = released, error in age includes J error, all errors 1 sigma
(36Ar through 40Ar are measured beam intensities, corrected for decay in age calculations)

Crystal	40Ar*/39ArK	Age (Ma)	1s.d.	anal err	37/39c	%39ArK	total39	mol 39Ar	Wmdata	WMs	wfactor	WxX
1	3.4991	13.29	0.36	0.33	7.441507	99.49	55.14	0	13.29	0.33	8.93	118.62
2	2.0867	7.94	0.48	0.48	6.340696	99.56		0	7.94	0.48	4.42	35.12
3	2.9580	11.24	0.99	0.98	5.467094	99.62		0	11.24	0.98	1.04	11.72
4	2.5541	9.71	0.23	0.2	5.839372	99.6		0	9.71	0.2	24.62	239.12
5	2.8963	11.01	0.44	0.42	7.734886	99.46		0	11.01	0.42	5.65	62.21
6	2.6817	10.20	0.49	0.48	6.400947	99.56		0	10.20	0.48	4.31	43.94
7	2.9335	11.15	0.25	0.22	5.442796	99.62		0	11.15	0.22	20.79	231.75
8	2.7084	10.30	0.22	0.19	6.068121	99.58		0	10.30	0.19	28.72	295.73
	Mean ± s.d. =	10.60	1.43						**WtdMean**	**1sd**	**wJ**	
	Wtd mean =	10.16	0.30						10.5417	0.1008	0.15	
	(5 single crystals)	No isochron										

Table A05. Sample #CCBM0305 ^{39}Ar/ ^{40}Ar Data (continued)

Crystal	39/40c	39/40err	36/40c	36/40err	R2	WtdAge39Ar	% 39Ar rlsd		Age (Ma)
1	0.1	0.5032	0	1.2910	0.4033	1.38	10.3	1	13.29
2	0.05	0.4019	0	0.7236	0.1280	0.89	11.2	2	7.94
3	0.16	0.3762	0	8.1105	0.0106	0.51	4.6	3	11.24
4	0.16	0.5133	0	1.4267	0.3862	0.96	9.9	4	9.71
5	0.13	0.5384	0	2.3858	0.2943	1.19	10.8	5	11.01
6	0.14	0.5467	0	2.9204	0.6527	0.74	7.3	6	10.20
7	0.18	0.5808	0	1.9508	0.5046	2.69	24.2	7	11.15
8	0.22	0.4189	0.01	0.9139	0.3842	2.24	21.7	8	10.30
								mean=	10.60
	4AMU	**39/40c**	**37/40c**					1s.d.=	1.43
	1.03025	1.00756	1.01513					± 2 s.d. =	7.75
									13.45

blank correction beam errors

Crystal	36c	39c	40c	%36err	%39err	%40err	36err	40err	%36err	%40err	K/Ca
1	0.12	5.68	53.97	0.70	0.08	0.32	0.0014	0.1790	1.19	0.33	0.05
2	0.36	6.15	115.54	0.49	0.12	0.1	0.0022	0.1167	0.61	0.1	0.06
3	0.03	2.51	16.03	2.35	0.05	0.04	0.0022	0.0074	8.1	0.05	0.07
4	0.07	5.42	33.14	0.47	0.22	0.27	0.0009	0.0926	1.35	0.28	0.06
5	0.09	5.94	44.08	1.23	0.03	0.38	0.0021	0.1719	2.32	0.39	0.05
6	0.06	4.01	28.89	0.36	0.15	0.36	0.0017	0.1079	2.87	0.37	0.06
7	0.12	13.27	72.14	0.71	0.10	0.43	0.0022	0.3148	1.87	0.44	0.07
8	0.29	11.92	54.36	0.45	0.03	0.19	0.0023	0.1056	0.81	0.19	0.06

Table A06. Sample #CCBSO0105 ^{39}Ar/ ^{40}Ar Data

Crystal	T (C)	t (min.)	36Ar	37Ar	38Ar	39Ar	40Ar	%40Ar*	Ca/K	37d	start d	end d
1	1600	4	0.066	0.789	0.087	1.173	5.25	91.2	25.19	13.99	13.96	14.02
2	1600	4	0.073	0.756	0.061	1.693	7.9	64.4	16.68			
4	1600	4	0.088	0.716	0.054	1.736	10.46	50.0	15.41			
5	1600	4	0.088	1.382	0.059	2.885	14.83	72.6	17.9			
6	1600	4	0.070	0.944	0.053	1.970	9.06	100.0	17.91			
7	1600	4	0.072	0.821	0.034	1.130	7.84	88.6	27.22			
8	1600	4	0.072	1.337	0.065	2.689	10.56	99.0	18.59			
9	1600	4	0.075	1.347	0.061	2.725	11.91	91.0	18.48			
10	1600	4	0.060	1.273	0.056	2.362	8.35	99.7	20.16			
11	1600	4	0.092	1.870	0.079	3.912	17.34	46.5	17.87			

note: isotope beams in mV rlsd = released, error in age includes J error, all errors 1 sigma (36Ar through 40Ar are measured beam intensities, corrected for decay in age calculations)

Table A06. Sample #CCBSO0105 ^{39}Ar/ ^{40}Ar Data (continued)

40Ar*/39ArK	Age (Ma)	1s.d.	anal err	37/39c	%39ArK	total39	mol 39Ar	Wmdata	WMs	wfactor	WxX
3.2606	12.52	0.59	0.58	9.268575	99.36	22.28	0	12.52	0.58	2.98	37.3
2.6119	10.04	0.93	0.92	6.153168	99.57		0	10.04	0.92	1.17	11.75
2.6168	10.06	0.37	0.36	5.683257	99.61		0	10.06	0.36	7.62	76.68
3.3929	13.03	0.25	0.22	6.600794	99.54		0	13.03	0.22	20.04	261.1
3.8881	14.92	0.47	0.45	6.602976	99.54		0	14.92	0.45	5.03	75.02
5.0623	19.41	1.38	1.37	10.011489	99.31		0	19.41	1.37	0.53	10.37
3.3513	12.87	0.88	0.87	6.851325	99.53		0	12.87	0.87	1.32	16.97
3.5199	13.52	0.38	0.36	6.811379	99.53		0	13.52	0.36	7.77	105.04
2.9243	11.24	0.33	0.31	7.426471	99.49		0	11.24	0.31	10.41	116.96
1.9043	7.33	0.16	0.14	6.586834	99.54		0	7.33	0.14	49.92	365.68
Mean ± s.d. =	12.49	3.09						**WtdMean**	**1sd**	**wJ**	
Wtd mean =								10.0837	0.0968	0.13	

Table A06. Sample #CCBSO0105 ^{39}Ar/ ^{40}Ar Data (continued)

Crystal	39/40c	39/40err	36/40c	36/40err	R2	WtdAge39Ar	% 39Ar rlsd			Age (Ma)
1	0.31	0.4721	0	84.8083	0.0071	0.66	5.3		1	12.52
2	0.26	0.3999	0	14.0211	0.0960	0.76	7.6		2	10.04
4	0.19	0.5978	0	3.1009	0.8155	0.78	7.8		4	10.06
5	0.21	0.3967	0	3.6025	0.0753	1.69	13.0		5	13.03
6	0.26	0.4647	0	13.76	0.0457	1.32	8.8		6	14.92
7	0.17	0.4513	0	56.4943	0.0134	0.98	5.1		7	19.41
8	0.29	0.4157	0	756.4800	0.0300	1.55	12.1		8	12.87
9	0.26	0.4885	0	27.5383	0.2524	1.65	12.2		10	13.52
10	0.34	0.6189	0	15.9939	0.2528	1.19	10.6		11	11.24
11	0.24	0.4173	0	3.0668	0.0286	1.29	17.6		12	7.33

	4AMU	39/40c	37/40c
	1.03025	1.00756	1.01513

mean= 12.49

1s.d.= 3.09

± 2 s.d. = 6.31

18.67

Table A06. Sample #CCBSO0105 ^{39}Ar/ ^{40}Ar Data (continued)

| Crystal | 36c | 39c | 40c | %36err | %39err | %40err | blank correction beam errors | | | | K/Ca |
							36err	40err	%36err	%40err	
1	0.00	1.17	3.77	0.10	0.14	0.01	0.0005	0.0097	84.81	0.26	0.04
2	0.00	1.69	6.42	0.07	0.01	0.01	0.0005	0.0097	14.02	0.15	0.06
4	0.02	1.73	8.98	0.27	0.05	0.39	0.0006	0.0419	3.04	0.47	0.06
5	0.02	2.87	13.34	0.27	0.11	0.05	0.0006	0.0122	3.58	0.09	0.06
6	0.01	1.96	7.58	0.90	0.22	0.1	0.0008	0.0133	13.76	0.18	0.06
7	0.00	1.12	6.37	1.81	0.19	0.07	0.0014	0.0111	56.49	0.18	0.04
8	0.00	2.68	9.08	2.84	0.09	0.11	0.0021	0.0151	756.48	0.17	0.05
9	0.00	2.71	10.43	0.96	0.07	0.26	0.0009	0.0325	27.53	0.31	0.05
10	0.00	2.35	6.86	0.84	0.29	0.31	0.0007	0.0276	15.98	0.4	0.05
11	0.02	3.89	15.85	0.17	0.18	0.03	0.0005	0.0110	3.04	0.07	0.06

Table A07. Sample #CCBD0205 ^{39}Ar/ ^{40}Ar Data

Padmore-UNLV, CCBD0205, single crystal, J = 0.00211953 ± 1.0432%

4 amu discrimination = 1.03025 ± 0.37%, 40/39K = 0.004667± 0.53927%, 36/37Ca = 0.0003059 ± 2.45%, 39/37Ca = 0.00068823 ± 1.84%

Crystal	T (C)	t (min.)	36Ar	37Ar	38Ar	39Ar	40Ar	%40Ar*	Ca/K	37d	start d	end d
1	1600	4	0.075	0.557	0.144	3.214	15.00	92.8	6.32	13.70	13.67	13.73
2	1600	4	0.111	0.978	0.115	2.202	19.18	38.5	16.25			
3	1600	4	0.091	0.429	0.753	47.641	131.44	95.4	0.33			
4	1600	4	0.115	0.250	0.448	19.206	65.89	80.0	0.47			
5	1600	4	0.116	1.254	0.115	2.903	22.21	42.2	15.8			
6	1600	4	0.076	0.741	0.203	5.420	19.39	94.2	4.99			
7	1600	4	0.417	0.226	1.012	70.818	285.3	64.8	0.12			
8	1600	4	0.191	2.365	0.452	10.421	65.93	50.1	8.29			
9	1600	4	0.074	0.194	0.705	53.436	141.43	99.0	0.13			
10	1600	4	0.092	0.280	0.280	22.612	67.28	90.5	0.45			
11	1600	4	0.081	0.203	0.850	61.966	166.53	98.0	0.12			
12	1600	4	0.104	0.263	1.170	83.393	220.67	95.4	0.11			
13	1600	4	0.221	0.311	1.504	104.715	309.43	85.8	0.11			
14	1600	5	0.187	0.460	1.137	74.960	227.36	85.1	0.22			

note: isotope beams in mV rlsd = released, error in age includes J error, all errors 1 sigma
(36Ar through 40Ar are measured beam intensities, corrected for decay in age calculations)

Table A07. Sample #CCBD0205 ^{39}Ar/ ^{40}Ar Data (continued)

Crystal	40Ar*/39ArK	Age (Ma)	1s.d.	anal err	37/39c	%39ArK	total39	mol 39Ar	Wmdata	WMs	wfactor	WxX
1	3.8938	14.83	0.36	0.32	2.338796	99.84	562.91	0	14.83	0.32	9.66	143.24
2	3.1105	11.86	0.49	0.47	5.993832	99.59		0	11.86	0.47	4.47	52.97
3	2.6172	9.98	0.12	0.07	0.121523	99.99		0	9.98	0.07	233.11	2326.44
4	2.6924	10.27	0.13	0.08	0.175665	99.99		0	10.27	0.08	160.78	1650.57
5	3.0287	11.54	0.39	0.37	5.829530	99.6		0	11.54	0.37	7.39	85.34
6	3.1097	11.85	0.24	0.2	1.845024	99.87		0	11.85	0.2	24.46	289.91
7	2.6130	9.96	0.14	0.09	0.043067	100		0	9.96	0.09	130.01	1295.45
8	3.1179	11.88	0.24	0.21	3.062702	99.79		0	11.88	0.21	23.68	281.37
9	2.6075	9.94	0.12	0.07	0.048995	100		0	9.94	0.07	216.59	2153.54
10	2.6432	10.08	0.13	0.07	0.167110	99.99		0	10.08	0.07	187.66	1891.45
11	2.6233	10.00	0.12	0.05	0.044211	100		0	10.00	0.05	389.59	3897.06
12	2.5225	9.62	0.11	0.05	0.042561	100		0	9.62	0.05	404.42	3890.48
13	2.5388	9.68	0.11	0.05	0.040081	100		0	9.68	0.05	389.49	3771.03
14	2.5801	9.84	0.12	0.05	0.082815	99.99		0	9.84	0.05	342.36	3368.44
	Mean ± s.d. =	10.81	1.40						WtdMean	1sd	wJ	
									9.9448	0.0199	0.11	

Table A07. Sample #CCBD0205 ^{39}Ar/ ^{40}Ar Data (continued)

Crystal	39/40c	39/40err	36/40c	36/40err	R2	36c	39c	40c	%36err	%39err	%40err	36err
1	0.25	0.6424	0	11.1707	0.7515	0.01	3.21	12.72	0.23	0.23	0.4	0.0006
2	0.13	0.6156	0	1.6414	0.7404	0.04	2.19	16.91	0.10	0.29	0.35	0.0006
3	0.37	0.4332	0	6.7439	0.1315	0.02	47.64	128.96	1.50	0.07	0.21	0.0015
4	0.3	0.4137	0	1.4415	0.4992	0.05	19.2	63.54	0.20	0.10	0.15	0.0007
5	0.14	0.4822	0	1.9268	0.4822	0.04	2.89	19.93	0.47	0.07	0.27	0.0008
6	0.31	0.4856	0	11.9723	0.4822	0.01	5.41	17.10	0.47	0.07	0.27	0.0007
7	0.25	0.3735	0	1.1727	0.0021	0.35	70.82	282.71	0.92	0.05	0.01	0.0039
8	0.16	0.5940	0	1.2656	0.4911	0.11	10.4	63.62	0.60	0.21	0.4	0.0013
9	0.38	0.3762	0	38.0130	0.0175	0.01	53.43	138.92	3.07	0.03	0.06	0.0024
10	0.35	0.4132	0	3.3436	0.1920	0.02	22.61	64.91	0.55	0.11	0.14	0.0008
11	0.38	0.3711	0	7.3236	0.0154	0.01	61.96	163.98	0.92	0.02	0.02	0.0010
12	0.38	0.4044	0	1.7878	0.7468	0.04	83.39	218.02	0.14	0.02	0.16	0.0006
13	0.34	0.3727	0	0.6870	0.0308	0.15	104.71	306.68	0.29	0.04	0.02	0.0009
14	0.33	0.3772	0	0.9217	0.1581	0.12	74.96	224.75	0.42	0.02	0.07	0.0010

Table A07. Sample #CCBD0205 ^{39}Ar/ ^{40}Ar Data (continued)

Blank correction beam errors

Crystal	36c	39c	40c	%36err	%39err	%40err	36err	40err	%36err	%40err	K/Ca
1	0.01	3.21	12.72	0.23	0.23	0.4	0.0006	0.0601	11.15	0.47	0.16
2	0.04	2.19	16.91	0.10	0.29	0.35	0.0006	0.0672	1.55	0.4	0.06
3	0.02	47.64	128.96	1.50	0.07	0.21	0.0015	0.2760	6.73	0.21	3.05
4	0.05	19.2	63.54	0.20	0.10	0.15	0.0007	0.0989	1.38	0.16	2.11
5	0.04	2.89	19.93	0.47	0.07	0.27	0.0008	0.0600	1.87	0.3	0.06
6	0.01	5.41	17.10	0.47	0.07	0.27	0.0007	0.0524	11.96	0.31	0.2
7	0.35	70.82	282.71	0.92	0.05	0.01	0.0039	0.0287	1.11	0.01	8.6
8	0.11	10.4	63.62	0.60	0.21	0.4	0.0013	0.2637	1.14	0.41	0.12
9	0.01	53.43	138.92	3.07	0.03	0.06	0.0024	0.0849	38.01	0.06	7.56
10	0.02	22.61	64.91	0.55	0.11	0.14	0.0008	0.0942	3.32	0.15	2.22
11	0.01	61.96	163.98	0.92	0.02	0.02	0.0010	0.0334	7.31	0.02	8.38
12	0.04	83.39	218.02	0.14	0.02	0.16	0.0006	0.3531	1.74	0.16	8.7
13	0.15	104.71	306.68	0.29	0.04	0.02	0.0009	0.0619	0.58	0.02	9.24
14	0.12	74.96	224.75	0.42	0.02	0.07	0.0010	0.1592	0.84	0.07	4.47

Table A07. Sample #CCBD0205 ^{39}Ar/ ^{40}Ar Data (continued)

Crystal	WtdAge39Ar	% 39Ar rlsd	Age (Ma)			
1	0.08	0.6	14.83			
2	0.05	0.4	11.86			
3	0.84	8.5	9.98			
4	0.35	3.4	10.27			
5	0.06	0.5	11.54	**4AMU**	**39/40c**	**37/40c**
6	0.11	1.0	11.85	1.03025	1.00756	1.01513
7	1.25	12.6	9.96			
8	0.22	1.9	11.88	mean=	10.81	
9	0.94	9.5	9.94	1s.d.=	1.40	
10	0.4	4.0	10.08	± 2 s.d. =	8.02	
11	1.1	11.0	10.00		13.60	
12	1.43	14.8	9.62			
13	1.8	18.6	9.68			
14	1.31	13.3	9.84			

Table A08. Sample CCBSC0606 ^{39}Ar/^{40}Ar Data

Padmore-UNLV, CCBSC0606, single crystal plagioclase, J = 0.00211321 ± 1.0766%

4 amu discrimination = 1.03025 ± 0.37%, 40/39K = 0.004667± 0.53927%, 36/37Ca = 0.0003059 ± 2.45%, 39/37Ca = 0.00068823 ± 1.84%

Crystal	T (°C)	t(min.)	^{36}Ar	^{37}Ar	^{38}Ar	^{39}Ar	^{40}Ar	%40Ar*	Ca/K			
1	1600	6	0.202	3.241	0.284	5.706	55.91	36.5	20.2			
2	1600	3	0.428	2.990	0.290	6.178	116.7	11.0	17.2			
3	1600	3	0.092	1.052	0.129	2.521	17.17	45.8	14.82			
4	1600	3	0.135	2.426	0.206	5.443	34.29	41.4	15.83			
5	1600	3	0.166	3.527	0.245	5.974	45.24	38.7	21	Mean ± s.d.	10.60	1.43
6	1600	3	0.127	1.967	0.245	4.026	29.9	38.0	17.36	Wtd mean	10.16	0.30
7	1600	3	0.198	5.532	0.539	13.316	73.19	53.5	14.75			
8	1600	3	0.369	5.546	0.369	11.974	55.41	58.9	16.45			

Crystal	^{40}Ar*/^{39}ArK	Age (Ma)	1s.d.	anal err	37/39c	%^{39}ArK	total39	mol ^{39}Ar	Wmdata	WMs	wfactor	WxX
1	3.4991	13.29	0.36	0.33	7.441507	99.49	55.14	0	13.29	0.33	8.93	118.62
2	2.0867	7.94	0.48	0.48	6.340696	99.56		0	7.94	0.48	4.42	35.12
3	2.9580	11.24	0.99	0.98	5.467094	99.62		0	11.24	0.98	1.04	11.72
4	2.5541	9.71	0.23	0.2	5.839372	99.6		0	9.71	0.2	24.62	239.12
5	2.8963	11.01	0.44	0.42	7.734886	99.46		0	11.01	0.42	5.65	62.21
6	2.6817	10.20	0.49	0.48	6.400947	99.56		0	10.20	0.48	4.31	43.94
7	2.9335	11.15	0.25	0.22	5.442796	99.62		0	11.15	0.22	20.79	231.75
8	2.7084	10.30	0.22	0.19	6.068121	99.58		0	10.30	0.19	28.72	295.73
									WtdMean	**1sd**	**wJ**	
									10.5417	0.1008	0.15	

Table A08. Sample CCBSC0606 ^{39}Ar/ ^{40}Ar Data (continued)

Blank correction beam errors

Step	40err	%36err	%40err	K/Ca	WtdAge39Ar	% 39Ar rlsd	Age (Ma)			
1	0.0601	11.15	0.47	0.16	0.08	0.6	14.83			
2	0.0672	1.55	0.4	0.06	0.05	0.4	11.86			
3	0.2760	6.73	0.21	3.05	0.84	8.5	9.98			
4	0.0989	1.38	0.16	2.11	0.35	3.4	10.27			
5	0.0600	1.87	0.3	0.06	0.06	0.5	11.54	**4AMU**	**39/40c**	**37/40c**
6	0.0524	11.96	0.31	0.2	0.11	1.0	11.85	1.03025	1.00756	1.01513
7	0.0287	1.11	0.01	8.6	1.25	12.6	9.96			
8	0.2637	1.14	0.41	0.12	0.22	1.9	11.88	mean=	10.81	
9	0.0849	38.01	0.06	7.56	0.94	9.5	9.94	1s.d.=	1.40	
10	0.0942	3.32	0.15	2.22	0.4	4.0	10.08	± 2 s.d. =	8.02	
11	0.0334	7.31	0.02	8.38	1.1	11.0	10.00		13.60	
12	0.3531	1.74	0.16	8.7	1.43	14.8	9.62			
13	0.0619	0.58	0.02	9.24	1.8	18.6	9.68			
14	0.1592	0.84	0.07	4.47	1.31	13.3	9.84			

Table A09. Sample #CCTC00105 ^{39}Ar/ ^{40}Ar Data

Padmore-UNLV, CCTC0105, single crystal, J = 0.00213473 ± 0.2300%
4 amu discrimination = 1.01784 ± 0.29%, 40/39K = 0.004667± 0.53927%, 36/37Ca = 0.0003059 ± 2.45%, 39/3
7Ca = 0.00068823 ± 1.84%

Crystal	T (C)	t (min.)	^{36}Ar	^{37}Ar	^{38}Ar	^{39}Ar	^{40}Ar	%^{40}Ar*	Ca/K
1	1600	4	0.308	0.349	6.083	491.438	874.73	91.5	0.0305505
2	1600	4	0.089	0.283	3.540	283.811	473.058	98.0	0.0428963
3	1600	4	0.089	0.289	3.952	320.295	531.3	98.7	0.0388159
4	1600	4	0.190	1.634	3.679	281.130	503.47	92.6	0.2500522
5	1600	4	0.083	0.288	4.233	344.370	567.151	98.6	0.0359774
6	1600	4	0.095	0.291	4.120	330.320	543.572	97.9	0.0378984
7	1600	4	0.092	0.227	2.083	167.883	284.664	96.5	0.0581679
8	1600	4	0.092	0.266	2.855	225.747	374.69	97.3	0.0506901
9	1600	4	0.137	0.290	3.613	285.523	494.73	95.2	0.0436938
10	1600	4	0.126	0.344	5.410	437.260	732.733	97.1	0.0338439
11	1600	4	0.098	0.279	0.359	290.133	484.58	97.5	0.0413685
12	1600	4	0.096	0.333	4.668	376.568	626.31	98.1	0.038042

note: isotope beams in mV rlsd = released, error in age includes J error, all errors 1 sigma
(^{36}Ar through ^{40}Ar are measured beam intensities, corrected for decay in age calculations)

Table A.09 CCTC0105 ^{39}Ar/ ^{40}Ar Data (continued)

Crystal	T (C)	t (min.)	36Ar	37Ar	38Ar	39Ar	40Ar	%40Ar*	Ca/K	37d	start d	end d
1	1600	4	0.075	0.557	0.144	3.214	15.00	92.8	6.324984874	13.70	13.673	13.726
2	1600	4	0.111	0.978	0.115	2.202	19.183	38.5	16.25074143			
3	1600	4	0.091	0.429	0.753	47.641	131.441	95.4	0.328140443			
4	1600	4	0.115	0.250	0.448	19.206	65.893	80.0	0.474354135			
5	1600	4	0.116	1.254	0.115	2.903	22.21	42.2	15.80347403			
6	1600	4	0.076	0.741	0.203	5.420	19.391	94.2	4.987931746			
7	1600	4	0.417	0.226	1.012	70.818	285.304	64.8	0.116285226			
8	1600	4	0.191	2.365	0.452	10.421	65.932	50.1	8.286857109			
9	1600	4	0.074	0.194	0.705	53.436	141.43	99.0	0.132290705			
10	1600	4	0.092	0.280	0.280	22.612	67.282	90.5	0.451248831			
11	1600	4	0.081	0.203	0.850	61.966	166.53	98.0	0.119372057			
12	1600	4	0.104	0.263	1.170	83.393	220.67	95.4	0.114917391			
13	1600	4	0.221	0.311	1.504	104.715	309.43	85.8	0.108220704			
14	1600	5	0.187	0.460	1.137	74.960	227.36	85.1	0.223614498			

note: isotope beams in mV rlsd = released, error in age includes J error, all errors 1 sigma

(36Ar through 40Ar are measured beam intensities, corrected for decay in age calculations)

Table A.09 CCTC0105 ^{39}Ar/ ^{40}Ar Data (continued)

Crystal	40Ar*/ 39ArK	Age (Ma)	1s.d.	anal err	37/39c	%39ArK	total39	mol 39Ar	Wm data	WMs	wfactor	WxX
1	3.8938	14.83	0.36	0.3217473	2.338796	99.838179	562.91	1.928E-16	14.83	0.321747316	9.659844	143.2362
2	3.1105	11.86	0.49	0.4731029	5.993832	99.585287		1.321E-16	11.86	0.473102943	4.467748	52.96516
3	2.6172	9.98	0.12	0.0654968	0.121523	99.991592		2.858E-15	9.98	0.065496753	233.1098	2326.435
4	2.6924	10.27	0.13	0.0788649	0.175665	99.987846		1.152E-15	10.27	0.078864947	160.78	1650.567
5	3.0287	11.54	0.39	0.3677857	5.829530	99.596655		1.742E-16	11.54	0.36778572	7.392822	85.34274
6	3.1097	11.85	0.24	0.2021933	1.845024	99.872343		3.252E-16	11.85	0.20219331	24.46056	289.9066
7	2.6130	9.96	0.14	0.0877015	0.043067	99.99702		4.249E-15	9.96	0.087701492	130.0128	1295.447
8	3.1179	11.88	0.24	0.2055068	3.062702	99.788092		6.253E-16	11.88	0.205506841	23.67813	281.3672
9	2.6075	9.94	0.12	0.0679489	0.048995	99.99661		3.206E-15	9.94	0.067948851	216.5887	2153.541
10	2.6432	10.08	0.13	0.072998	0.167110	99.988438		1.357E-15	10.08	0.07299803	187.6626	1891.451
11	2.6233	10.00	0.12	0.0506637	0.044211	99.996941		3.718E-15	10.00	0.050663666	389.5891	3897.06
12	2.5225	9.62	0.11	0.0497263	0.042561	99.997055		5.004E-15	9.62	0.049726305	404.4153	3890.476
13	2.5388	9.68	0.11	0.0506702	0.040081	99.997227		6.283E-15	9.68	0.050670208	389.4885	3771.028
14	2.5801	9.84	0.12	0.0540457	0.082815	99.99427		4.498E-15	9.84	0.054045707	342.3557	3368.438
Mean ± s.d. =		10.81	1.40									

	WtdMean	1sd	wJ
	9.9448	0.0199	0.105636

Table A.09 CCTC0105 ^{39}Ar/ ^{40}Ar Data (continued)

Crystal	39/40c	39/40err	36/40c	36/40err	R2
1	0.250328	0.6424	0.0004323	11.1707	0.7515
2	0.128703	0.6156	0.0022904	1.6414	0.7404
3	0.366634	0.4332	0.0001671	6.7439	0.1315
4	0.29996	0.4137	0.0007172	1.4415	0.4992
5	0.143953	0.4822	0.0021301	1.9268	0.4822
6	0.314126	0.4856	0.0003345	11.9723	0.4822
7	0.24861	0.3735	0.0011984	1.1727	0.0021
8	0.162223	0.5940	0.0017406	1.2656	0.4911
9	0.38176	0.3762	4.323E-05	38.0130	0.0175
10	0.345687	0.4132	0.0003563	3.3436	0.1920
11	0.375036	0.3711	7.783E-05	7.3236	0.0154
12	0.379624	0.4044	0.0001598	1.7878	0.7468
13	0.338881	0.3727	0.0004833	0.6870	0.0308
14	0.33101	0.3772	0.0005099	0.9217	0.1581

Table A.09 CCTC0105 ^{39}Ar/ ^{40}Ar Data (continued)

Step	40err	%36err	%40err	K/Ca	WtdAge 39Ar	% 39Ar rlsd	Age (Ma)	4AMU	39/40c	37/40c
1	0.0601	11.15461	0.4721464	0.1581031	0.08466	0.6	14.83			
2	0.0672	1.548937	0.3974039	0.0615357	0.04637	0.4	11.86			
3	0.2760	6.730349	0.2140585	3.0474756	0.84465	8.5	9.98			
4	0.0989	1.384488	0.1556174	2.1081296	0.35027	3.4	10.27			
5	0.0600	1.866832	0.3011696	0.0632772	0.05953	0.5	11.54	**4AMU**	**39/40c**	**37/40c**
6	0.0524	11.96266	0.3065706	0.2004839	0.11412	1.0	11.85	1.03025	1.00756	1.01513
7	0.0287	1.112805	0.0101411	8.5995447	1.25355	12.6	9.96			
8	0.2637	1.137092	0.4145577	0.120673	0.21999	1.9	11.88	mean=	10.81	
9	0.0849	38.01114	0.061119	7.5591101	0.94388	9.5	9.94	1s.d.=	1.40	
								± 2 s.d.		
10	0.0942	3.319868	0.1451735	2.2160722	0.40487	4.0	10.08	=	8.02	
11	0.0334	7.314176	0.0203842	8.3771699	1.10115	11.0	10.00		13.60	
12	0.3531	1.741582	0.1619516	8.7019031	1.42517	14.8	9.62			
13	0.0619	0.57854	0.0202005	9.2403761	1.8011	18.6	9.68			
14	0.1592	0.84121	0.070825	4.471982	1.31022	13.3	9.84			

THERMAL IONIZATION MASS SPECTROMETRY RESULTS

Sr data are referenced to NBS-987 ^{87}Sr/^{86}Sr = 0.71025, and Nd data are referenced to La

Jolla Nd ^{143}Nd/^{144}Nd = 0.511860. For both systems, the data reported are adjusted to agree with

these values. Analyses for Sr and Nd are internally consistent to $\pm$ 20 ppm (~0.000020 for

^{87}Sr/^{86}Sr and ~0.000010 for ^{143}Nd/^{144}Nd). Blanks run concurrently with samples were all

less than 200 pg for Sr, and less than 100 pg for Sm and Nd. Sr isotopic compositions are

normalized to ^{86}Sr/^{88}Sr = 0.1194. Nd data are presented as present-day isotopic compositions

and as eNdt (normalized to ^{146}Nd/^{144}Nd = 0.7219 and ^{143}Nd/^{144}Nd = 0.512638 for CHUR), where

't' is the age of the sample. Pb data are normalized using NBS-981 with ^{207}Pb/^{206}Pb = 0.91464.

Average fractionation for repeat runs on the standard is 0.11 $\pm$ 0.05/amu. Blanks run with

samples are typically 20 pg or less.

Table B.01 Thermal Ionization Mass Spectrometry Results

Sample	Age (Ma)	143/144 corr	Tot. Sm (ppm)	Tot. Nd (ppm)	Sm/Nd (Wt.)	εNd (NOW)	εNd (AGE)	εNd (DM)
CCTC 0105	8	0.512528	2.11	14.35	0.1469	-2.15	-2.04	6.68
CCBSC 0605	8	0.512448	2.73	22.54	0.1212	-3.70	-3.57	6.64
CCBSP 0105	8	0.512424	5.16	30.67	0.1683	-4.17	-4.08	6.14
CCHC 0105	8	0.512497	2.14	13.71	0.1558	-2.76	-2.69	6.51
CCBSP 0405	8	0.512521	3.00	17.24	0.1737	-2.28	-2.19	6.42
CCBSP 0505	8	0.512520	2.25	13.49	0.1669	-2.31	-2.21	6.48
CCBSC 0105	8	0.512552	2.65	14.24	0.1864	-1.68	-1.60	6.39
CCBSC 0205	8	0.512549	2.49	16.57	0.1500	-1.73	-1.63	6.73
CCBSC 0606	8	0.512528	2.13	12.65	0.1685	-2.15	-2.05	6.49
CCBSP 0305	8	0.512590	2.38	13.53	0.1756	-0.93	-0.83	6.65
CCHC 0305	8	0.512507	2.64	15.18	0.1737	-2.56	-2.46	6.36
CCBSC 0602	8	0.512560	2.67	14.30	0.1866	-1.53	-1.44	6.42
CCBSC 0604	8	0.512613	2.66	13.75	0.1937	-0.49	-0.41	6.55
BM0305	8	0.512584	5.37	36.88	0.1457	-1.05	-0.94	6.87
CCBSC 0601	8	0.512561	2.03	10.84	0.1870	-1.50	-1.42	6.42
CCBD 0205	8	0.512566	3.19	20.06	0.1589	-1.41	-1.31	6.71

Table B.01 Thermal Ionization Mass Spectrometry Results (continued)

Sample	87Sr/86Sr meas	87Sr/86Sr cor	(206/204)obs	206/204corr	error
CCTC 0105	0.706089	0.706093	17.791	17.830	0.018
CCBSC 0605	0.705445	0.705448	17.964	18.004	0.018
CCBSP 0105	0.705869	0.705873	18.040	18.079	0.018
CCHC 0105	0.705844	0.705848	18.031	18.071	0.018
CCBSP 0405	0.707582	0.707586	18.143	18.183	0.018
CCBSP 0505	0.706501	0.706505	18.188	18.228	0.018
CCBSC 0105	0.709281	0.709285	18.137	18.177	0.018
CCBSC 0205	0.705634	0.705637	18.047	18.087	0.018
CCBSC 0606	0.706549	0.706553	18.120	18.160	0.018
CCBSP 0305	0.709278	0.709282	18.162	18.202	0.018
CCHC 0305	0.706924	0.706928	18.223	18.263	0.018
CCBSC 0602	0.709787	0.709791	18.161	18.201	0.018
CCBSC 0604	0.708853	0.708857	18.136	18.176	0.018
BM0305	0.704680	0.704684	18.181	18.221	0.018
CCBSC 0601	0.709335	0.709339	18.151	18.191	0.018
CCBD 0205	0.705181	0.705184	18.275	18.315	0.018

Table B.01 Thermal Ionization Mass Spectrometry Results (continued)

Sample	207/204	207/204 corr	error	208/204	208/204 corr	error
CCTC 0105	15.459	15.510	0.023	37.472	37.637	0.075
CCBSC 0605	15.479	15.530	0.023	37.608	37.773	0.076
CCBSP 0105	15.462	15.513	0.023	37.634	37.800	0.076
CCHC 0105	15.478	15.529	0.023	37.647	37.813	0.076
CCBSP 0405	15.471	15.522	0.023	37.698	37.864	0.076
CCBSP 0505	15.466	15.517	0.023	37.702	37.868	0.076
CCBSC 0105	15.462	15.513	0.023	37.744	37.910	0.076
CCBSC 0205	15.499	15.550	0.023	37.746	37.912	0.076
CCBSC 0606	15.502	15.553	0.023	37.759	37.925	0.076
CCBSP 0305	15.495	15.546	0.023	37.768	37.934	0.076
CCHC 0305	15.495	15.546	0.023	37.790	37.956	0.076
CCBSC 0602	15.487	15.538	0.023	37.818	37.984	0.076
CCBSC 0604	15.485	15.536	0.023	37.821	37.987	0.076
BM0305	15.469	15.520	0.023	37.826	37.992	0.076
CCBSC 0601	15.489	15.540	0.023	37.839	38.005	0.076
CCBD 0205	15.501	15.552	0.023	37.931	38.098	0.076

APPENDIX C

MAJOR AND TRACE ELEMENT X-RAY REFRACTION RAW DATA

CCBD0205

1/16/2007 3:09:51 PM
PANalytical
View result

Type: Routine
Archive: rhybas
Application: rhybas
Sample: ccbd0205
Sum (%): 99.3453
Init weight: 1.0002 g
Flux weight: 6.0004 g
Final weight: 7.0006 g

Compound Value Unit Status

SiO2   72.97 %
Al2O3   13.99 %
TiO2   0.242 %
Fe2O3   1.31 %
MgO   0.25 %
Na2O   5.12 %
K2O   4.68 %
MnO   0.069 %
CaO   0.67 %
P2O5   0.052 %
1/16/2007 3:33:27 PM
PANalytical
View result

Type: Routine
Archive: Trace1a
Application: trace1
Sample: ccbd0205
Sum (%): 99.6622
Init weight: 12 g
Flux weight: 3 g
Final weight: 15 g

Compound Value   Unit Status

Sc   0.741 ppm
V   4.212 ppm
Ni   5.641 ppm
Cu   4.222 ppm

Ga   17.134 ppm
Rb   101.052 ppm
Sr   86.711 ppm
Y   23.865 ppm
Zr   209.700 ppm
Nb   54.112 ppm
Ba   550.133 ppm
La   46.964 ppm
Hf   4.885 ppm
Pb   22.249 ppm
Th   21.844 ppm
U   5.870 ppm
Meas. LOI   0.140 %
BM0305
1/16/2007 3:10:18 PM
PANalytical
View result

Type: Routine
Archive: rhybas
Application: rhybas
Sample: bm0305
Sum (%): 93.7037
Init weight: 1.0003 g
Flux weight: 6.0002 g
Final weight: 7.0005 g

Compound Value Unit Status

SiO2   63.79 %
Al2O3   14.96 %
TiO2   0.509 %
Fe2O3   2.37 %
MgO   0.47 %
Na2O   5.77 %
K2O   3.91 %
MnO   0.103 %
CaO   1.64 %
P2O5   0.173 %

BM0305B
1/16/2007 3:41:05 PM
PANalytical
View result

Type: Routine

Archive: rhybas2
Application: rhybas
Sample: bm0305
Sum (%): 98.6594
Init weight: 1 g
Flux weight: 6 g
Final weight: 7 g

Compound Value Unit Status

SiO2   67.32 %
Al2O3   15.96 %
TiO2   0.513 %
Fe2O3   2.47 %
MgO   0.55 %
Na2O   5.94 %
K2O   3.96 %
MnO   0.104 %
CaO   1.66 %
P2O5   0.171 %

BMO305/16/2007 3:35:10 PM
PANalytical
View result

Type: Routine
Archive: Trace1a
Application: trace1
Sample: bm0305
Sum (%): 99.3414
Init weight: 12 g
Flux weight: 3 g
Final weight: 15 g

Compound Value   Unit Status

Sc   2.816 ppm
V   34.628 ppm
Ni   4.512 ppm
Cu   2.911 ppm
Ga   18.004 ppm
Rb   74.066 ppm
Sr   483.283 ppm
Y   24.614 ppm
Zr   341.326 ppm
Nb   52.395 ppm

Ba   1558.209 ppm
La   72.122 ppm
Hf   9.914 ppm
Pb   20.956 ppm
Th   19.125 ppm
U   7.039 ppm
Meas. LOI   0.340 %

CCBSC0105
1/16/2007 3:08:08 PM
PANalytical
View result

Type: Routine
Archive: rhybas
Application: rhybas
Sample: ccbsc0105
Sum (%): 99.6586
Init weight: 1 g
Flux weight: 6 g
Final weight: 7 g

Compound Value Unit Status

SiO2   77.28 %
Al2O3   11.90 %
TiO2   0.109 %
Fe2O3   0.73 %
MgO   0.06 %
Na2O   1.97 %
K2O   7.31 %
MnO   0.041 %
CaO   0.23 %
P2O5   0.018 %
CCBSC0105
1/16/2007 3:31:59 PM
PANalytical
View result

Type: Routine
Archive: Trace1a
Application: trace1
Sample: ccbsc0105
Sum (%): 100.1108
Init weight: 12 g

Flux weight: 3 g
Final weight: 15 g

Compound Value   Unit Status

Sc   0.332 ppm
V   negative ppm
Ni   5.648 ppm
Cu   4.487 ppm
Ga   11.974 ppm
Rb   285.195 ppm
Sr   44.342 ppm
Y   18.651 ppm
Zr   93.423 ppm
Nb   45.916 ppm
Ba   314.182 ppm
La   22.392 ppm
Hf   2.633 ppm
Pb   25.473 ppm
Th   21.747 ppm
U   6.748 ppm
Meas. LOI   0.300 %

CCBSC0205
1/16/2007 3:38:28 PM
PANalytical
View result

    Type: Routine
   Archive: rhybas2
 Application: rhybas
    Sample: ccbsc0205
    Sum (%): 96.1241
 Init weight: 1 g
 Flux weight: 6 g
Final weight: 7 g

Compound Value Unit Status

SiO2   70.88 %
Al2O3   13.65 %
TiO2   0.218 %
Fe2O3   1.26 %
MgO   0.38 %

Na2O   4.49 %
K2O   4.01 %
MnO   0.064 %
CaO   1.13 %
P2O5   0.051 %
BSC 0205
1/16/2007 3:07:45 PM
PANalytical
View result

    Type: Routine
   Archive: rhybas
 Application: rhybas
    Sample: ccbsc0205
    Sum (%): 85.4561
 Init weight: 1 g
 Flux weight: 6 g
Final weight: 7 g

Compound Value Unit Status

SiO2   63.01 %
Al2O3   11.99 %
TiO2   0.204 %
Fe2O3   1.19 %
MgO   0.30 %
Na2O   3.96 %
K2O   3.66 %
MnO   0.059 %
CaO   1.03 %
P2O5   0.050 %
BSC0205
1/16/2007 15:38
PANalytical
View result

    Type: Routine
   Archive: rhybas2
 Application: rhybas
    Sample: ccbsc0205
    Sum (%): 96.0858
 Init weight: 1 g
 Flux weight: 6 g
Final weight: 7 g

Compound Value Unit Status

SiO2   70.71%
Al2O3   13.65%
TiO2   0.22%
Fe2O3   1.25%
MgO   0.46%
Na2O   4.60%
K2O   3.97%
MnO   0.06%
CaO   1.12%
P2O5   0.05%

CCBSC0205

1/16/2007 3:30:19 PM
PANalytical
View result

      Type: Routine
     Archive: Trace1a
    Application: trace1
       Sample: ccbsc0205
       Sum (%): 97.1399
    Init weight: 12 g
    Flux weight: 3 g
    Final weight: 15 g

Compound Value   Unit Status

Sc   3.410 ppm
V   1.418 ppm
Ni   5.099 ppm
Cu   6.030 ppm
Ga   15.670 ppm
Rb   126.422 ppm
Sr   310.265 ppm
Y   17.383 ppm
Zr   194.647 ppm
Nb   34.332 ppm
Ba   1212.936 ppm
La   50.012 ppm
Hf   5.639 ppm
Pb   24.603 ppm
Th   16.554 ppm
U   5.244 ppm

Meas. LOI   0.760 %

CCBSC0601
1/16/2007 3:06:20 PM
PANalytical
View result

      Type: Routine
     Archive: rhybas
    Application: rhybas
       Sample: ccbsc0601
       Sum (%): 98.2238
    Init weight: 1 g
    Flux weight: 6 g
    Final weight: 7 g

Compound Value Unit Status

SiO2   75.60 %
Al2O3   12.43 %
TiO2   0.113 %
Fe2O3   0.75 %
MgO   0.14 %
Na2O   3.77 %
K2O   4.78 %
MnO   0.062 %
CaO   0.56 %
P2O5   0.020 %

CCBSC0601
1/16/2007 3:39:53 PM
PANalytical
View result

      Type: Routine
     Archive: rhybas2
    Application: rhybas
       Sample: ccbsc0601
       Sum (%): 98.7873
    Init weight: 1 g
    Flux weight: 6 g
    Final weight: 7 g

Compound Value Unit Status

SiO2   75.92 %
Al2O3   12.51 %
TiO2   0.115 %
Fe2O3   0.76 %
MgO   0.15 %
Na2O   3.89 %
K2O   4.81 %
MnO   0.062 %
CaO   0.57 %
P2O5   0.017 %
CCBSC0601
1/16/2007 3:26:17 PM
PANalytical
View result

Type: Routine
Archive: Trace1a
Application: trace1
Sample: ccbsc0601
Sum (%): 99.3046
Init weight: 12 g
Flux weight: 3 g
Final weight: 15 g

Compound Value   Unit Status

Sc   1.500 ppm
V   negative ppm
Ni   4.719 ppm
Cu   4.778 ppm
Ga   13.650 ppm
Rb   125.140 ppm
Sr   35.765 ppm
Y   20.874 ppm
Zr   100.727 ppm
Nb   49.786 ppm
Ba   272.376 ppm
La   31.712 ppm
Hf   2.745 ppm
Pb   28.435 ppm
Th   24.509 ppm
U   7.949 ppm
Meas. LOI   0.390 %

CCBSC0602

1/16/2007 3:07:25 PM
PANalytical
View result

Type: Routine
Archive: rhybas
Application: rhybas
Sample: ccbsc0602
Sum (%): 98.4713
Init weight: 1 g
Flux weight: 6 g
Final weight: 7 g

Compound Value Unit Status

SiO2   77.80 %
Al2O3   10.83 %
TiO2   0.103 %
Fe2O3   0.68 %
MgO   0.09 %
Na2O   1.98 %
K2O   6.71 %
MnO   0.041 %
CaO   0.21 %
P2O5   0.022 %

CCBSC0602
1/16/2007 3:33:09 PM
PANalytical
View result

Type: Routine
Archive: Trace1a
Application: trace1
Sample: ccbsc0602
Sum (%): 98.8720
Init weight: 12 g
Flux weight: 3 g
Final weight: 15 g

Compound Value   Unit Status

Sc   0.715 ppm
V   negative ppm
Ni   5.710 ppm

Cu   10.879 ppm
Ga   12.620 ppm
Rb   192.318 ppm
Sr   29.593 ppm
Y   17.411 ppm
Zr   86.462 ppm
Nb   43.089 ppm
Ba   237.734 ppm
La   34.121 ppm
Hf   3.471 ppm
Pb   21.823 ppm
Th   20.499 ppm
U   6.896 ppm
Meas. LOI   0.260 %

CCBSC0604

1/16/2007 3:06:47 PM
PANalytical
View result

     Type: Routine
    Archive: rhybas
  Application: rhybas
    Sample: ccbsc0604
    Sum (%): 100.0538
 Init weight: 1 g
 Flux weight: 6 g
Final weight: 7 g

Compound Value Unit Status

SiO2   78.46 %
Al2O3   11.71 %
TiO2   0.102 %
Fe2O3   0.68 %
MgO   0.13 %
Na2O   3.68 %
K2O   4.76 %
MnO   0.053 %
CaO   0.45 %
P2O5   0.027 %

CCBSC06041/16/2007 3:33:46 PM
PANalytical

View result

     Type: Routine
    Archive: Trace1a
  Application: trace1
    Sample: ccbsc0604
    Sum (%): 100.4044
 Init weight: 12 g
 Flux weight: 3 g
Final weight: 15 g

Compound Value   Unit Status

Sc   0.715 ppm
V   negative ppm
Ni   4.917 ppm
Cu   4.698 ppm
Ga   13.657 ppm
Rb   130.779 ppm
Sr   33.711 ppm
Y   18.621 ppm
Zr   86.355 ppm
Nb   46.469 ppm
Ba   243.459 ppm
La   35.071 ppm
Hf   1.611 ppm
Pb   24.943 ppm
Th   22.321 ppm
U   6.846 ppm
Meas. LOI   0.220 %

CCBSC0605

1/16/2007 15:03
PANalytical
View result

     Type: Routine
    Archive: rhybas
  Application: rhybas
    Sample: ccbsc0605
    Sum (%): 98.2522

Init weight: 1 g
 Flux weight: 6 g
Final weight: 7 g

Compound Value Unit Status

SiO2   72.27 %
Al2O3   14.27 %
TiO2   0.238 %
Fe2O3   1.37 %
MgO   0.13 %
Na2O   4.80 %
K2O   3.87 %
MnO   0.058 %
CaO   1.20 %
P2O5   0.061 %
CCBSC0605
1/16/2007 3:41:34 PM
PANalytical
View result

    Type: Routine
   Archive: rhybas2
 Application: rhybas
    Sample: ccbsc0605
    Sum (%): 98.7911
 Init weight: 1 g
 Flux weight: 6 g
Final weight: 7 g

Compound Value Unit Status

SiO2   72.57 %
Al2O3   14.36 %
TiO2   0.237 %
Fe2O3   1.37 %
MgO   0.20 %
Na2O   4.83 %
K2O   3.89 %
MnO   0.059 %
CaO   1.22 %
P2O5   0.060 %

CCBSC0605
1/16/2007 3:31:10 PM
PANalytical

View result

    Type: Routine
   Archive: Trace1a
 Application: trace1
    Sample: ccbsc0605
    Sum (%): 99.1570
 Init weight: 12 g
 Flux weight: 3 g
Final weight: 15 g

Compound Value   Unit Status

Sc   2.431 ppm
V   1.790 ppm
Ni   5.396 ppm
Cu   6.354 ppm
Ga   15.426 ppm
Rb   80.271 ppm
Sr   380.431 ppm
Y   16.354 ppm
Zr   192.784 ppm
Nb   27.743 ppm
Ba   1427.462 ppm
La   41.001 ppm
Hf   4.758 ppm
Pb   24.146 ppm
Th   13.251 ppm
U   4.691 ppm
Meas. LOI   0.080 %

CCBSC0606
1/16/2007 3:03:59 PM
PANalytical
View result

    Type: Routine
   Archive: rhybas
 Application: rhybas
    Sample: ccbsc0606

124

Sum (%): 100.6481
Init weight: 1 g
Flux weight: 6 g
Final weight: 7 g

Compound Value Unit Status

SiO2   76.73 %
Al2O3   13.18 %
TiO2   0.147 %
Fe2O3   0.89 %
MgO   0.20 %
Na2O   4.03 %
K2O   4.72 %
MnO   0.062 %
CaO   0.64 %
P2O5   0.044 %
CCBSC0606

1/16/2007 3:34:29 PM
PANalytical
View result

    Type: Routine
    Archive: Trace1a
  Application: trace1
    Sample: ccbsc0606
    Sum (%): 101.2971
 Init weight: 12 g
 Flux weight: 3 g
Final weight: 15 g

Compound Value   Unit Status

Sc   0.467 ppm
V   negative ppm
Ni   5.000 ppm
Cu   6.994 ppm
Ga   14.032 ppm
Rb   115.779 ppm
Sr   96.749 ppm
Y   19.525 ppm
Zr   104.160 ppm
Nb   37.222 ppm
Ba   919.836 ppm
La   38.188 ppm

Hf   2.486 ppm
Pb   25.384 ppm
Th   20.096 ppm
U   5.369 ppm
Meas. LOI   0.450 %

CCBSP0105
1/16/2007 3:30:39 PM
PANalytical
View result

    Type: Routine
    Archive: Trace1a
  Application: trace1
    Sample: ccbsp0105
    Sum (%): 99.3457
 Init weight: 12 g
 Flux weight: 3 g
Final weight: 15 g

Compound Value   Unit Status

Sc   2.052 ppm
V   negative ppm
Ni   5.270 ppm
Cu   5.079 ppm
Ga   16.316 ppm
Rb   91.517 ppm
Sr   275.643 ppm
Y   20.781 ppm
Zr   172.792 ppm
Nb   35.350 ppm
Ba   1462.020 ppm
La   54.897 ppm
Hf   4.062 ppm
Pb   26.393 ppm
Th   16.333 ppm
U   5.021 ppm
Meas. LOI   0.270 %

CCBSP0305
1/16/2007 3:40:24 PM
PANalytical

View result

Type: Routine
Archive: rhybas2
Application: rhybas
Sample: ccbsp0305
Sum (%): 98.6742
Init weight: 1 g
Flux weight: 6 g
Final weight: 7 g

Compound Value Unit Status

Compound	Value	Unit	Status
SiO2	75.98	%	
Al2O3	12.66	%	
TiO2	0.142	%	
Fe2O3	0.90	%	
MgO	0.19	%	
Na2O	3.77	%	
K2O	4.43	%	
MnO	0.037	%	
CaO	0.54	%	
P2O5	0.020	%	

CCBSP0305

1/16/2007 3:05:58 PM
PANalytical
View result

Type: Routine
Archive: rhybas
Application: rhybas
Sample: ccbsp0305
Sum (%): 97.9942
Init weight: 1 g
Flux weight: 6 g
Final weight: 7 g

Compound Value Unit Status

Compound	Value	Unit	Status
SiO2	75.12	%	
Al2O3	12.45	%	
TiO2	0.142	%	
Fe2O3	0.90	%	
MgO	0.19	%	

Compound	Value	Unit
Na2O	4.16	%
K2O	4.43	%
MnO	0.037	%
CaO	0.53	%
P2O5	0.024	%

CCBSP 0305
1/16/2007 3:29:55 PM
PANalytical
View result

Type: Routine
Archive: Trace1a
Application: trace1
Sample: ccbsp0305
Sum (%): 99.1733
Init weight: 12 g
Flux weight: 3 g
Final weight: 15 g

Compound Value   Unit Status

Compound	Value	Unit	Status
Sc	1.348	ppm	
V	negative	ppm	
Ni	5.805	ppm	
Cu	6.660	ppm	
Ga	14.390	ppm	
Rb	109.760	ppm	
Sr	70.329	ppm	
Y	20.230	ppm	
Zr	106.205	ppm	
Nb	38.232	ppm	
Ba	662.248	ppm	
La	45.630	ppm	
Hf	2.841	ppm	
Pb	25.618	ppm	
Th	20.659	ppm	
U	5.417	ppm	
Meas. LOI	0.340	%	

CCBSP0405
1/16/2007 3:08:57 PM
PANalytical
View result

Type: Routine

Archive: rhybas
Application: rhybas
   Sample: ccbsp0405
   Sum (%): 97.7079
Init weight: 1 g
Flux weight: 6 g
Final weight: 7 g

Compound Value Unit Status

SiO2   74.47 %
Al2O3   12.69 %
TiO2   0.132 %
Fe2O3   0.87 %
MgO   0.31 %
Na2O   3.96 %
K2O   4.68 %
MnO   0.033 %
CaO   0.53 %
P2O5   0.032 %
1/16/2007 3:40:44 PM
PANalytical
View result

   Type: Routine
   Archive: rhybas2
Application: rhybas
   Sample: ccbsp0405
   Sum (%): 99.3220
Init weight: 1 g
Flux weight: 6 g
Final weight: 7 g

Compound Value Unit Status

SiO2   76.00 %
Al2O3   13.09 %
TiO2   0.131 %
Fe2O3   0.87 %
MgO   0.30 %
Na2O   3.66 %
K2O   4.69 %
MnO   0.032 %
CaO   0.53 %
P2O5   0.022 %
CCBSP0405

1/16/2007 3:29:33 PM
PANalytical
View result

   Type: Routine
   Archive: Trace1a
Application: trace1
   Sample: ccbsp0405
   Sum (%): 99.8769
Init weight: 12 g
Flux weight: 3 g
Final weight: 15 g

Compound Value   Unit Status

Sc   1.208 ppm
V   negative ppm
Ni   5.555 ppm
Cu   0.435 ppm
Ga   14.358 ppm
Rb   113.852 ppm
Sr   60.715 ppm
Y   19.072 ppm
Zr   108.030 ppm
Nb   38.901 ppm
Ba   631.721 ppm
La   41.581 ppm
Hf   3.542 ppm
Pb   25.610 ppm
Th   18.036 ppm
U   5.413 ppm
Meas. LOI   0.390 %

CCBP0505
1/16/2007 3:04:24 PM
PANalytical
View result

   Type: Routine
   Archive: rhybas
Application: rhybas
   Sample: ccbsp0505
   Sum (%): 98.6009

Init weight: 1 g
Flux weight: 6 g
Final weight: 7 g

Compound Value Unit Status

SiO2   74.19 %
Al2O3   13.43 %
TiO2   0.176 %
Fe2O3   1.04 %
MgO   0.14 %
Na2O   4.22 %
K2O   4.61 %
MnO   0.060 %
CaO   0.71 %
P2O5   0.035 %

CCBSP0505
1/16/2007 3:31:35 PM
PANalytical
View result

   Type: Routine
   Archive: Trace1a
Application: trace1
   Sample: ccbsp0505
   Sum (%): 99.2529
Init weight: 12 g
Flux weight: 3 g
Final weight: 15 g

Compound Value   Unit Status

Sc   0.571 ppm
V   negative ppm
Ni   4.132 ppm
Cu   3.928 ppm
Ga   16.048 ppm
Rb   111.432 ppm
Sr   121.578 ppm
Y   19.795 ppm
Zr   138.905 ppm
Nb   38.726 ppm
Ba   811.574 ppm
La   29.827 ppm
Hf   3.360 ppm

Pb   24.886 ppm
Th   18.757 ppm
U   7.126 ppm
Meas. LOI   0.460 %

CCTC0105
1/16/2007 3:04:47 PM
PANalytical
View result

   Type: Routine
   Archive: rhybas
Application: rhybas
   Sample: cctc0105
   Sum (%): 98.8097
Init weight: 1 g
Flux weight: 6 g
Final weight: 7 g

Compound Value Unit Status

SiO2   76.31 %
Al2O3   12.00 %
TiO2   0.145 %
Fe2O3   0.93 %
MgO   0.13 %
Na2O   4.03 %
K2O   4.57 %
MnO   0.049 %
CaO   0.61 %
P2O5   0.027 %
CCTC0105
1/16/2007 3:32:42 PM
PANalytical
View result

   Type: Routine
   Archive: Trace1a
Application: trace1
   Sample: cctc0105
   Sum (%): 99.1826
Init weight: 12 g
Flux weight: 3 g

Final weight: 15 g

Compound Value   Unit Status

Sc   negative ppm
V   negative ppm
Ni   5.495 ppm
Cu   2.881 ppm
Ga   13.938 ppm
Rb   134.565 ppm
Sr   39.542 ppm
Y   15.073 ppm
Zr   92.215 ppm
Nb   29.784 ppm
Ba   182.876 ppm
La   33.668 ppm
Hf   2.472 ppm
Pb   22.733 ppm
Th   20.432 ppm

U   5.573 ppm

CCHC0105
1/16/2007 3:22:30 PM
PANalytical
View result

    Type: Routine
   Archive: rhybas
 Application: rhybas
    Sample: cchc0105
    Sum (%): 98.6206
 Init weight: 1 g
 Flux weight: 6 g
Final weight: 7 g

Compound Value Unit Status

SiO2   73.78 %
Al2O3   13.73 %
TiO2   0.201 %
Fe2O3   1.19 %
MgO   0.18 %
Na2O   4.42 %
K2O   4.05 %

MnO   0.025 %
CaO   0.99 %
P2O5   0.043 %
1/16/2007 3:22:55 PM
PANalytical
View result

    Type: Routine
   Archive: rhybas
 Application: rhybas
    Sample: cchc0105
    Sum (%): 99.0085
 Init weight: 1 g
 Flux weight: 6 g
Final weight: 7 g

Compound Value Unit Status

SiO2   73.83 %
Al2O3   13.97 %
TiO2   0.205 %
Fe2O3   1.22 %
MgO   0.21 %
Na2O   4.39 %
K2O   4.14 %
MnO   0.040 %
CaO   0.97 %
P2O5   0.043 %

CCHC0105
1/16/2007 3:07:05 PM
PANalytical
View result

    Type: Routine
   Archive: rhybas
 Application: rhybas
    Sample: cchc0105
    Sum (%): 98.6206
 Init weight: 1 g
 Flux weight: 6 g
Final weight: 7 g

Compound Value Unit Status

SiO2   73.78 %

Al2O3   13.73 %
TiO2   0.201 %
Fe2O3   1.19 %
MgO   0.18 %
Na2O   4.42 %
K2O   4.05 %
MnO   0.025 %
CaO   0.99 %
P2O5   0.043 %

CCHC0105
1/16/2007 3:32:22 PM
PANalytical
View result

      Type: Routine
      Archive: Trace1a
   Application: trace1
      Sample: cchc0105
      Sum (%): 99.2608
 Init weight: 12 g
 Flux weight: 3 g
Final weight: 15 g

Compound Value   Unit Status

Sc   2.156 ppm
V   2.879 ppm
Ni   4.840 ppm
Cu   3.388 ppm
Ga   15.028 ppm
Rb   91.801 ppm
Sr   258.441 ppm
Y   15.548 ppm
Zr   168.243 ppm
Nb   34.054 ppm
Ba   1033.143 ppm
La   26.131 ppm
Hf   4.945 ppm
Pb   25.590 ppm
Th   17.879 ppm
U   5.788 ppm
Meas. LOI   0.410 %

CCHC0305
1/16/2007 3:09:28 PM

PANalytical
View result

      Type: Routine
      Archive: rhybas
   Application: rhybas
      Sample: cchc0305
      Sum (%): 98.5130
 Init weight: 1.0002 g
 Flux weight: 5.9999 g
Final weight: 7.0001 g

Compound Value Unit Status

SiO2   74.34 %
Al2O3   13.15 %
TiO2   0.174 %
Fe2O3   1.04 %
MgO   0.19 %
Na2O   4.38 %
K2O   4.52 %
MnO   0.042 %
CaO   0.66 %
P2O5   0.024 %

CCHC0305
1/16/2007 3:34:07 PM
PANalytical
View result

      Type: Routine
      Archive: Trace1a
   Application: trace1
      Sample: cchc0305
      Sum (%): 98.9619
 Init weight: 12 g
 Flux weight: 3 g
Final weight: 15 g

Compound Value   Unit Status

Sc   1.045 ppm
V   0.157 ppm
Ni   4.837 ppm
Cu   7.353 ppm
Ga   13.793 ppm

130

Rb   109.930 ppm
Sr   113.308 ppm
Y   21.069 ppm
Zr   138.292 ppm
Nb   38.034 ppm
Ba   805.519 ppm
La   37.771 ppm
Hf   4.385 ppm
Pb   26.005 ppm
Th   18.577 ppm
U   5.332 ppm
Meas. LOI   0.250 %

INDUCTIVELY COUPLED MASS SPECTROMETRY RESULTS, TRACE ELEMENTS

	La	Ce	Pr	Nd	Sm	Eu	Gd	Tb	Dy	Ho	Er	Tm	Yb
BMO305	80.66	126.52	12.68	40.69	6.31	1.56	4.82	0.74	4.27	0.88	2.43	0.40	2.48
CCBSCO105	27.76	48.82	5.02	15.76	3.11	0.39	2.58	0.48	3.04	0.63	1.78	0.30	1.96
CCBSC0205	45.68	74.23	7.32	23.06	3.76	0.78	2.84	0.45	2.77	0.56	1.60	0.25	1.64
CCBSC0601	30.09	53.64	5.46	17.08	3.35	0.43	2.89	0.53	3.37	0.70	2.03	0.33	2.21
CCBSC0602	26.69	46.14	4.87	15.38	3.02	0.38	2.54	0.47	2.94	0.61	1.76	0.29	1.90
CCBSC0604	25.74	46.94	4.87	15.28	3.07	0.39	2.65	0.49	3.12	0.63	1.83	0.29	1.98
CCBSC0605	45.47	72.23	7.41	23.78	3.92	0.91	2.97	0.46	2.72	0.55	1.51	0.24	1.56
CCBSC0606	35.47	59.12	5.98	18.85	3.41	0.55	2.88	0.50	3.18	0.65	1.88	0.30	1.96
CCBSP0105	50.97	75.02	9.50	31.75	5.65	1.08	4.23	0.66	3.72	0.72	1.94	0.29	1.90
CCBSP0405	41.55	69.44	7.18	23.00	4.21	0.72	3.45	0.60	3.61	0.74	2.09	0.33	2.15
CCBSP0505	40.19	66.73	6.71	21.15	3.64	0.63	2.97	0.52	3.23	0.67	1.91	0.30	2.01
CCBSP0305	34.66	57.69	6.23	20.02	3.75	0.60	3.12	0.54	3.32	0.69	1.94	0.31	2.02
CCHC0105	39.33	65.93	6.48	20.28	3.35	0.70	2.62	0.42	2.54	0.52	1.47	0.23	1.54
CCHC0305	33.43	56.27	5.76	18.14	3.34	0.53	2.83	0.49	3.05	0.64	1.78	0.29	1.95
CCBD0205	56.71	89.51	9.24	28.86	4.84	0.81	3.95	0.66	3.96	0.82	2.30	0.37	2.44
CCTC0105	39.90	60.80	5.56	15.95	2.45	0.37	2.04	0.35	2.24	0.48	1.45	0.25	1.74
CCBSC0205 ®	45.51	74.03	7.28	23.12	3.71	0.79	2.82	0.45	2.75	0.56	1.60	0.25	1.68
CCBSP0505 ®	40.06	66.48	6.66	21.00	3.66	0.64	2.92	0.52	3.22	0.65	1.88	0.31	2.05

	Lu	Ba	Th	Nb	Y	Hf	Ta	U	Pb	Rb	Cs	Sr	Sc	Zr	W

BMO305	0.41	1669	19.42	52.11	24.20	7.44	3.64	5.84	21.40	73.1	1.72	488	3.3	312	74
CCBSCO105	0.31	364	21.88	43.78	17.67	3.29	4.51	6.72	23.98	273.8	11.16	44	2.1	84	141
CCBSC0205	0.27	1274	15.45	31.96	15.60	4.65	2.97	4.82	24.25	118.2	3.06	303	2.1	161	114
CCBSC0601	0.35	310	24.10	47.62	20.05	3.53	4.73	7.66	27.06	118.6	4.13	35	2.3	90	93
CCBSC0602	0.30	272	20.59	39.72	17.11	3.00	4.43	6.65	21.00	183.1	9.88	29	1.9	76	213
CCBSC0604	0.31	272	21.74	44.49	17.95	3.05	4.82	6.12	23.89	127.0	23.79	32	2.1	76	165
CCBSC0605	0.26	1526	13.43	26.76	14.89	4.58	2.45	4.07	23.74	78.5	1.49	379	1.9	161	94
CCBSC0606	0.31	998	17.91	35.38	18.45	3.37	3.55	5.76	25.16	113.6	3.58	97	2.1	95	103
CCBSP0105	0.29	1486	16.51	33.24	19.70	4.29	3.36	4.55	25.36	87.7	1.79	271	2.0	143	149
CCBSP0405	0.34	849	19.05	36.31	20.01	3.91	3.45	5.51	25.10	107.1	3.76	112	2.3	115	107
CCBSP0505	0.33	861	18.54	36.66	18.72	3.94	3.46	6.09	25.05	105.6	3.94	119	2.2	117	83
CCBSP0305	0.33	724	19.13	36.03	19.40	3.46	3.64	5.14	24.35	107.5	3.21	69	2.2	99	109
CCHC0105	0.24	1126	17.05	33.70	14.65	4.34	3.02	4.25	24.25	90.5	1.61	262	2.1	147	71
CCHC0305	0.31	685	19.01	37.38	18.09	3.42	3.64	5.01	23.83	111.4	2.91	59	2.2	92	79
CCBD0205	0.38	591	22.29	52.45	23.18	5.50	4.34	6.17	21.52	100.3	2.50	86	2.5	184	77
CCTC0105	0.29	221	19.37	28.27	14.82	3.09	3.28	5.38	21.91	131.8	4.41	39	2.0	78	160
CCBSC0205 ®	0.27	1270	15.57	31.86	15.46	4.69	2.97	4.86	24.15	117.6	3.01	302	2.1	162	113
CCBSP0505 ®	0.32	859	18.40	36.50	18.64	3.93	3.44	6.02	24.93	105.7	3.97	118	2.2	116	82

APPENDIX E

INDUCTIVELY COUPLED MASS SPECTROMETRY RESULTS TESTING PROCEDURES

The ICP-MS at the lab at Washington State University consists of a quadrupole mass spectrometer with an inductively coupled argon plasma as an ion source. Sciex Elan model 250 ICP-MS equipped with a Babington nebulizer, water cooled spray chamber, and Brooks mass flow controllers. all 14 naturally occurring rare earth elements (La through Lu) together with Ba, Rb, Y, Nb, Cs, Hf, Ta, Pb, Th, U, Sr and Zr. Zr is measured only as a check for complete dissolution of the sample.

The samples were digested using a technique modified technique from Crock and Lichte (1982). The samples were first ground into a fine powder in an iron bowl in a shatterbox swing mill. Two grams of the powder was mixed with an equal amount of lithium tetraborate (Li2B4O7) flux, and fused in a carbon crucible at 1000° for 30 minutes. The resulting fusion bead was then reground. 250 mg of this powder was dissolved on a hotplate at 110°C, using 6 ml HF, 2 ml HNO_3, and 2 ml $HClO_4$ in an open teflon vial. Moisture was driven off the sample until dry, then additional drying was accomplished using by heating the sample with 2 ml HClO4 at 165°C, to convert insoluble fluorides to soluble perchlorates. 3 ml HNO_3, 8 drops H_2O_2, 5 drops of HF and an internal standard of In, Re, and Ru were then added to the sample. It was diluted to 60 ml (1:240 final dilution). Samples are introduced into the argon plasma at 1.0 ml/min using a peristaltic pump and an automatic sampler. Plasma power is 1500 watts. Under these conditions MO+/M+ (the proportion of metal ions forming oxides) is minimized. The instrument is run in

"multi-element" mode averaging 10 repeats of 0.5 sec/element for a total integrated count time of 5 sec/element.

The instrument is calibrated by running unknown samples in sets of 17. Along with the unknowns, an acid blank and two samples of each of the 3 in-house rock standards are run totaling 24 standard and unknown samples per batch.

The three in-house standards have been calibrated against 17 international standards. Their elemental concentrations so derived are listed in table 2. Independent values on these three in-house standards by Walsh (Kings College, London, U.K., by ICP-OES), Meier (U.S.G.S., Denver, by ICP-MS), Bailey and Conrey (WSU, Pullman, WA, by INAA) are also listed.

A spreadsheet program is used to correct raw intensities for oxide and isobaric interferences, and to correct for drift using the In, Re, and Ru internal standards (after Doherty, 1989). Calibration curves for each element are then constructed from the six (2x3) standard samples and single acid blank by plotting given values (table 2) against the corrected intensities. Concentrations for the unknown samples are then computed from this curve. These calculations assume that the isotopic proportions of the unknowns and standards do not vary significantly from the average of the earth's crust.

BULK DISTRIBUTION COEFFICIENTS

Element	Quartz	Sanidine	Plagioclase	Biotite	Zircon	Allanite	Apatite	Magnetite	cpx	opx
Sc	0.00	0.04	0.17	15.5	68.65	55.85	0	8.81	131	22
Rb	0.00	0.48	0.25	4.2	0	0.19	0	0.04	0	0.01
Sr	0.00	4	11.8	7.2	0	1.8	2	0.09	0	0.17
Y	0.00	0.04	0.05	2.4	60	95.5	40	3.21	0	1.1
Zr	0.00	0.1	0.09	0.5	6400	0.29	0.1	0.62	2.31	0.05
Nb	0.00	0.16	0.27	4.6	50	0.12	0.1	2.5	0.01	0.31
Cs	0.00	0.01	0.05	2.3	0	0	0	0	0	0
Ba	0.00	4.7	13.5	5.37	0	0	2	0	0	0.9
La	0.00	0.06	0.1	3.18	16.9	2595	20	21.5	17.6	14.4
Ce	0.00	0.02	0.06	2.8	16.75	2279	35	17.85	10.25	12.3
Sm	0.00	0.01	0.01	1.55	14.4	867	63	8.14	10.36	7.87
Eu	0.00	5.85	4.75	0.87	16	111	30	4.05	7.47	2.85
Tb	0.00	0.01	0.02	1.05	37	273	20	4.75	5.5	5.5
Yb	0.00	0	0.02	0.61	641	33	25	1.4	7.08	2.7
Lu	0.00	0.03	0.02	0.61	641	33	25	1.4	7.08	2.7
Hf	0.00	0.02	0.04	0.6	3193	18.9	0.1	4.41	1.51	0
Ta	0.00	0.02	0.05	1.34	47.5	3.15	0	0.87	0.91	1.13
Th	0.00	0	0.03	1.23	76	538	2	7.36	2.34	6.53
U	0.00	0.02	0.15	0.17	0	14.3	0	0.85	0.58	0.28
Pb	0	0.75	0.7	2.1	0	0	0	0.8	0	0

Partition coefficients gathered from: Higuchi and Nagasawa (1969); Schnetzler and Philpotts (1970); Nagsawa and Schnetzler (1971); Arth (1976); Mahood and Hildreth (1983); Michael (1983); Nash and Crecraft (1985); Stix and Gorton (1990); Ewart and Griffen (1994); Streck and Grunder (1997).

REFERENCES

Aldrich, M.J., Jr., 1986, Tectonics of the Jemez lineament in the Jemez Mountains and the Rio Grande rift: Journal of Geophysical Research, v. 91, p. 1753-1762.

Aldrich, M.J., Jr., Chapin, C.E., and Laughlin, A.W., 1986, Stress History and Tectonic Development of the Rio Grande Rift, New Mexico: Journal of Geophysical Research, v. 91, no. B6, p. 6199-6211.

Aprea, C.M., Hildebrand, S., Fehler, M., Steck, L., Baldridge, W.S., and Roberts, P., 2000, Three-dimensional Kirchhoff migration: Imaging of the JVC using teleseismic data: Journal of Geophysical Research, v. 107, p. 2253-2268.

Arth, J.G., 1976, Behavior of trace elements during magmatic processes-A summary of theoretical models and their applications: Journal of Research, United States Geological Survey v. 4 p. 41-47.

Bachman, O., and Bergantz, G.W., 2004, On the Origin of crystal-poor rhyolites: Extracted from batholithic crystal mushes: Journal of Petrology, 45, 1565-1582.

Bailey, R.A., Smith, R.L., and Ross, C.S., 1969, Stratigraphic nomenclature of volcanic rocks in the Jemez Mountains, New Mexico, United States Geological Survey Bulletin 1274-P 19 p.

Broxton, D., Woldegabriel, G., Peters, L., and Budahn, J., 2007, Pliocene volcanic rocks of the Tschicoma Formation, East-Central Jemez Volcanic Field: Chemistry, petrography, and age constraints *in* Field Conference, Geology of the Jemez Mountains Region II: New Mexico Geological Society Guidebook 58, p. 284-295

Chamberlin, R.M., Pazzaglia, F.J., Wegmann, K.W., and Smith, G.A., 1999, Preliminary geologic map of Loma Creston Quadrangle, Sandoval County, New Mexico: New Mexico Bureau of Mines and Mineral Resources.

Chapin, C.E., Wilks, M., McIntosh, W.C., 2004, Spacetime patterns of Late Cretaceous to present magmatism in New Mexico—comparison with Andean volcanism and potential for future volcanism: New Mexico Bureau of Geology & Mineral Resources Bulletin 160.

DePaolo, D.J., 1981, Trace-element and isotopic effects of combined wallrock assimilation and fractional crystallization: Earth and Planetary Science Letters, v. 53, p. 189-202

Doell, R.R., Dalrymple,G.B., Smith, R.L., and Bailey, R.A., 1968, Paleomagmatism, potassium-argon ages, and geology of rhyolites and associated rocks of the Valles Caldera, New

Mexico: Memoirs of the Geological Society of America, 116, p. 116-248.

Ellisor, R., Wolff, J., Gardner, J., 1996, Outline of the petrology and geochemistry of the Keres Group lavas and Tuffs: New Mexico Geological Society Guidebook, 47th Conference, Jemez Mountains Region

Ewart, A., and Griffin, W.L., 1994, Application of Proton-Microprobe Data to Trace-Element Partitioning in Volcanic-Rocks. Chemical Geology, v. 117 no.1-4, p. 251-284.

Gardner, J.N., and Goff, F., 1984, Potassium-argon dates from the Jemez volcanic field-- Implications for tectonic activity in the north-central Rio Grande Rift, New Mexico Geological Society Guidebook, 35th Field Conference, Rio Grande Rift: Northern New Mexico, p.75-81.

Gardner, J.N., 1985, Tectonic and petrologic evolution of the Keres Group: Implications for the development of the Jemez Volcanic Field, New Mexico: PhD dissertation, University of California, Davis, CA unpublished.

Gardner, J.N., Goff, F., Garcia, S., and Hagan, R.C., 1986, Stratigraphic Relations and Lithologic Variations in the Jemez Volcanic Field, New Mexico: Journal of Geophysical Research, v. 91, p. 1763-1778.

Gibler, K., 2007, Postcollapse volcanism in the Valles Caldera, New Mexico: The Transition from Large Volume Explosive to Small Volume Effusive Eruptions, MS. Degree Thesis, University of Nevada, Las Vegas, unpublished.

Goff, F., and Gardner, J.N., 1994, Evolution of a mineralized geothermal system, Valles Caldera, New Mexico: *Economic Geology, v. 89 no. 8 1803-1832.*

Golombek, M.P., 1981, Geometry and rate of extension across the Pajarito fault zone, Española basin, Rio Grande Rift, northern New Mexico: *Geology* v. 9, p. 21-24.

Gorman, A.R., Clowes, R.M., Ellis, R.M., Henstock, T.J., Spence, G.D., Keller, G.R., Levander, A., Snelson, C.M., Burianyk, J.A., Kanasewich, E.R., Asudeh, I., Hajnal, Z., and Miller, K.C., 2002, Deep Probe: Imaging the roots of western North America: Canadian Journal of Earth Science, v. 39, p. 375-398.

Guilbeau, K.P., 1982, Geology, geochemistry and petrogenesis of the upper Keres Group, Ruiz Peak area, Jemez Mountains, New Mexico: MS thesis, University of New Mexico.

Halliday, A.N., Mahood, G.A., Holden, P., Metz, J.M., Dempster, T.J., and Davidson, J.P., 1989, Evidence of long residence times of rhyolitic magma in the Long Valley magmatic system: The isotopic record in precaldera lavas of Glass Mountain: Earth and Planetary Science Letters, v. 68 p. 274-290.

Hanson, G.N., 1980, Rare Earth Elements in Peterogenetic Studies of Igneous Systems: Annual

Review of Earth and Planetary Science, v. 8, 371-406.

Haskin, M.A. and Haskin, L.A., 1966, Rare earths in European shales; a redetermination: Science v. 154 p. 507-509.

Heiken, G., Goff, F., Gardner, J., and Baldridge, 1990, The Valles/Toledo complex, Jemez volcanic field, New Mexico: Annual Review of Earth and Planetary Sciences Letters v. 18, p. 27-53.

Hildreth, W., 1981, Gradients in silicic magma chambers: Implications for lithospheric magmatism: Journal of Geophysical Research v. 86, 10,153-10,192.

Hildreth, W., 1979, The Bishop Tuff: Evidence for the origin of compositional zonation in silicic magma chambers: Geological Society of America Special Paper 180, 170 p.

Hildreth, W., and Wilson, C.J.N., 2007, Compositional Zoning of the Bishop Tuff: Journal of Petrology, v. 48, no. 5, p. 951-999.

Huppert, H.E., and Sparks, R.S.J., 1988a, The fluid dynamics of crustal melting by injection of basaltic sills, Transactions-Royal Society of Edinburgh: Earth Sciences v.79, p. 237-243.

Huppert, H.E., and Sparks, R.S.J., 1988b, The generation of granitic magmas by intrusion of basalt into continental crust: Journal of Petrology, v. 29, p. 599 -624.

Huppert, H.E., and Sparks, R.S.J., 1990,

Izett, G.A., and Obradovich, J.D., 2001, $^{40}Ar/^{39}Ar$ ages of Miocene tuffs in basin-fill deposits (Santa Fe group, New Mexico, and troublesome formation, Colorado) of the Rio Grande rift system: Mountain Geologist, v 38, p. 77-86.

Jellinek, M.A., DePaolo, 2003, A model for the origin of large silicic magma chambers: Precursors of caldera-forming eruptions: Bulletin of Volcanology and Geothermal Research, v. 65 p. 363-381.

Johnson, D.M., Hooper, P.R., Conrey, R.M., 1999, XRF analysis of rocks and minerals for major and trace elements single low dilution Li-tetraborate fused Bead: International Center for Diffraction data.

Johnson, S.Y., Stephenson, W.J., Morgan, L.A., and Pierce, K.L., 2002, Hydrothermal and tectonic activity in northern Yellowstone Lake, Wyoming: Geological Society of America Bulletin, v. 115, p. 954-971.

Justet, L., 2003, Effects of basalt intrusion on the multi-phase evolution of the Jemez volcanic field, NM: PhD Dissertation, University of Nevada, Las Vegas, unpublished.

Justet, L., and Spell, T., 2001, Effusive eruptions from a large silicic magma chamber: The

Bearhead Rhyolite, Jemez volcanic field, NM: Journal of Volcanology and Geothermal Research, v. 107, p. 241-264.

Karlstrom, K.E., Bowring, S.A., Chamberlain, K.R., Dueker, K.G., Eshete, T., Erslev, E.A., Farmer, G.L., Heizler, M., Humphreys, E.D., Johnson, R.A., Keller, G.R., Kelley, S.A., Levander, A., Magnani, M.B., Matzel, J.P., McCoy, A.M., Miller, K.C., Morozova, E.A., Pazzaglia, F.J., Prodehl, ., Rumpel, H.-M., Shaw, C.A., Sheehan, A.F., Shoshitaishvili, E., Smithson, S.B., Snelson, C.M., Stevens, L.M., Tyson, A.R., and Williams, M.L., 2002, Structure and Evolution of the Lithosphere Beneath the Rocky Mountains: Initial Results from the CD-ROM Experiment, GSA Today, v. 12, no.3.

Kelley, S.A., McIntosh, W.C., Goff, F., Kempter, K.A., Wolff, J.A., Esser, R., Braschayko, S., Love, D., and Gardner, J.N., 2013, Spatial and temporal trends in pre-caldera Jemez Mountains volcanic and fault activity: Geosphere, v. 9, no. 3, p. 614-646.

Knaack, C., Cornelius, S.B., and Hooper, P.R., 1994, Trace element analyses of rocks and minerals by ICP-MS: Open file report, Washington State University.

Krogh, T.E., 1973, A low-contamination method for hydrothermal decomposition of zircon and extraction of U and Pb for isotopic age determinations, Geochimica et Cosmochimica Acta, v. 37, no. 3, p 485-494.

Krogh, T.E., 1982. Improved accuracy of U–Pb zircon ages by the creation of more concordant systems using an air abrasion technique. *Geochimica et Cosmochimica Acta*, v. **46,** 637–649.

Lebas, M.J., Lemaitre, R.W., Streckeisen, A. and Zanettin, B., 1986, A Chemical Classification of Volcanic-Rocks Based on the Total Alkali Silica Diagram: Journal of Petrology v. 27 no. 3 p. 745-750.

Lee, C.T.A., Lee, C.T., and Wu, C.T., 2014, Modeling the compositional evolution of recharging, evacuating, and fractionating (REFC) magma chambers: Implications for differentiation of arc magmas: Geochimica et Cosmochimica Acta v. 143 p. 8–22

Leudke, R.G., and Smith, R.L., 1978, Map showing distribution, composition and age of Late Cenozoic volcanic centers in Arizona and New Mexico: U.S. Geologic Survey Map I-1091-A.

Levander, A., Zelt, C., and Magnani, M.B., 2004, Crust and upper mantle velocity structure of the southern Rocky Mountains from the Jemez Lineament to the Cheyenne Belt: American Geophysical Union 10.1029 Series Letters Chapters.

Lipman, P.W., 1984, The Roots of ash flow calderas in western North America: Windows into the tops of granitic batholiths: Journal of Geophysical Research, v. 89, p. 8801-8841.

Loeffler, B.M., Vaniman, D.T., Baldridge, W.S., and Shafiqullah, M., 1988, Neogene Rhyolites of the northern Jemez Field, New Mexico: Journal of Geophysical Research, v. 93, p. 6157-6167.

Magnani, M.B., Miller, K.C., Levander, A., and Karlstrom, K., 2004, The Yavapai-Mazatzal Boundary: A long-lived tectonic element in the lithosphere of the southwestern North America, Geological Society of America Bulletin, v. 116, p.1137-1142.

Magnani, M.B., Miller, K., Levander, A., Eshete, T., and Karlstrom, K., 2002, Seismic reflection image of the Jemez Lineament of New Mexico: Evidence for a south-dipping paleosubduction boundary between the Yavapai and Mazatzal Provinces: Rocky Mountains III: Post-Laramide Uplift and Erosion of the Rocky Mountains and Colorado Plateau (Posters) paper 207-9

Mahood, G.A., and Hildreth, E.W. (1983). Large partition coefficients for trace elements in high-silica rhyolites. *Geochimica et Cosmochimica Acta 47: 11-30. doi: 10.1016/0016-7037(83)90087-X.*

Maluski, H.,1989, Argon[39] Argon[40] dating: Nuclear Methods of Dating, Kluwer Academic Publishers, London, p. 325-351

McCalpin, J.P., 2005, Late Quaternary activity of the Parajito fault, Rio Grande Rift of northern New Mexico, USA: Tectonophysics, v. 408, p. 213-236.

Measuring Rio Grande Rift Crustal Deformation Retrieved on May 10, 2016 from http://aconcagua.geol.usu.edu/~arlowry/RGR/faq.html#WHAT

Montinmy, R., 1989, The conventional Potassium-Argon method: Nuclear Methods of Dating, Kluwer Academic Publishers, London, p. 225-324

Morgan, P., Seager, W.R., and Golombek, M.P., 1986, Cenozoic Thermal, Mechanical and Tectonic Evolution of the Rio Grande Rift: Journal of Geophysical Research, v. 91, no. B6, p. 6263-6276

Nagasawa, H. and Schnetzler, C.C., 1971**,** Partitioning of rare Earth, alkali, and alkaline Earth elements between phenocrysts and acidic igneous magmas: Geochimica et Cosmochimica Acta v. 35 p. 953-968.

New Mexico Museum of Natural History and Science Images Accessed December 5, 2015 at http://nmnaturalhistory.org/volc_valles.html

Oppenheimer, C., 2003, Climate, environmental and human consequences of the largest known historical eruption: Tambora Volcano (Indonesia) 1815: Progress in Physical Geography, v. 27, no. 2, p. 230-259

Patchett, P.J., and Ruiz, J., 1987, Nd isotopic ages of crust formation and metamorphism in the

Precambrian of eastern and southern Mexico: Contributions to Mineralogy and Petrology, v. 96, p. 523-528.

Perry, F.V., Baldridge, W.S., DePaolo, and Shafiqullah, A., 1990, Evolution of a magmatic system during continental extension: The Mount Taylor volcanic field, New Mexico: Journal of Geophysical Research v. 95, p. 19,327-19,348.

Phillips, E.H., Goff, F., Kyle, P.R., McIntosh, W.C., Dunbar . N.W., and Gardner, J.N., 2007, The $^{40}Ar/^{39}Ar$ age constraints on the duration of resurgence at the Valles caldera, New Mexico: Journal of Geophysical Research, v. 112, B08201. 15 p.

Reid, M.R., 2008, How long does it take to supersize an Eruption: Elements v. 4 p.23-28.

Reneau, S.L., Gardner, J.N., and Forman, S.L., 1996, New Evidence for the age of the youngest eruptions in the Valles Caldera, New Mexico: Geology, v. 24, p 7-10

Ross, C.S. & Smith, R.L., 1961, Ash-flow tuffs: their origin, geologic relations, and identification. US Geological Survey, Professional Papers 366, 1-81.

Rowe, M.C., Wolff, J.A., Gardner, J.N., Ramos, F.C., Teasdale, R., and Heikoop, C.E., 2007, Development of a Continental Volcanic Field: Petrogenesis of Pre-caldera Intermediate and Silicic Rocks and Origin of the Bandelier Magmas, Jemez Mountains (New Mexico, USA): Journal of Petrology v. 48 no.11 p. 2063-2091

Schnetzler, C.C., and Philpotts, J.A., 1970, Partition coefficients of rare-earth elements between igneous matrix material and rock-forming mineral phenocrysts: II. Geochimica et Cosmochimica Acta v. 34 no. 3 p. 331-340.

Self, S., 1992, Krakatau Revisited: The Course of Events and Interpretation of the 1883 Eruption:
GeoJournal v. 28, no. 2, p. 109-121.

Self, S., Goff, F., Gardner, J.N., Wright, J.V., and Kite, W.M., 1986, Explosive rhyolitic volcanism in the Jemez Mountains: Vent locations caldera development and relation to regional structure: Journal of Geophysical Research, v. 91, p. 1779-1798.

Singer, B.S. and Kudo, A.M., 1986, Assimilation - fractional crystallization of Polvadera Group rocks in the northwestern Jemez Volcanic Field, New Mexico: Contributions to Mineralogy and Petrology v. 94, p. 374-386

Smith, R.L., and Bailey, R.A., 1968, Resurgent Cauldrons: *Geological Society of America Memoirs, v. 116, p. 613-662*

*Smith, R.L., Bailey, R.A., and Ross, C.S., 1961, Structural Evolution of the Valles caldera, New Mexico, and its bearing on the emplacement of ring Dikes, USGS professional p*aper 424-D D145-D149.

Smith, R.L., Bailey, R.A., and Ross, C.S., 1970, Geologic Map of the Jemez Mountains, New Mexico: United States Geologic Survey.

Smith, R.L., Bailey, R.A., 1966, The Bandelier Tuff: A Study of Ash-flow eruption cycles from zoned magma chambers: Bulletin of Volcanology, v. 29, p. 83-103

Smith, R.L., 1979, Ash flow magmatism, Geological Society of America Special Paper 180, p. 5-27

Spell, T.L., McDougall, I., and Doulgeris, A.P., 1996, Cerro Toledo Rhyolite, Jemez Volcanic Field, New Mexico: 40AR/39Ar geochronology of eruptions between two caldera forming Events. GSA Bulletin, v. 108, no. 12, p. 1549-1566

Spell, T.L., Kyle, P.R., Thurwall, M.F., and Campbell, A.R., 1993, Isotopic and geothermal constraints on origin and evolution of postcollapse rhyolites in the Valles Caldera, New Mexico: Journal of Geophysical Research, v. 98, p. 19,723-19,739.

Stix, J., Goff, F., Gorton, M.P., Heiken, G., and Garcia, S.R., 1988, Restoration of compositional zonation in the Bandelier silicic magma chamber between two caldera-forming eruptions: Geochemistry and Origin of the Cerro Toledo Rhyolite. Jemez Mountains, New Mexico: Journal of Geophysical Research, v. 93, p. 6129-6147

Sun, S.S. and McDonough, W.F., 1989, Chemical and isotopic systematics of oceanic basalts; implications for mantle composition and processes. Magmatism in the ocean basins. Saunders, A.D. and Norry, M.J. (Editors), Geological Society of London, London. V. 42 p. 313-345

Suneson, H., 2012, My Favorite Outcrop: Black Mesa Basalt: Shaleshaker, July-August

USGS Volcano Hazards Program, 2016 Retrieved on 4/27/16 from https://volcanoes.usgs.gov/volcanoes/yellowstone/yellowstone_geo_hist_50.html

Wilson, D., Aster, R., West, M., Ni, J., Grand, S., Gao, W., Baldridge, W.S., Semken, S., and Patel, P., 2005, Lithospheric structure of the Rio Grande Rift, Nature, v. 433, p. 851-854.

Wisniewski, P. and Pazzaglia, F.J., 2002, Epeirogenic controls on Canadian River incision and landscape evolution, High Plains of northeastern New Mexico: Journal of Geology, v. 110, n. 4, p. 437-456

Wolff, J.A., and Gardner, J.N., 1995, Is the Valles Caldera entering a new cycle of activity?: Geology, v. 23, p. 411-414.

Wolff, J.A., Rowe, M.C., Teasdale, J.N., Gardner, J.N., Ramos F.C., and Heikoop, C.E., 2005, Petrogenesis of pre-caldera mafic lavas, Jemez Mountains volcanic field (New Mexico,

USA): Journal of Petrology, v. 46 p. 407-439.

Zimmerer, M.T., Lafferty, J., and Coble, M.A., 2015, The eruptive and magmatic history of the youngest pulse of volcanism at the Valles Calder: Implications for successfully dating late Quaternary eruptions: Journal of Volcanology and Geothermal Research v. 310, p. 50-57.

CURRICULUM VITAE

Penelope Padmore
PO Box, 7064, Cave Creek AZ 85327
phone 602.733.8924
email: penelopempadmore@gmail.com

EDUCATION

Master's Degree in Education, Grand Canyon University, Phoenix (online program)
April 2009 to November, 2011
Special Education. Graduated with a 4.0 G.P.A. Also completed requirements for full K-12 Structured English Immersion endorsement.

Master's Degree Candidate, University of Nevada Las Vegas
2005-2007, Spring 2016
Completed all courses for M.S. in Geology. December 2016 is anticipated graduation date.

B.Sc. in Geology Salem State University
1999

B.A. in Theater Arts Salem State University
1989

RELATED EXPERIENCE

Staff Scientist, SECOR, International, Inc., now Stantec Consulting Corporation
May 2007 to September, 2008
*Phase I site assessments for two sites in Gilbert, AZ.
*Supervision of monitoring well installation, development and abandonment.
*Groundwater monitoring at sites in Arizona, Washington State, and Oregon. Sampling techniques included micro-purge, PDB, discrete interval sampling. Also bailed free product and assisted with slug testing.
*Report preparation included Health and Safety Plans, well installation reports, quarterly groundwater monitoring reports, among others.
*Quality Control Officer for first phase construction of the remediation system for the Sinclair Refinery in Wellsville, New York.
*GIS modeling of High Consequence Areas assessment for gas pipeline.
*Clients included state agencies, major oil companies and real estate development firms.

University of Nevada, Las Vegas, Department of Geologic Sciences Teaching Assistant
January 2005- May 2007
Metallic Ore Deposits: Subjects included mineral identification, assisting with overnight field trips to northern Nevada, and presenting 30 to 45 minute lectures on a range of topics.
Geographic Information Systems: Taught two laboratory sections in this subject

Geology 101: Taught three semesters, two sections each. In final semester, Student evaluations averaged 3.6 and 3.8 out of 4.0.

Site Supervisor, Copper State Engineering, Scottsdale, AZ
December 2004
Two week project included preparing and running perc tests and supervising field personnel for a housing development.

Environmental Geologist; Onsite Environmental/Aerotek
2002-2004, occasional, part time
*Temporary assignments included semi annual groundwater sampling events at Superfund Sites in Maine.

Soil Testing Technician; GeoTesting Express, Boxborough MA
2000 - 2002
* Field/lab soil sampling and testing. Tests included index, permeability, compaction, density and other ASTM /AASHTO- standard tests of contaminated and non-contaminated soils, and geosynthetics, in both the laboratory and in the field.
* Responsible for compliance with foreign soil regulations.
*Assisted engineers in creating reports. Used Plaxis 7.0 for sub-surface modeling.

TEACHING EXPERIENCE

Special Education Teacher Arizona State Hospital
September 2015 to Present
I teach a wide variety of subjects, including both academic skills from elementary to college level, as well as transitional life skills to disabled adults.

Middle School Teacher, Greenway Middle School, 3001 E. Nisbet Road, Phoenix Arizona
Academic Year 2013-2014
First half of the year, taught small self contained classes for students in math, and supported 8th grade language arts teachers as part of full inclusion. Second half of the year, taught Honors Core (Gifted) Language Arts classes for 7th and 8th Graders, Future Problem Solving, as well as a remedial reading class. Students in the reading class showed dramatic increases in reading levels; up to four grade levels in one quarter.

Volunteer: Literacy Volunteers of Maricopa County 729 E. Hatcher Road Phoenix, AZ 85020
October 2011 to Present
Tutor adult English Language Learners and GED students.

Teacher's Aid: The Children's Center for Neurodevelopmental Studies 5430 West Glenn Drive
Glendale, AZ 85301
December 2010 to August 2011
Worked with high school aged and students in sixth to eight grade classes as well as providing

respite care for students with severe disabilities.

Teaching Assistant: University of Nevada, Las Vegas, Department of Geologic Sciences 4505 S. Maryland Pkwy. Las Vegas, NV 89154
2005-2007
Subjects taught included Metallic Ore Deposits, Geographic Information Systems and Geology 101.

Tutor: Salem State College 352 Lafayette St, Salem, MA 01970
1997-1999 Part time
Tutored college a student with severe learning disabilities in college level courses, in subjects ranging from English to advanced geology courses.

Staff Member: Fidelity House, Inc., Lawrence Massachusetts
1990 -1993
Assistant House Manager 1992-1993
Helped establish volunteer newsletter *Connecting Links.*

PUBLICATIONS

Padmore, P., and Spell, T., 2008, The Canovas Canyon Rhyolite, Jemez Volcanic Field, New Mexico: Early Eruptions From A Large Silicic Magma System, or Not? American Geophysical Union, Fall Meeting 2008.

CURRENT CERTIFICATIONS

Arizona Department of Education Certificate number 4518862:
Provisional Cross Categorical Special Education K-12
Secondary Language Arts
Middle School Language Arts
Middle School Science
Provisional Adult Education